Evaluating Retinal Blood Vessels' Abnormal Tortuosity in Digital Image Fundus

Submitted in fulfilment of the requirements for the

Degree of MSc by research

School of Computer Science

University Of Lincoln

Mowda Abdalla

June 30, 2016

Acknowledgements

This project would not have been possible without the help and support of many people. My greatest gratitude goes to my supervisors Dr. Bashir Al-Diri, and Prof. Andrew Hunter who were abundantly helpful and provided invaluable support, help and guidance. I am grateful to Dr. Majed Habeeb, Dr. Michelle Teoailing, Dr. Bakhit Digry, Dr. Toke Bek and Dr. Areti Triantafyllou for their valuable help with the new tortuosity datasets and the manual grading. I would also like to thank my colleagues in the group of retinal images computing and understanding for the great help and support throughout the project.

A special gratitude goes to Mr. Adrian Turner for his invaluable help and support. Deepest gratitude are also for my parents, Ali Shammar and Hawa Suliman, and to my husband who believed in me and supported me all the way. Special thanks also go to my lovely daughters Aya and Dania. Finally, I would like to convey warm thanks to all the staff and lecturers of University of Lincoln and especially the group of postgraduate students of the School of Computer Science.

Abstract

Abnormal tortuosity of retinal blood vessels is one of the early indicators of a number of vascular diseases. Therefore early detection and evaluation of this phenomenon can provide a window for early diagnosis and treatment. Currently clinicians rely on a qualitative gross scale to estimate the degree of vessel tortuosity. There have been many attempts to develop an accurate automated measure of tortuosity, yet it seems that none of these measures has gained universal acceptance. This can be attributed to the fact that descriptions and definitions of retinal vessel tortuosity are ambiguous and non-standard. In addition unified public datasets for different disease are not regularly available. I have propose a tortuosity evaluation framework in order to quantify the tortuosity of arteries and veins in two dimensional colour fundus images. The quantification methods within the framework include retinal vessel morphology analysis based on the measurements of 66 features of blood vessels. These features are grouped as follows: 1) Structural properties 2) Distance approach features 3) Curvature approach features 4) Combined approach features 5) Signal approach features. The features numbered 1 to 4 above are derived from literature. Item number five are new features which I have proposed and developed in this thesis.

These features have been evaluated using a manually graded retinal tortuosity dataset as controlled set. I have also built three tortuosity datasets, each of which contains two manual gradings. These datasets are: 1) A general tortuosity dataset 2) A diabetic retinopathy dataset 3) A hypertensive retinopathy dataset. In addition, I have investigated the differences in tortuosity patterns in hypertensive and diabetic retinopathy. New pathology based datasets were used in this investigation. These are the major contributions of this thesis.

Attestation

I understand the nature of plagiarism, and I am aware of University of Lincoln's policy on this. I certify that this study reports original work by myself during my university project except for the following:

* The retina image shown in figure 2.2 was taken from (http://www.stlukeseye.com/anatomy/retina.html).

* Images of the vision and parts of the eye in Section 2.5 were taken from (http://www.allaboutvision.com/resources/anatomy.html) and (http://www.tedmontgomery.com/the-eye/index.html)

* The tortuous vein image in Section 2.6, Figure 2.5 was taken from (http://www.merckmanuals.com/home/heart_and_blood_vessel_disorders/venous_disorders/varicose_veins.html)

Signature: Date:

Glossary

ANN Artificial Neural Network. 57, 59

AOC Arc Over Chord ratio. 45

Backpropagation backwards propagation of error. 119

CT Computed Tomography. 25

DTFT Discrete Fourier Transform of aperiodic signals. 55

FFT Fast Fourier transform. 52

FSHD facioScapuloHumeral Muscular Dystrophy. 17

FT Fourier Transform. 21, 52, 55, 56

ICC Intraclass Correlation Coefficient. 22

ICM Inflection Count Metric. 46

L-O-Out Leave-One-Out cross validation. 120

MDAC Mean direction angle change. 98

ML Machine Learning. 58

MRI Magnetic Resonance Imaging. 25

RF Random Forests. 57

RLV Relative Length Variation. 45

ROP Retinopathy of Prematurity. 17

RVTDS Retinal Vessel Tortuosity Dataset. 21, 22, 58, 66, 91, 100, 150

SOAM Sum Of Angles Measure. 46

X-ray Energetic High-Frequency Electromagnetic Radiation. 25

Contents

List of Figures

List of Tables

Chapter 1

Introduction

The aim of this chapter is to introduce retinal blood vessels tortuosity, which is a medical phenomenon that affects the retina. It also highlights the importance of its accurate evaluation. In addition, this chapter presents the researcher's motivation and the rationale behind conducting the research and states the set of aims and objectives of the thesis. A description of tasks and investigations that were carried out throughout the project is also included. A general overview of the flow of the thesis structure is presented at the end of this chapter.

1.1 Introduction

Retinal blood vessel tortuosity has been associated with the presence and progression of a number of vascular diseases such as Diabetic Retinopathy, Hypertensive Retinopathy, Retinopathy of Prematurity (ROP), facioScapuloHumeral Muscular Dystrophy (FSHD), Coats Disease and many more [54, 62]. First of all, what is retinal vessels tortuosity and how can it be estimated or graded accurately? The word "Tortuous", according to the Oxford Dictionary is defined as: "full of turns and twists" [22]. However, this is not exactly a helpful definition when it comes to describing retinal blood vessels tortuosity, bearing in mind that the blood vessels are already spread in a semi sphere shaped eye and they are already slightly curved and twisted. Therefore, I introduce the term "Increased tortuosity" or "Abnormal tortuosity" instead. This is more meaningful and accurate in describing this phenomenon.

There are a number of measures that have been proposed to evaluate abnormal tortuosity in the past 42 years. The evaluation of the accuracy of these methods varies depending on the types of the ground truth used. Some of these evaluation methods are: 1) Classifying vessels as either tortuous or non-tortuous. 2) Ordering a number of retinal vessel segments by increased tortuosity. 3) Grading the tortuosity of the whole vascular tree. However, none of these measures has gained a universal acceptance, [see section 2.7].

In this thesis I investigated retinal blood vessels abnormal tortuosity and morphological changes of vessels with respect to tortuosity. In addition, a review of most of the tortuosity measures proposed in the literature has been completed. [See chapter 2]. Subsequently, a framework for evaluating abnormal tortuosity has been proposed. The next sections present the rationale and motivation behind investigating this phenomenon and proposing my framework.

1.2 Rationale

Recent advances in computing and information technology have had a huge impact on all aspects of our lives, especially in the health care sector. Medical image analysis has played a significant role in improving the way that diseases are detected, diagnosed and treated. As improvement continues in some of the medical imaging fields such as CT, X-rays and MRI scans, additional investigations are being carried out to replace some of the old conventional diagnostic methods. Methods such as naked eye inspections of medical imaging, and subjective qualitative diagnostic decisions, like retinal fundus images, to be replaced by automated diagnostic systems that are capable of providing accurate quantitative measurements or even diagnosis. Along with the improvement in medical imaging technologies such as image registration and fusion; and image capturing tools there have been a general improvement in equipment in terms of quality and resolutions within the medical sciences in general. Investigations are still being undertaken to find ways of marrying these advances in imaging with the emerging medical discoveries, that might utterly change the conventional methods of disease diagnosis and treatment. As possible outcome is that, diseases could be predicted and either prevented or treated earlier.

One of the interesting findings in ophthalmology is the strong positive correlation which has been found between retinal blood vessels abnormal tortuosity and the presence and progression of some vascular diseases [54, 62]. This discovery could lead to a leap forward in the development of robust non-invasive diagnostic tools. Since the retina is the only place where blood vessels can be directly visualized, non-invasively, in vivo, it provides easy access for studying the micro-circulation and the haemo-dynamic of blood flow in the human body. For basic background knowledge of the retina and its arterial and venous systems, see the following sections under the literature review, Section 2.5, about the human eye, Section 2.5.1, about retinal venous and arterial systems.

At present, ophthalmologists estimate retinal vessels morphology changes, and retinal vascular abnormalities in general, through naked eye inspection. These inspections are either performed through an ophthalmoscope, which is an instrument used by ophthalmologists, to directly inspect the fundus of the eye; or through images captured by special cameras known as retinal fundus images. Then, the degree of tortuosity is estimated, mostly based on clinician experience and knowledge since there is no standard guide for tortuosity evaluation. This is mostly evaluated using a qualitative scale such as "mild", "moderate", "severe" and "extreme". Occasionally, this is useful however, it is not that effective especially when it comes to early accurate tortuosity detection, and hence early diagnosis and treatment.

Ophthalmologists' reliance on manual tools and techniques to monitor and qualitatively evaluate the changes in retinal vessels morphology can lead to devastating outcomes such as losing eyesight. With improved image processing techniques and software, accurate results can be obtained and further complications can be prevented.

1.3 Motivation

Globally, the estimated prevalence of diabetes in adults between the ages of 20 and 79 worldwide for 2012 was 382 million and it is expected to affect 592 million people by 2035 [21]. It is estimated that 175 million people have undiagnosed type two diabetes. Diabetic retinopathy alone accounts for about 7% of people who are

registered blind in England and Wales, and it is also considered the leading cause of preventable sight loss in people of working age in the UK. Nevertheless, diabetic retinopathy represents one of the diseases that have been found to have correlations between its progression and the tortuosity of retinal blood vessels [72, 64]. Therefore, developing an automated tortuosity evaluation tool is equally important to finding cures to all these diseases.

1.4 Hypothesis

1.4.1 Aims and objectives

Aims

The aims of this thesis are: A) to develop a quantitative tortuosity evaluation framework to evaluate abnormal or increased tortuosity of human retinal blood vessels using two dimensional digital image. The framework consists of a number of features that represent most aspects of structural changes in retinal blood vessels. B) To develop new features. C) To build a pathology based tortuosity dataset of diabetic and hypertensive retinopathy, and a large general dataset. D) To investigate tortuosity differences between diabetic and hypertensive retinopathy.

Objectives

In order to achieve the stated aims, a set of objectives have to be accomplished first as follows:

1) Evaluate the existing tortuosity measures from the literature for grading tortuosity.

2) Investigate the development of new tortuosity evaluating features based on Fourier Transform.

3) Combine the best selection of tortuosity features to build a robust framework for evaluating tortuosity.

4) Create a new dataset, which consists of two subsets: diabetic and hypertensive sets, in addition to the development of manual grading, in which retinal blood

vessels, in this new dataset, will be graded by volunteer ophthalmologists.

5) Evaluate the developed framework by reference to a public dataset, which is Retinal Vessel Tortuosity Dataset (RVTDS) foracchia2005luminosity.

6) Evaluate the developed framework by reference to the developed private dataset mentioned in 4.

7) Evaluate the tortuosity differences between hypertension and diabetic retinopathy by reference to the developed private dataset mentioned in 4.

1.5 Investigations

At the start of this project, I conducted a literature review on the evaluation of retinal blood vessels tortuosity in retinal image fundus, in which I critically evaluated and analysed previous work conducted in this field. I also selected and sourced information closely related to the topic, which was later used to provide the context for my thesis. In addition, I highlighted some of the good existing research built upon that research, and identified gaps that needed to be addressed and investigated. Moreover, in the course of the literature investigations, I visited two of the biggest eye screening centres in the UK; Sunderland eye infirmary and Boston retinal screening center, and I had the opportunity to have informative discussions with a number of expert ophthalmologists and clinicians.

At the second stage of the project, and fully equipped with the right knowledge and clear plans, I started the process of building an evaluation framework that included a large number of features. I also developed a number of new features most of which were based on Fourier Transform (FT). I used various statistical analysis methods to analyse my framework performance and presented the results. Meanwhile, I also started on developing tortuosity datasets. At the beginning, and with help of my supervisors, we built a semi-automated system that: A) segmented retinal blood vessels from 2D fundus images, B) labelled vessel segments as vein and arty, C) Graded the degree of tortuosity. However, things did not go to plan, in terms of automation, and I had to plan and prepare for a manual grading. Thus, three new datasets were proposed.

At the third stage of this project. and based on facts obtained during the literature review, I analysed arteries and veins of patients with hypertension and diabetic retinopathy with regard to vessel structural properties, to see if there were any differences in vessels behaviour between these diseases. At the final stage I reported and documented all work done throughout the project, in addition to discussing results and stating future plans for improvements, projects and publications.

1.6 Thesis overview

This section provides an overview of the thesis structure. The first chapter provides an introduction to the thesis problem, which is retinal blood vessels evaluation, from both the medical and the computing sides. It provides the medical definition of the described phenomenon, in addition to the urgent need of an accurate measure on the part of the health professionals in this field. It also outlines some of the previous work done regarding this problem and some reflections upon them, see Section 2.7. This chapter extends to state the rationale and motivations that has drawn the researcher to conduct such research. This is followed by the thesis hypothesis, a statement of the aims and objectives, and details of the initial comprehensive investigation.

The second chapter documents the literature review conducted on both the medical and the computing sides of the research. On the computing side, the chapter provides an introduction to digital image processing and analysis, in particular medical imaging and more specifically retinal image analysis. Then, the chapter provides a detailed description of retinal blood vessels tortuosity in general, in addition to an introduction to the anatomy of the retina and its components. Following this there is a comprehensive review of measures to evaluate blood vessels tortuosity which are most frequently proposed in the literature.

The third chapter of this thesis describes the development, and the analysis processes involved, of the proposed tortuosity evaluation framework. It outlines the features that constitute the framework, whether they are taken from the literature, or proposed in this study. Implementation and statistical evaluation of these features, using the RVTDS and the new tortuosity dataset, are also included in this chapter.

The fourth chapter of this thesis documents the process of building a general image tortuosity dataset that consists of 130 segments of diabetic and hypertensive patients. This dataset was then divided to create two pathology based datasets, hypertensive and diabetic with 77 and 53 segments respectively. Grading systems are discussed and graders are outlined, then after detailed implementation process the Intraclass Correlation Coefficient (ICC) of the graders is analysed. Consequently three new datasets were proposed.

The fifth chapter of this thesis, is mainly focused on investigating differences in tortuosity between diseases. The diseases datasets proposed in chapter four are used. The proposed frameworks features were measured using these datasets, results are then analysed and reported.

The sixth and final chapter concludes the thesis by outlining contributions made and discusses plans for future work improvement. It starts by highlighting results obtained in this project and it concludes by suggesting improvements and outlining plans for future projects.

1.7 Conclusion

Increased or abnormal retinal blood vessels tortuosity has been proven to be an early indicator of the presence or advancement of a number of vascular and non vascular diseases. Several attempts have been made to accurately evaluate this abnormal tortuosity, however there is still no universal evaluation method. After a comprehensive investigation of all aspects that surround this phenomenon, I propose an evaluation framework with a clear set of aims and objectives as outlined in the thesis overview and set out in detail over the next chapters.

Chapter 2

Literature review

This chapter provides a detailed literature review of the evaluation of retinal blood vessels tortuosity in digital fundus image in both medical and computing fields. The first two sections provide a general introduction to the field of digital image processing and analysis, followed by an overview of medical imaging technologies and approaches in particular, retinal imaging. The chapter then proceeds to describe retinal blood vessels tortuosity and provides an overview of the anatomy and structure of the retina and its components. The last three sections of this chapter, provide a broad overview of most frequently proposed evaluation methods in the literature, touch also upon evaluation methods used in other disciplines, and considers some issues raised by ophthalmologists regarding the type of measures and methods to be used in the evaluation. Previous data analysis methods used are also discussed in this chapter.

2.1 Introduction

A great number of tortuosity evaluation methods have been proposed within the last 42 years. In this chapter, different approaches to tortuosity evaluation are outlined and critically evaluated. These approaches are different in terms of tortuosity quantification methods, types of blood vessel segments used and the various approaches to validation techniques. Although some of the tortuosity evaluation methods which have been suggested showed good results, none of these measures has gained acceptance as a universal tortuosity evaluation feature or measure.

A review paper, based on this chapter has been presented at the Science and Information Conference (SAI 2015) and recorded in the conference proceedings published by IEEE. The paper can be found in Appendix .1.

2.2 Digital image processing and analysis

Digital image processing is a branch of computer vision, which in turn is a branch of computer science. Before proceeding to define the image processing and image analysis fields, a basic understanding of images and their components is needed. An image, as described by Gonzales and Woods [38], is a two dimensional function, $f(x, y)$, where x and y are spatial planes or coordinates. The amplitude of f at any pair of coordinates (x, y) is called the intensity or grey level of the image at that point. When x, y and the amplitude values of f are all finite, discrete quantities, then the image is called a digital image.

Gonzales and Woods also noted that the field of image processing refers to processing digital images by means of using a digital computer. In other words, as described by Zhou et al. [94], digital image processing is the technology of applying a set of computer algorithms to process digital images. Moreover, Vernon [89] stated that image processing can be thought of as a transformation, which takes an image and produces an image, i.e. it starts with an image and produces a modified or enhanced image, whereas digital image analysis is the transformation of an image into something other than an image, i.e. it produces some information representing a description or decision about the initial image. There are three main fields or categories in image processing: A) Image restoration, in which noise and blur are removed from an image using particular operations and algorithms. B) Segmentation of regions of interest, which is the process of isolating particular parts of an image, for example the background, foreground or specific textured or coloured object or area. C)Image enhancement, which is the enhancement of the image brightness, sharpness, etc. In medical image processing systems, most of these techniques and processes are used to process and improve images of the human body or parts of it for further analysis i.e. for diagnosis or examination purposes. Examples of medical images are Energetic High-Frequency Electromagnetic Radiation (X-RAY), Computed

Tomography (CT) scan images, Magnetic Resonance Imaging (MRI), ultrasound images, etc. The next section will provide more information about medical image processing.

2.3 Medical image processing and analysis

Medical image analysis is the field in which images of the human body or part of it, are digitally processed for research or clinical purposes, such as diagnosis, finding more information about or investigations of diseases. Over the last few decades, as stated by Arnulf Oppelt [71], enormous improvements have been made in the area of imaging systems for use in medical diagnostics, and new techniques such as magnetic resonance tomography have been developed. This has opened up new avenues in early diagnosis, especially, but not limited to conditions related to the brain such as strokes, spine injuries and abnormal tissues in the human body in general.

Since the field of medical image processing has been an interdisciplinary research field attracting expertise from applied mathematics, engineering, computer science, physics, statistics, biology and medicine, huge improvements have been made in conventional techniques such as X-rays [94]. Image processing and analysis of medical images normally go through a number of stages or phases. These phases start with the image acquisition process and include: 1) image formation/reconstruction. 2) Image enhancement. 3) Image compression and storage. 4) Image analysis. 5) Visualisation of the processed image. The process ends with the evaluation and validation of obtained results [26]. This study is mainly focused on retinal image processing and analysis. The next section provides more details about image analysis stages with reference to retinal imaging.

2.3.1 Retinal image analysis

One of the interesting facts about the eye that it is the only organ in the body where blood vessels can be directly visualised in vivo without any medical intervention. Ophthalmologists have put that fact into use for many years as can be seen in the following statement by Gowers in 1876:" ... When the retina is free from local disease, there is no reason to believe that the retinal artery and vein differ in

their condition from other arteries and veins of the same size, and, therefore, any marked change in their state, apart from cerebral or ocular disease, may be taken as evidence of a similar change throughout the vascular system", [40]. Subsequent studies confirmed that there are correlations between brain diseases and changes in the retinal vascular [87, 73], in particular vascular dementia [67, 93], and stroke [76].

There has been rapid development in image processing technologies relevant to ophthalmology over the past few years including progress towards developing automated diagnostic systems for conditions such as diabetic retinopathy, age-related macular degeneration and retinopathy of prematurity [74]. In retinal image analysis studies, retinal images are processed, in similar ways that images in general are processed, to extract desired information or diagnosis needed; these process are staged as follow:

A) Image acquisition and pre-processing: At this stage images of patients' retinas are acquired or retrieved from sources such as image databases. These images are then pre-processed through operations such as enhancement or smoothing. The set-up of the cameras, in addition to the quality of the captured images and the outcome of the pre-processing, play a significant role in the success of subsequent stages. The quality of retinal images, has been considered as one of the problems in successfully capturing images of the ocular fundus because of factors such as defocus, medial opacities or the presence of artefact [56, 60]. The preprocessing stage therefore also includes image restoration, in which damages caused by the image capturing process, noise or blurriness are reversed.

B) Segmentation: The second stage is the segmentation of regions of interests, which in this case means those regions in the retina that could possibly be segmented such as the retinal vasculature (retinal arteries and veins) or abnormal anomalies such as lesions. There are different segmentation techniques for different tasks. The outcome of this stage is normally a binary image or a measurement mask with the white colour marking the regions of interests and black representing the background. Morphological operations can be used at this stage for further enhancement or correction using operations such as opening, closing, and dilation or eroding.

C) Evaluation and visualization: At this stage, measurement can be carried out in addition to basic or advanced evaluation of the data resulting from these measurements, and/or image visualization. [See Figure 2.1 for the stages of image analysis.]

In conclusion, increasing technology leading to the development of digital imaging systems over the past two decades has revolutionised fundal imaging [74]. Automated diagnosis of retinal fundal images using digital image analysis offers huge potential time and cost benefits such as the ability to examine a large number of images, and offering more objective measurements than current observer driven techniques [74]. Nowadays retinal image analysis is considered a standard clinical practice with an increasing number of retinal medical applications.

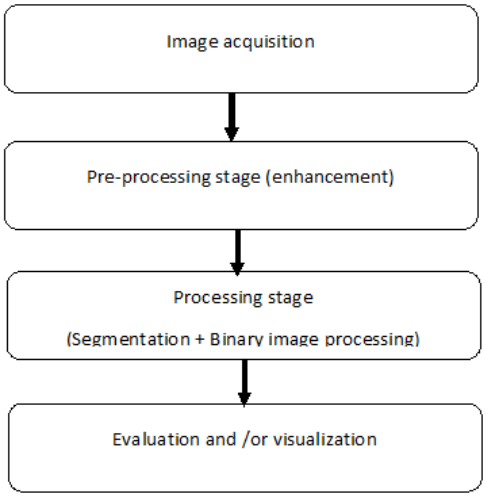

Figure 2.1: A graph shows the stages of image analysis

2.4 Blood vessel's tortuosity

The word "tortuous" is defined in the Oxford Dictionary as: "full of turns and twists". Nevertheless, tortuosity observation is not just confined to blood vessels, it has been studied and measured in various disciplines, for example, tortuosity has been used to describe rivers, animals' pathways, materials, tubes, etc. However, in the medical field the term tortuous has been particularly associated with blood vessels and in some cases with nerves. When it comes to describing structural

changes in blood vessels, the use of tortuous seems not quite precise, given the nature and the functionality of blood vessels. Blood vessels in general as described by [86] consist of arteries, arterioles, capillaries, venules and veins. All blood in the human body is carried in these vessels. The arteries, which are strong, flexible and resilient, carry blood away from the heart and bear the highest blood pressures. Since the arteries are elastic, they tend to narrow (recoil) passively to help maintain blood pressure. Arteries normally branch into smaller vessels called arterioles; both arteries and arterioles have muscular walls that can adjust their diameter to increase or decrease blood flow to a particular part of the body.

Capillaries as defined by Mary Bird [6] are fine, hair like, vessels consisting of one cell thick coats. Since they are only one cell thick, they act as a bridge between arteries and veins. They consist of fluid containing oxygen, nutrients and other substances which are able to flow into the tissues, consequently supplying the individual cells with their requirements.

Veins, which return blood to the heart, can widen (dilate) as the amount of fluid in them increases. Some veins have valves in them, to prevent blood from flowing backward. If these valves leak, the back-flow of the blood can cause the veins to stretch and become elongated and convoluted (tortuous) [86]. [See figure 2.5 for a tortuous vein]. Bearing all these structural properties in mind, the researcher suggests that the use of "abnormal tortuosity" would provide a more logical description of the abnormal structural changes in blood vessels. Abnormal tortuous vessels can occur in several places in the body, and some of these tortuous vessels might indicate a medical condition, especially in structures like the retina, the brain (cerebral) or abdomen.

2.5 The retina

The human eye is the organ which gives the sense of sight; it allows humans to observe and learn more about their surrounding environment, more than they normally do with any of their other senses. The eyes are located in the front half of the orbits surrounded by fat and connective tissues and supported by a facial hammock. They rest in these two bony cavities, the orbits, on either side of the nose [19]. The

concave interior part of the human eye, consists of the retina, the choroid, the sclera, the optic disk, and blood vessels, which can be seen through the ophthalmoscope by the naked eye. The retina has been known as the most complex organ in the human body. It is the sensory layer of the eye extending from the optic disk to the ora serrata [59]. This layer is a delicate nervous membrane, upon the surface of which images of external objects are received, as stated in Gray's Anatomy [41].

The retina consists of the macula, which is the most sensitive area of the retina characterised by its richness of cons, or bulbous particles which are ones of the light sensitive elements that convert electromagnetic waves into nerve impulses. Retinal blood vessels usually end at the margins of the macula [58]. Retinal blood vessels are discussed in detail in Section 2.5.1. Another important part of the retina is the fovea, located in the centre of the macula, which has the densest concentration of cons, and is responsible for acute vision and the production of bright reflex. [See Figure 2.2 illustrates the anatomy and parts of the retina.] An effective way of obtaining a deep understanding of the parts that make up the eye and their functionalities, is to go through the process of vision. The process by which vision happens in the eye is similar to the work flow of a digital camera. The reflected light waves from an object, such as a tree, enter the eye first through the cornea, which is the clear dome of the front part of the eye. The light then travels through the pupil, which is the circular opening in the centre of the coloured iris. The pupil adjusts itself by contracting and dilating with the change of light intensity entering through it. The entering light is first bent or converged by the cornea, and then bent further by the crystalline lens, located immediately behind the iris and the pupil, to a nodal point (N) located immediately behind the back surface of the lens. [See Figure 2.3]. The image at that point becomes reversed and turned upside-down, while the light continues through the vitreous humor, the clear gel that makes up about 80% of the eye's volume, and then back to the clear focus on the retina behind the vitreous [70].

2.5.1 Retinal blood vessels

There are two types of vessels that supply blood to the eye. The choroidal blood vessels, which supply the external parts of the eye with an amount that represents

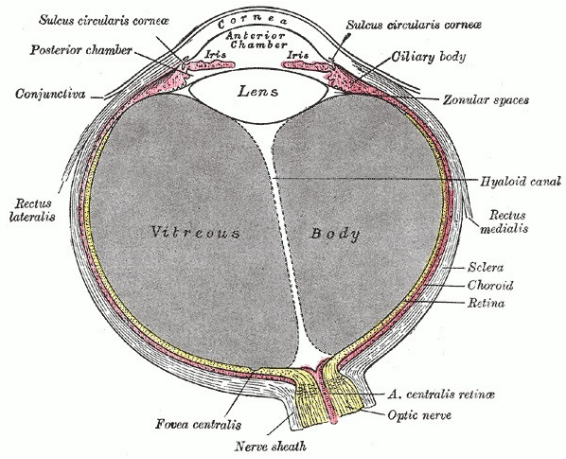

Figure 2.2: The anatomy of the eye

around 65-85% of the whole amount of blood that the eye receives; and the central retinal artery, which is, on the contrary, the eye's internal blood supplier that extends and branches to arterioles.

This study mainly revolves around the internal vascular of the retina especially the retinal blood vessels, arteries and veins, that extend from the optic disc to the peripheral or the edges of the retina.

Retinal arterial system

Arteries in general, as defined in Gray's anatomy [41], are cylindrical tubular vessels, which serve to convey blood from the heart to every part of the body. Therefore, they deal with a high blood pressure flow. They are characterised by thick muscular walls with a lot of smooth muscles, for flexibility, and also by a relatively small lumen, which is the cylindrical hole through which the blood flows.

The retinal arterial system consists of the central retinal artery, and the retinal arterioles. The central retinal artery, which is the main blood supply to the retina, is fed by the ophthalmic artery which branches off the carotid artery. It is an end artery without any anastomoses that enters the optic nerve estimated as $1cm$ behind the globe. Central artery occlusion might cause irreparable damage, such as vision loss, due to ischemia. The retinal arterioles arise from the central retinal artery; they have smooth muscle within their walls, but they differ from the arteries in their internal elastic lamina, which is discontinuous in nature [54].

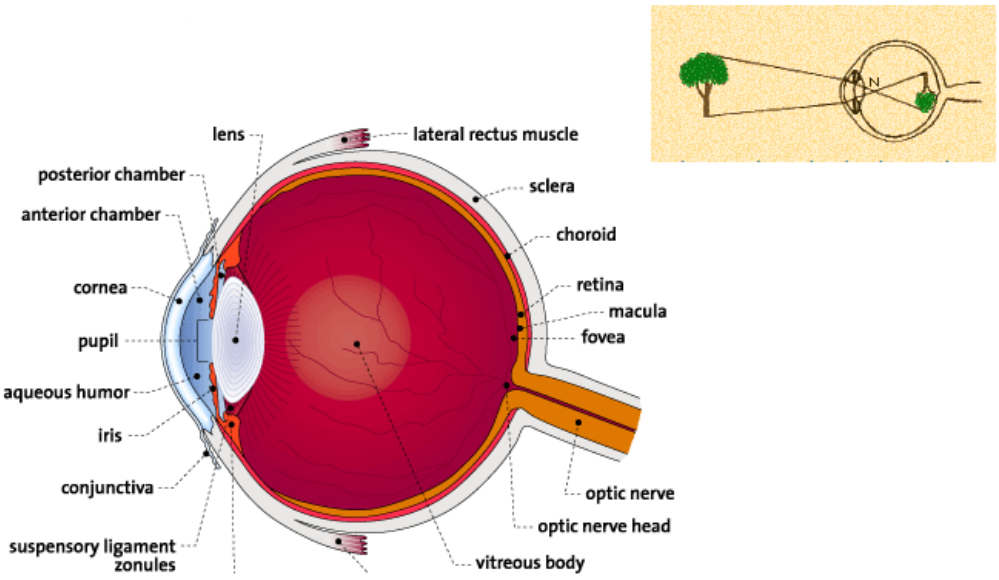

Figure 2.3: Vision process and parts of the human eye

Retinal venous system

The veins are the vessels which serve to return the deoxygenated blood from the capillaries of different parts of the body to the heart, therefore they deal with low blood pressure [41]. Veins are very similar to arteries in their structure, but they have larger lumens compared to arteries and relatively thin muscular walls, which means less smooth muscle or less elastic fibres. Moreover, veins have valves to prevent back flow of the deoxygenated blood, which allow veins to deal effectively with the low blood pressure flow.

The venous system also includes the small venules, which have a similar structure to capillaries, but are larger in size. Larger venules, which contain smooth muscle gradually join to form veins. In addition to the smooth muscle, veins contain elastic tissue in their walls and they are to some extent distensible; they gradually expand in width as they pass posteriorly towards the central retina as described by Kanski [54]. Figure 2.4 illustrates the positions of macula, fovea, veins and arteries in a retinal funds image.

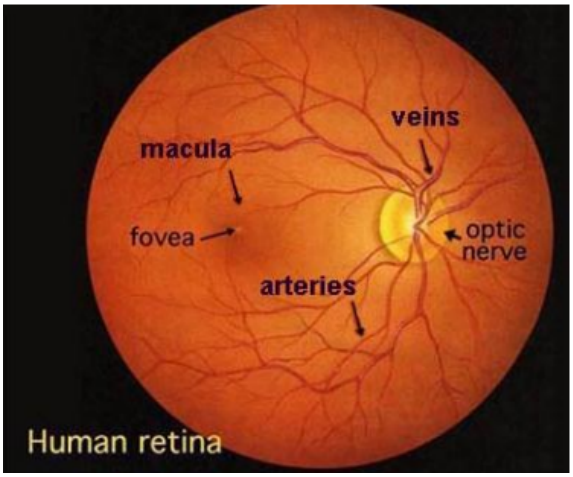

Figure 2.4: Retinal Arteries, Veins, Fovea and Optic nerve

2.5.2 Retinal fundus

In the retina and retinal imaging, the fundus represents the inner part of the eyeball. It includes parts such as the retina, optic disc, and the macula. The fundus of the eye can be seen through the pupil with an ophthalmoscope, which is an instrument used by ophthalmologists to inspect the interior or fundus of the eye.

2.6 Retinal vessel's tortuosity

In the previous sections, it has been indicated that the use of the word tortuous with blood vessels in general is not precisely accurate, especially with blood vessels located in structures like the retina. This is because the blood vessels are spread in a semi-spherical shaped eye and these vessels are already slightly curved and twisted. Normal retinal blood vessels are straight or slightly curved but in some diseases they become dilated and start to take different paths. This dilation, as explained by William E. Hart, et al. [48] is caused by radial stretching of the blood vessel, and the serpentine path occurs because of longitudinal stretching. Tortuosity can be focal, which occurs only in a small region of the retina or individual segment, or general which involves the entire retinal vascular tree, Figure 2.6 shows retinal images with tortuous and non-tortuous retinal blood vessels.

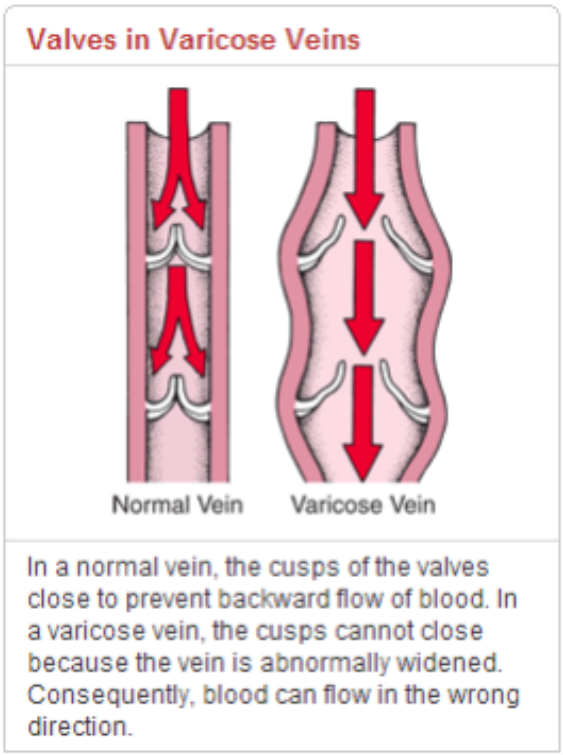

Figure 2.5: Tortuous vein (varicose vein)

Retinal vessels tortuosity and hypertension

Retinopathy is a general term that refers to any form of non-inflammatory damage to the retina of the eye. Hypertensive retinopathy is a disease that affects the retina that occurs because of hypertension-induced changes to the small vessels in the eyes. Cholesterol is formed in larger arteries, just like elsewhere in the body and this arteriosclerosis in the eye leads to tiny infarcts and superficial bleeding on the retina. The arteriosclerotic changes will remain until overall cholesterol is treated. However, hypertensive retinopathy will get better as the underlying cause, hypertension, is treated. Signs of hypertensive retinopathy that can be examined and identified in the fundus oculi are generalised and localized arteriolar narrowing, increased light reflex, arteriovenous crossing phenomena, arterial attenuation (decrement in the arterial attenuation) and more severe signs such as exudates, haemorrhages and papilloedema. These signs have long been considered indicative of the stages of, and prognosis in, systemic arterial hypertensive disease [53, 54]. It is clear that tortuosity is one of the earliest signs that can be spotted. Mostly people with hypertensive retinopathy are usually symptoms free. They will not

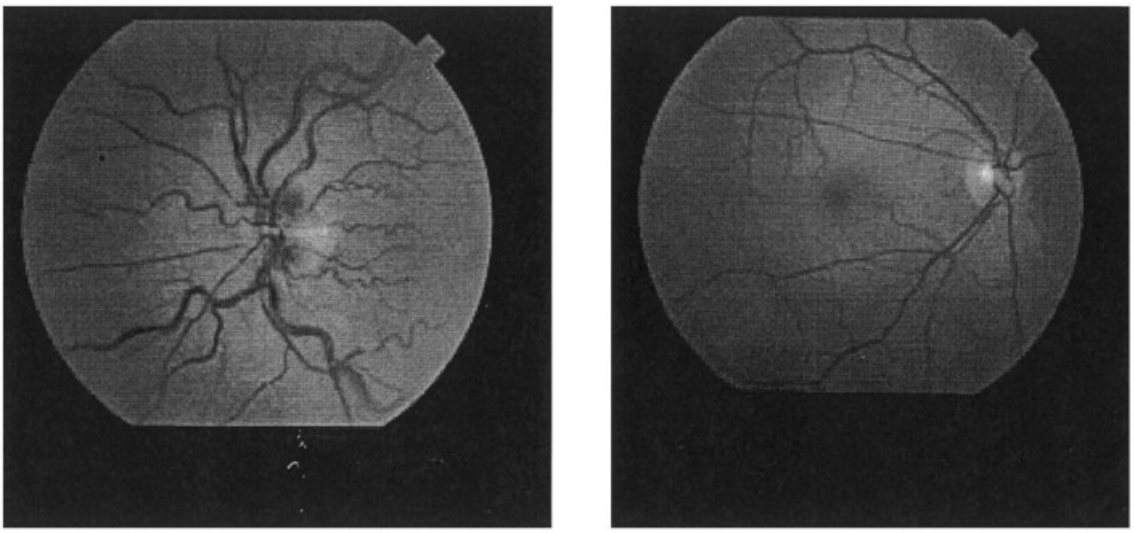

(a) (b)

Figure 2.6: (a) tortuous and (b) non-tortuous retinal fundus images

have changes in their vision and they may not even know that they have high blood pressure. Often, hypertensive retinopathy is spotted during an eye examination, when the doctor observes the classical changes in the eye associated with hypertensive retinopathy and the required treatment will then begin. Clinically, weeks to months after successful treatment of hypertension, an eye exam should show that the retinopathy changes have resolved.

Retinal vessels tortuosity and diabetes

Diabetic retinopathy is the most common diabetic eye disease and the leading cause of blindness in adults. It is caused by changes in the blood vessels in the retina. Blood vessels may swell and leak fluids, or abnormal new blood vessels may grow on the surface of the retina. Diabetic retinopathy is a progressive disease; in which changes may not be noted at first, but with time, retinopathy gets worse and eventually leads to vision loss. Intermittent blurring of vision is a usual complaint and is caused by the swelling or edema of the lens due to changes in blood sugar levels. It usually affects both eyes [1]. There are four stages or types of diabetic retinopathy:

1) Mild Nonproliferative Retinopathy: This is the earliest stage of diabetic retinopathy, in which small balloon-like swelling occurs in the retina's tiny blood vessels.

2) Moderate Nonproliferative Retinopathy: At this stage some blood vessels in an area are blocked.

3) Severe Nonproliferative Retinopathy: At this stage more blood vessels become blocked and the retina begins to grow new blood vessels in an effort to provide nourishment to areas that suffer from lack of blood supply.

4) Proliferative Retinopathy: This is an advanced stage, in which new vessels are formed in the retina but they are very fragile and abnormal; they are not the cause of blindness, but when they leak, due to weakness, severe loss of vision and then blindness can occur.

It is extremely important for diabetic patients to have their eyes examined regularly by an ophthalmologist. Keeping blood sugars, as well as cholesterol and blood pressure under control will help limit the damage to eyes and help keep valuable eyesight. One of the main differences between the two retinopathies is that hypertensive retinopathy is reversible, and diabetic retinopathy is not.

2.7 Previous work on grading retinal vessels tortuosity

In the past, there have been many attempts to develop an accurate tortuosity grading measure or system. This section provides a brief overview of the measures which have been most commonly proposed in the past 42 years of research in chronological order. The majority of the proposed measures can be classified into three main groups: 1) measures based on the ratio between the curve length and the chord length. 2) Measures based on the local curvature at each point, or changes in the curve direction or sign along the blood vessel segment.3) Combined measures; these measures are the product of the combination of the previous measures. Recently researchers have started to incorporate additional structural properties or behaviours of blood vessels, (such as segment width, number of sub-curves in a blood vessel segment, etc.), into curvature measures. This is because ophthalmologists carrying out clinical observations, rely on these basic structural properties to estimate the degree of tortuosity.

One of the earliest attempts to mathematically evaluate retinal blood vessels abnormalities was conducted in 1967 by Kagan et al. [53], The study focused on measuring the width and artery to vein ratio. They also investigated signs in fundus oculi secondary to hypertension, such as generalised and local arteriolar narrowing, increased light reflex, and arteriovenous crossing phenomena and so on. Their aim was to differentiate between hypertensive and non-hypertensive retinas and to distinguish and separate the stages of hypertension from each other. They assessed three subject groups: normal, hypertensive and hypertensive with abnormalities. The width of the main upper and lower temporal arteriol and venule were measured using a curvometer (an instrument normally used for map reading). The measures were at a distance of one disc diameter from the periphery of the disc, to the nearest mm. Their study revealed that there are differences between hypertensive and non-hypertensive retinas. They reported that there is smaller width of arterioles with the hypertension group in addition to retinal abnormalities as well as with the venules, but without significance. Also, they reported a smaller A/V ratio with the abnormalities group compared to the normal.

A few years later, the relative length variation method was proposed. It was first introduced by Lotmart [63], and altered later by Bracher [7]. This method was based on the measurement of the length of blood segment and its underlying chord. This is one of the first methods that is based on distance measurement. The measure subdivides a single vessel segment into series of single sub-arcs with curve height h_i, and chord lengths l_i, tortuosity is then estimated as the relative length variation Equation 2.2, where L is the length of the blood vessel, and the approximation is derived using a sinusoidal model of a blood vessel segment. Unfortunately, the technique is not fully automated and it requires manual selection of points on the fundus photograph to divide the vessel into a series of single arcs. Bracher [8] also noted that blood vessels may take sinusoidal form, but are more often irregular in as much as bends alternate with straight parts, and there is no rule for the distance of the bend from the disc. The study also estimated the integral width and length of blood vessels. Using this measure as a part of a suite of tortuosity measures, 91% was achieved in the classification of individual retinal vessel segments as tortuous or non-tortuous and 95% in the classification of a whole vascular tree as tortuous

and non-tortuous, the study was conducted by Hart et al. in 1999 [49] using a private dataset without an indication to a particular disease, and a logit model for the classification.

As cited in [49] Kaupp et al. have reported unpublished results of an automated tortuosity measure that uses a Fourier transform of the perpendicular along the blood vessel segment. Smedby et al. [83] introduced five measures to grade tortuosity of femoral arteries, included a number of integral curvature measures and a measure that is based on the number of inflection points along the blood vessel, in addition to another which calculates the number of fractions of the blood vessel segment that has a high curvature. Capowski, Kylstra and Freedmen [14] proposed a tortuosity index based on spacial frequencies. It was built on a grade index system, in which retinal images were classified as either tortuous or non-tortuous. Although it had been found that the index forms an objective measure of the ROP disease state, it has been stated that it is not sensitive to non-ROP changes. Hart, et al. [49] described a suite of automated tortuosity measures of the tortuosity of retinal vessel segments. The suite included arc over chord measure, the total curvature and the total squared curvature. The latter two measures were each averaged by their chord and curve lengths. The blood vessel segments used were manually and automatically extracted. The measures have zero value for a straight segment and an increasing positive values for a tortuous one. They also proceeded to prove two hypotheses concerning the proposed measures: first the transformation properties of measured vessel segments, and secondly the vessel composition and scaling. Regarding vessel composition, they believed that if a segment in a vessel is tortuous, it means the entire vessel is tortuous too, and also assumed that the direction and orientation of vessel do not affect the vessel tortuosity. Their proposed measures were tested on two classification problems: 1) the classification of segments as either tortuous or non-tortuous. 2) The classification of a whole vascular tree. The achieved classification rate of the first problem was 91% and 95% for the other. However, their measures have been found to fail to differentiate between the tortuosities of structures that visually appear to be different in tortuosity. Two years later Hart, et al. explored the relative length variation which had been introduced earlier by Lotmart Freiburghaus and extended by Bracher [63, 7] as previously noted. They used the curvature of

a parametrized curve as defined in Equation 2.1 (Where $\alpha(t)$ is the angle of the tangent line at t, and s is the distance at t). However they found that there is still difficulty in accurately estimating the degree of tortuosity especially with the subjectivity gross scale, which increases the difficulty of identifying changes between classes.

$$Tortuosity(t) = \frac{d\alpha}{d(s)}(t) \tag{2.1}$$

Geoffrey Dougherty [25] proposed a novel index for measuring abdominal arterial tortuosity, which is caused by the compression of the spine with age. The proposed index is based on the second differences of the coordinates of the vessel mid line, or derived from the standard deviation of successive differences, $d_{Xo}, d_{X1}, \ldots, d_{XN}$, in the horizontal co-ordinates. Thus, the index depends on the vessel length and the sampling interval. However, the author noted that it can be made independent of both by dividing by the sampling interval. This variant based measure the author referred to as the Standard Deviation Tortuosity (SDT). The index assigns a value of zero, if the measured vessel is straight. The measure is independent of the magnification, resizing of the image or the sampling frequency.

Kheng Goh et al. [37] described twelve tortuosity measures, and used a data mining algorithms to classify retinal images as either tortuous or non-tortuous. Using arc over chord, and the curvature measure suite in addition to the direction angle change. Kheng Goh et al. stated that these measures of curvature do not give a reliable and consistent indication of the overall measure of tortuosity of the vessel segment under consideration if used individually. However, they observed that if some of these attributes of the different curvature definitions are used collectively, the degree of reliability and accuracy in measuring the curvature of a particular segment of the retinal vessel is increased. In their proposed Automatic Diabetic Retinal Image Screening system ADRIS, they combined all the data of the 12 attributes associated with the four curvature definitions or measures and fed the data into an association based data mining classification tool known as CBA. The output of CBA consists of a set of association rules governing the relationship between the 12 attributes that reliably and accurately classify the input vessel segments as either tortuous or otherwise. Heneghan, Conor et al. [51]measured the width and tortuosity of

retinal vessels that were extracted from retinas of ROP patients. They used the ratio between the arc and chord length to estimate tortuosity. Their algorithm consistently overestimated the degree of tortuosity by approximately 0.07, which they attributed to the discrete nature of a digital image. They added that since pixels have a finite size, this means that measuring distance from centre to centre of each pixel will force a theoretically smooth curve to follow a zig-zag path with a longer length. However, they explained that the estimate is consistently biased over the range of tortuosities of interest, so that measurements of tortuosity can be considered as reliable in a relative sense. After applying a simple retrospective screening paradigm, they yield a screening test with a sensitivity and specificity of 82% and 75%. Factors confounding a more accurate test include poor image quality, inaccuracies in vessel segmentation, inaccuracies in measurement of vessel width and tortuosity, and limitations inherent in screening based solely on examination of the posterior pole. Bullit et al. [13] proposed an innovative method based on 3-D curvature estimated via a geometric technique. They used three of the existing tortuosity metrics: Distance metric (DM) which is the ratio between the arc length and the chord length normally used on 2D images; Inflection Count Metric (ICM) in which the DM is multiplied by the number of inflection points in a vessel; the Sum of Angles Metric (SOAM) which is implemented by integrating the total curvature along the curve. Although their proposed method was the most sensitive in detecting two types of abnormal tortuosity, it has been found to be ineffective with tight curves. Grisan, Enrico et al.[43] suggested that there are important aspects that should be considered before measuring vessel tortuosity, such as the factors that influence the vessel to be tortuous or non-tortuous in the first place. Their approach was to provide some solutions to problems encountered in previous studies such as long vessel tortuous classification. The three transformation properties they suggested that might influence the evaluation of vessels tortuosity are:

1) Translation, rotation and scaling: Grisan et al. stated that translation and rotation are not supposed to influence the perception of tortuosity. But with scaling, they believed that a single vessel does not affect clinical perception. However, they questioned that especially when it came to vessel calibre.

2) Composition: They introduced a new definition of composition property, which

completely contradicts the Hart, William et al. definition [48]. They stated that a vessel s with a combination of various segments s_i, will not have a tortuosity measure less than any of its composing parts.

3) Modulation: They assumed that the greater the number of changes in the curvature sign or the twist, the more tortuous the vessel is considered. Similarly, they added, the greater the amplitude (maximum distance of the curve from the underlining cord) of the twist is, the greater is the tortuosity associated with it.

Grisan et al. investigated all the existing algorithms, then added additional features and proposed a new improved algorithm [28, 44]. They believed that, compared with the previous algorithms, their technique was more reliable and robust. However, a more extensive evaluation based on a larger set of images is needed. Longmuir, Susannah Q., et al. [62] presented a paper that investigated Facioscapulohumeral Muscular Dystrophy, which is an autosomal-dominant disease, and it has been found that retinal blood vessel tortuosity to be one of its several signs. Their methodology was based on the extraction of the centreline of each artery and vein. Their calculation was then determined by the number of changes in curvature sign, the angle of curvature of the vessel, the ratio of arc length to the respective chord length and total length of the vessel. The tortuosity was calculated by the ratio of the arc length to the respective chord length. Their results showed that there is a correlation between the subjective tortuosity of arteries, and the severity of FSHD. However, these results were not that significant compared with the tortuosity of veins. Trucco, Emanuele, et al. [29] supported the notion of incorporating vessel features in the tortuosity calculation process. They stated that curvature may not be the only quantity involved in modelling tortuosity, and they assumed features like vessel thickness, or calibre, may also play a role in tortuosity estimation. Danu Onkaew et al. [20] used previous algorithms in developing their method. They went on to upgrade an algorithm that was developed based on curvature to estimate the vessel tortuosity using chain code. However, the algorithm did not show any compatibility with the transformation properties that ophthalmologist use to define tortuosity measures.

Recently Rodriguez, Martin et al.[65] introduced a different approach for

evaluating tortuosity; they used the fast Fourier transform of the vessel's curvature as a tortuosity evaluation method. Results were promising especially when it came to aspects such as the variation of amplitude, frequency and length of vessels.

Diedrich, Karl T., et al. [23] carried out research that investigated the brain's arteries and their relation to arterial vascular diseases mainly focused on hypertension. A centreline extraction algorithm was used and a distance based tortuosity metric was applied to magnetic resonance angiography (MRA) of brain images to quantitatively measure the tortuosity of arterial vessel centrelines. The study resulted in a correlation between tortuosity and hypertension. In recent years, Turior, Rashmi, and Bunyarit Uyyanonvara. [88] used existing curvature measurement algorithms as a base of their new algorithm. They introduced two new methods for curvature measurement: a numerical integration method and a numerical differentiation method to calculate the curvature of vessel segments. Ghadiri, Farnoosh et al. [35] developed an automated algorithm to grade tortuosity of an entire vessel network. Their technique was primarily based on the vessel direction. Hence, they evaluated vessel network tortuosity without using vessel centreline tracing. During the same year Ghodasra, Devon H., et al. [36] set out to describe the rate of change in retinal vessel tortuosity and width in eyes that developed type one Retinopathy of Prematurity (ROP). They used a computer assisted image analysis system to grade vessels tortuosity and width. The rate of change per day was calculated using a linear regression model and the results showed a relation between tortuosity and the width of the vessels.

The literature also includes attempts to build automated or semi-automated integrated systems, (such as the Retinopathy Of Prematurity Tool (ROPtool) [90] and Computer Assisted Image Analysis of the Retina (CAIAR))that respectively segment, classify and measure blood vessels tortuosity [92]. However, this study focuses on methods and algorithms that evaluate the tortuosity of individually blood vessel segments.

In conclusion, the literature review shows that most studies have been based on the ratio between the curve length and the chord length. However, this measure has proven to lack accuracy because it assigns the same tortuosity value to an intuitively very tortuous curve as to a simple, gently curve with the same average

deviation from the chord [29, 48]. On the other hand, the measures based on the local curvature at each point along the course of vessel segment have also been found to be unable to capture some of the important aspects related to blood vessels walls or boundaries such as aneurysms [5]. Consequently, suggestions have been made that curvature may not be the only quantity involved in modelling tortuosity, and that vessel features should also play a role in curvature estimation [43, 29]. However the right combination of features needs to be identified and tested. As clearly indicated above, in addition to a number of innovative approaches such as grading tortuosity on 3D images, researchers also tried to incorporate the clinical perception aspects of tortuosity in their methods with consideration to the properties that influence blood vessels to become tortuous in the first place such as the length of the vessel, and how smooth the vessel is, etc. With all these studies in mind, and with consideration to the advantages and drawbacks encountered in these studies, a tortuosity evaluation framework is proposed in an attempt to capture most of vessels curvature and to automatically and accurately grade retinal blood vessel tortuosity. A number of improved tortuosity measures are also proposed and incorporated in the framework.

2.7.1 Grading tortousity in other disciplines

Beside the studies of retinal blood vessels' tortuosity, this phenomenon has also been investigated in various parts of the human body. Vessels tortuosity in general has been associated with the presence of disease, for example the study of the tortuosity of abdominal arterial and compression of the spine, conducted by [25], proved that there is a significant correlation between the tortuosity of the abdominal aorta and subjects' age. In another example, blood vessels tortuosity also has been found to be relevant as a detector of the beginning of malignant tumours in the human brain [13, 27]. There are also studies of the tortuosity of the microarchitecture of the trabecular bone in an investigative study that aims to improve fracture risk prediction [75].

Furthermore, tortuosity also has been investigated and measured in other non-medical disciplines. In civil and environmental studies, tortuosity is considered as one of the geometrical properties of cracks and so has been investigated in that context and measured in cement and concrete cracks [2]. In physics, tortuosity is

investigated, studied and measured in porous media [66]; In electricity and lightning research the tortuosity of lightning spark is expressed using the mean absolute value of angle change, which is a measure frequently used in measuring tortuosity of blood vessels.[4]. In agricultural science particularly in animal behaviour studies, the tortuosity of an animal's path resulting from seasonal migrations was also investigated and its characteristics and tortuosity were calculated [31].

2.7.2 Tortuosity measure properties

Although ophthalmologists fail to agree on a universal definition of vessels tortuosity, they mostly seem to agree on what a tortuosity measure needs to satisfy to become clinically meaningful. They suggest that a tortuosity measure should be invariant to translation, rotation and scaling. Moreover the position and the orientation of the blood vessel should not affect the perception or the degree of the tortuosity. This seems to be a strong beginning towards setting corner stones in the quest for the perfect tortuosity measure. Few studies have investigated these properties. Hart, et al. [48] discussed two tortuosity properties, vessel composition and scaling. Enrico Grisan, et al. [43] discussed three of the vessels transformation properties: translation, rotation and scaling, composition and modulation.

2.8 Existing tortuosity evaluating features

This section outlines some of the most used tortuosity evaluating features from the literature that are based on various approaches to estimating tortuosity in addition to a number of basic blood vessels structural properties' measurements. It also provides a critical evaluation of these features, their strengths and limitations in order to be incorporated in the proposed tortuosity evaluating framework.

2.8.1 Distance approach

These features are mainly constructed to evaluate tortuosity by measuring the length of the blood vessel segment or curve, or the length of the path that the blood vessel takes, known as the Arc and denoted by L_C; and the length of the straight line between the two end points of the blood vessel segment or arc, known as the Chord

and denoted by L_X. Tortuosity is then estimated mainly by taking the ratio between those two lengths. The next sections provide some measures based on this approach.

Relative length variation

This was the first distance based feature. It was introduced first by Lotmart Freiburghaus [63], and altered later by Bracher [7]. This feature subdivides a vessel segment into a series of single arcs with heights h_i, and chord lengths l_i. Tortuosity is then estimated as the Relative Length Variation (RLV) 2.2, where L is the length of the blood vessel, l_i represents chord lengths and h_i is arrow heights. The approximation is derived using a sinusoidal model of a blood vessel segment. Unfortunately, the technique is not fully automated and it requires manual selection of points on the fundus photograph to divide the vessel into a series of single arcs. Using this measure as a part of a suite of tortuosity measures, 91% was achieved in the classification of segments as tortuous or non-tortuous and 95% in the classification of a whole vascular tree [49] on a private dataset with no particular disease,

$$RLV = \frac{L_C}{l} \approx \frac{8}{3} \sum_{i=1}^{n} (\frac{h_i}{l_i}) \tag{2.2}$$

.

Arc over chord ratio

The Arc Over Chord ratio (AOC) is the most simple, basic and most used distance based tortuosity evaluation feature. It is introduced by [48]. Given the blood vessel segment as a curve o arc (S), and the length of the curve as (L_C), 2.5 or 2.6, and the straight distance between the two end points of the blood vessel segment, known as the chord length as (L_X) equation 2.7. This feature simply examines how long the curve is, compared with the straight distance between its two end points. The feature has zero value for straight vessel segments and increasing positive value for segments as they become tortuous. It is also free of any manual manipulations or interactions. See Equation 2.3;

$$AOC = \frac{L_C 2(S)}{L_X(S)} - 1, \tag{2.3}$$

or

$$POC = \frac{L_C(S)}{L_X(S)} - 1 \tag{2.4}$$

Implementation	Dataset	Performance
William E Hart (1997) [48]	Private Dataset	Has a classification rate of 91% $*^1$ and 95%$*^2$ as one of 7 measures.
Conor Heneghan (2002) [51]	Private Dataset	Average increase in tortuosity with the severity of the disease(ROP).
David Wallace (2003)[91]	Private Dataset	80% sensitivity and 91% specificity.
Elizabeth Bullitt (2003)[13]	Private Dataset	It does not differentiate between tight coils and smooth curves.
Julien Jomier (2003)[52]	Private Dataset (ROP)	80% sensitivity and 92% specificity in the prediction of retinopathy compared to experts
Enrico Grisan (2003)[43]	Retinal Vessel Tortuosity DataSet(Public)	Arteries P =0.857, and veins P= 0.036 $*^3$
Enrico Grisan (2006) [28]	Retinal Vessel Tortuosity DataSet(Public)	Arteries P= 0.792, and veins P= -0.656$*^4$.
Enrico Grisan (2008) [44]	Retinal Vessel Tortuosity DataSet(Public)	Arteries P= 0.792, and veins P= -0.656. $*^4$
Crystal S. Y. Cheung etal (2011) [17]	Private Dataset	Significant reductions in all vascular measurements were observed compared to pre-treatment$*^6$
Rashmi Turior (2012)[88]	Private Dataset	Achieved a classification rate of 73% $*^5$
Arunava Chakravarty (2013)[15]	Retinal Vessel Tortuosity DataSet(Public)	It can distinguish between the relative size, shapes and orientations of vessel bends.
Amir Mohsenin (2013) [69]	Private Dataset	80% sensitivity and 92% specificity in predicting retinopathy .

Table 2.1: Some of the implementations, datasets and performances achieved using Arc Over Chord Lengths Ratio: (1) as one of a suite of measures they achieved 91% for classifying individual segments; (2) 95% for the classification of whole retinal vascular trees as tortuous or non-tortuous; (3) Spearman's Rank Correlation with the clinical order, using numerical differentiation;(4) Spearman's Rank Correlation with the clinical order; (5), using K-nearest neighbour classifier; (6) Comparative study between ROP patients pre and post treatment.

$$L_C = \sum_{i=1}^{n-1} \sqrt{(x_i - x_{i+1})^2 + (y_i - y_{i+1})^2}, \tag{2.5}$$

$$L_C 2 = \int_{t_0}^{t_1} \sqrt{x\prime(t)^2 + y\prime(t)^2}, \tag{2.6}$$

$$L_X = \sqrt{(x_n - x_1)^2 + (y_n - y_1)^2}. \tag{2.7}$$

This feature is found to work very well with short segments. However it assigns the same tortuosity value for a long nicely curved vessel as to a very twisted similar length segment. [See figure 4.1]. To sum up, Distance based features have failed in evaluating retinal vessels tortuosity and, as explained by Emmanuel Trucco [29], that the ratio between the curve and the chord is simply a measure of deviation from a straight line, which is more of a global measure, whereas tortuosity seems more directly related to local measures such as curvature. See Table 2.1 for some of the implementations, datasets used and performances achieved using distance approach features.

2.8.2 Curvature approach

Curvature, in mathematics, is the amount by which a surface deviates from a straight line. This deviation or twist can be measured in many ways: Geometrically, for each point along a curve by calculating the magnitude or rate of change of the angle theta θ, which is the angle made by the tangent line and the positive x-axis, with respect to the curve length or by the measurement of geometrical changes along a blood vessel such as angles between consecutive tangents' lines and changes in concavity, such as the Sum Of Angles Measure (SOAM) Equation 2.20 and the Inflection Count Metric (ICM) Equation 2.26.

Algebraically, by finding the physical rate of change along the blood vessel or the derivative of a function at each point, based on difference operators for data that are equally spaced, it is possible to calculate forward difference, middle difference, backwards difference. This provides a close estimation of curvature at each point along the curve or the blood vessel segment.

Through interpolation, in which curvature is estimated by splines interpolation, given a function $f_n = f(x_n)$, where $n = 0, ..., N$, a spline, which is a polynomial would be fitted between each two pairs of consecutive points, one of whose coefficients are determined. Cubic splines, normally, produce an interpolated function that is continuous through to the second derivative. Splines in general tend to be more stable than fitting a polynomial through the $N+1$ points, with less possibility of wild oscillations between consecutive points. The curvature evaluation features used to estimate tortuosity in the literature vary between these methods. The following sections set out some of these features as proposed in the literature.

The signed and unsigned curvature

These measures calculate the signed and unsigned curvature at each single point along a blood vessel segment. The sign of the signed curvature C indicates the direction in which the unit tangent vector rotates as a function of the parameter t along the blood vessel segment. If the unit tangent rotates counter-clockwise, then $C > 0$ (positive), if it rotates clockwise, then $C < 0$(negative). Given a blood vessel segment (S), as a plane curve, where S is represented by centre line points represented by $S = [(x_1, y_1), (x_2, y_2), ..., (x_{n-2}, y_{n-2})), (x_{n-1}, y_{n-1}), (x_n, y_n)]$,

and given parametrically in the Cartesian coordinates as $y(t) = (x(t), y(t))$, the curvature C at point t, $C(t)$, can be estimated as follows:

$$Signed\_C(t) = \frac{x\prime(t)y\prime\prime(t) - y\prime(t)x\prime\prime(t)}{[x\prime(t)^2 + y\prime(t)^2]^{\frac{3}{2}}}, \tag{2.8}$$

$$Unsigned\_C(t) = abs(Signed\_C). \tag{2.9}$$

Total signed and unsigned curvature of a blood vessel segment

Given the previous curve (S), and the x_n, y_n points representing the centre line points, the total signed and unsigned curvature of this segment is the integral curvature along the blood vessel segment with respect to it's length expressed as follows:

$$TSC(S) = \int_{t_0}^{t_n} Signed\_C(t)\ dt \tag{2.10}$$

$$TUSC(S) = \int_{t_0}^{t_n} Unsigned\_C(t)\ dt \tag{2.11}$$

Total squared signed curvature of a blood vessel segment

Given the same blood vessel segment S tortuosity as the total squared curvature is estimated as :

$$TSSC(S) = \int_{t_0}^{t_n} Signed\_C(t)^2\ dt \tag{2.12}$$

Total signed/unsigned curvature normalised by the blood vessel arc length

Tortuosity here is estimated by normalising the total signed or unsigned curvature by the blood vessels' arc length as:

$$Signed\_C\ normlised\ by\ L_C = \frac{TC_{(S)}}{L_{C_{(S)}}} \tag{2.13}$$

Total squared signed curvature normalised by the blood vessels' arc length

Tortuosity here is estimated by normalizing the total squared signed curvature by the blood vessel arc length as:

$$TSSC\ normalised\ by\ L_C = \frac{TSC_{(S)}}{L_{C_{(S)}}} \tag{2.14}$$

Total signed/ unsigned curvature normalised by the blood vessels' chord length

Tortuosity here is estimated by normalising the total signed or unsigned curvature by the blood vessel arc length as:

$$TSC\ normalised\ by\ L_x = \frac{TC_{(S)}}{L_{X_{(S)}}} \tag{2.15}$$

Total squared signed curvature normalised by the blood vessels' chord length

Tortuosity here is estimated by normalising the total signed curvature by the chord length between the two end points of the blood vessel segment

$$TSSC\ normalised\ by\ L_C = \frac{TSC_{(S)}}{L_{X_{(S)}}} \tag{2.16}$$

Tortuosity using numerical differentiation

This measure is introduced by Rashmi et al. [88]. Given a blood vessel segment (S), where S is represented by centre line points as
$S = [(x_1, y_1), (x_2, y_2), ..., (x_{n-1}, y_{n-1})), (x_{n-1}, y_{n-1}), (x_n, y_n)]$ this measure estimate curvature based on numerical differentiation between the points along the blood segment calculated as follow:
first differences between the x_n points

$$x_{(1)} = [x_2.....x_n], \text{ and } x_{(2)} = [x_1.....x_{n-1}]$$

$$y_{(1)} = [y_2.....y_n], \text{ and } y_{(2)} = [y_1.....y_{n-1}]$$

then the calculation of the slopes m

$$m_{(1)} = [m_2 - m_n] = \frac{x_{(1)}}{y_{(1)}}$$

$$m_2 = [m_1 - m_{n-1}] = \frac{x_{(2)}}{y_{(2)}}$$

$$Tortuosity = \sum_{i=1}^{n} D = [m_1 - m_2] \tag{2.17}$$

Tortuosity coefficient

This measure proposed by Geoffrey Dougherty [25]. It is based on the second differences of the vessel mid line. Tortuosity is estimated by summing the absolute values of these second differences, represented by δ_i which are the differences between the gradients between two successive segments, then it is divided by P which is the sampling interval. The measure is claimed to be easily converted and generalised to the use of three dimensional measurements. The measure is expressed mathematically as follows:

$$Tortuosity\_Coe = \{\sum_{j=1}^{N} |\delta_i|\}/P \tag{2.18}$$

Tortuosity based on chain code

The Slope Chain Code tortuosity measure is built on a chain code called Slope Chain Code (SCC). The measure is proposed by Ernesto Bribiesca [11]. It is simply based on converting a continuous curve to a discrete one by placing straight-line segments of constant length around the curve (the end points of the straight-line segments always touching the curve), and calculating the slope changes a_i between contiguous straight-line segments scaled to a continuous range from -1 to $+1$. The SCC of a curve is independent of translation, rotation, and optionally of scaling, which is considered an important advantage for computing tortuosity. For the mathematical representation of this measure see Equation 2.19.

$$T\_SCC = \sum_{i=1}^{n} |a_i| \tag{2.19}$$

There are similar measures in the literature such as the signed and the unsigned tortuosity evaluation measures, and Rashmi's method. Both methods evaluate tortuosity by taking the differences between consecutive slops along the blood vessel segment [88].

Sum of angles metric (SOAM)

This measure is proposed by Semdby, [83] and improved by Elizabeth Bullitt et al. [13, 27]. It measures tortuosity through evaluating the angles between consecutive trios of points along the space curve represented by a vessel skeleton, then normalised

by path length. Results are in a form of radians/cm. Vessels of high curvature have been noted to have elevated $SOAM$ values. The measure has been found to be an effective tool in detecting high-frequency, low-amplitude coils or sine waves. See Equation 2.20, where P_k is curvature at point k and CP_k is the total angle at P.

$$SOAM = \frac{\sum_{k=1}^{n-3} CP_k}{\sum_{k=1}^{n-1} |P_k - P_{(k-1)}|} \tag{2.20}$$

Mean curvature (MC)

This measure is proposed by Chanjira Sinthanayothin et al. [82]. The main principle of MC is fitting circles that fit curves or sub-curves perfectly along a curve. The radiuses of all circle representing curves will then be obtained for the tortuosity of the image to be calculated as the mean curvature (MC). Where 0 is image with low tortuosity and close to 1 is high tortuosity. [See Equation 2.21.]

$$MC = AVG\left[\sum_{i=1}^{n} \frac{1}{r_i}\right] \tag{2.21}$$

Mean direction angle change (MDAC)

This measure is proposed by Chandrinos et al. [16]. It measures tortuosity by averaging the change of angles calculated at reasonable discrete steps along the blood vessel. The measure works by considering two centerline pixels, $P - s$ and $P + s$ for each pixel indicated in the track list, P, pixels that lie ahead and after P, respectively. Consequently two vectors $(P - s, P)$ and $(P, P + s)$ are formed and normalised by dividing each with its norm. Lastly, the dot product is calculated and the inverse cosine of this product. MDAC is then estimated by averaging those angles over the number of points used along the vessel track. This measure does not work with short segments for instance segments with 10 or less points.

$$MDAC = \frac{1}{(t_{length-2*step})} \sum_{n=step}^{t_length-step} arccos(UV(P_{n-step}), P_n).UV(P_n, P_{n+step}) \tag{2.22}$$

Absolute direction angle change (ADAC)

This measure is proposed by K. G. Goh, et al. [37]. It is based on tracking the vessel centreline and accumulating any direction change along the path of the vessels. At

the end of this tracking, the number of changes in direction will indicate how tortuous the segment of the blood vessel is.

$$ADAC = \sum_{i=i+1}^{N-n} (\theta(i) \geq \frac{\pi}{6}) \tag{2.23}$$

Fast Fourier transform based methods

Recently Martin Rodriguez et al. [65] have introduced a different approach for evaluating tortuosity. The Fast Fourier transform (FFT) of the vessel's curvature is used as an evaluating method for tortuosity. The method computes the angle variations in three dimensions along the path of the vessel, and then each angle θc is divided by the Euclidean distance Dc between the two points.

$$\theta_C = Cos^{-1}(\frac{\overrightarrow{T_{C-1}}\overrightarrow{T_{C+1}}}{|\overrightarrow{T_{C-1}}||\overrightarrow{T_{C+1}}|}) \tag{2.24}$$

The overall total curvature in rad/mm is calculated as the sum of curvatures at each centroid as follows:

$$TSCC = \sum_{C} \frac{\theta_C}{D_C} \tag{2.25}$$

The amplitude spectra obtained clearly showed differences in tortuosity for the two segments. However, the TSCC obtained for two different tortuous segments were similar although they were completely different in shape, [See section 2.9 in this chapter for a review on FT].

To sum up, measures expressed by equations (2.8) to (2.16) are proposed by Hart, William et al. [48]. These measures combined together were able to achieve a classification rate of 91% for the classification of a group of independent retinal blood vessels' segments and to achieve 95% for the classification of the whole vascular tree of independent retinal images. The total squared curvature measure was recommended as best measure. See Table 2.2 for some of the curvature and combined methods implementations.

2.8.3 Combined methods

These are the methods that result from the combination of two or more of the previous methods. Some of these methods may also incorporate other blood vessels

Measure	Implementations
Total curvature (TC)	Enrico Grisan [43, 28, 44], Chanjira Sinthanayothin (2010) , Rashmi Turior (2012), Arunava Chakravarty (2013).
Total squared curvature (TSC)	Enrico Grisan(2003, 2006, 2008), Arunava Chakravarty (2013).
Total curvature normalised by arc length	Enrico Grisan(2003, 2006, 2008), Arunava Chakravarty (2013).
Total squared curvature normalised by the arc length	Enrico Grisan (2003, 2006, 2008).
Total curvature normalised by the chord length	Enrico Grisan (2003, 2006, 2008), Arunava Chakravarty (2013).
Total squared curvature normalised by the chord length	Enrico Grisan (2003, 2006, 2008)
Tortuosity Coefficients	Geoffery Dougherty (2000).
Sum of Angles Metric (SOAM)	Enrico Grisan (2006), Elizabeth Bullitt (2003, 2005), Sodi A,(2013), Arunava Chakravarty (2013).
Inflection count metric (ICM)	Elizabeth Bullitt (2003, 2005), Arunava Chakravarty (2013)
Mean direction angle change (MDAC)	Conor Heneghan (2002),Enrico Grisan (2003, 2006, 2008). , Arunava Chakravarty (2013)
Absolute Direction Angle Change (ADAC)	Enrico Grisan (2006) [28] Arunava et al. (2013) [15] .
Tortousity based on curvature and improved chain code (TCCC)	Onkaew et al. (2011) [20], Abbadi et al. (2013) [30] .
Mean Direction Angle Change (MDAC)	Enrico Grisan (2003, 2008) [43, 44], Conor Heneghan et al. (2002) [51], Arunava et al. (2013) [15] .

Table 2.2: Some of the curvature and the mixed tortousity measures' implementations

.

structural properties such as thickness, width, inflection points counts, etc.

Inflection count metric (ICM)

This measure is proposed by Smedby for 2D curves [83] and extended by Elizabeth Bullitt [13, 27] to be implemented on 3D images or space curves. This measure counts "inflection points" along each space or plane curve and multiplies this number (plus one) times the total curve length and then divides by the distance between end points. [See equation 2.26.]

$$ICM = (n_{i_{c+1}})\frac{L_X}{L_C} \tag{2.26}$$

Tortuosity based on curvature and improved chain code (TCCC)

This measure proposed by Danu Onkaew et al. [20]. It is an automatic tortuosity measure that classifies retinal images as tortuous and non-tortuous. It is based on the curvature calculated from an improved chain code algorithm and the number

of inflection points, where, n_{i_c} and L are the number of inflections and arc length respectively. This measure evaluates vessel tortuosity by summing curvature at every pixels of vessel and also considers the number of inflection points at each sub-vessel. This formula has a dimension of 1=L and thus may be interpreted as a tortuosity density, so it can be compared in vessels that have a different length. The advantage of this formula is that it does not depend on segmentation of the vessel tree.

$$TCCC = \frac{(n_{i_{c+1}})}{n_{i_c}} \frac{1}{L} \sum_{n=1}^{n} K(P_i, K) \tag{2.27}$$

Sub-curves and distance based measures (Grisan measure)

Enrico Grison proposed a new tortuosity measure and improved it over the years [43, 28, 44]. The algorithm based on the partitioning of each vessel into segments of constant-sign curvature and on the combination between the number of such segments and their curvature values. However, this measure requires manual vessel extraction and inflection point placement. The following are the three equations in which the measure has been improved.

$$T1 = \frac{n-1}{L_C} \sum_{n=1}^{n} \left[\frac{L_{C_S i}}{L_{X_S i}} \right], \tag{2.28}$$

$$T2 = \frac{n-1}{L_C} \frac{1}{L_C} \sum_{n=1}^{n} \left[\frac{L_{C_S i}}{L_{X_S i}} \right], \tag{2.29}$$

$$T3 = \frac{n-1}{n} \frac{1}{L_C} \sum_{n=1}^{n} \left[\frac{L_{C_S i}}{L_{X_S i}} \right], \tag{2.30}$$

where n is the number of curves in a segment.

Tortuosity index (TI)

This measure is proposed by [62]. It evaluates tortuosity by identifying the number of changes in curvature sign. Where n is the number of segments in a single vessel, m represents the angles of curvature θ_i, length of the respective area is denoted by L_C and the length of the chord is represented by L_X.

$$TI = \left[\frac{(n+1) * [\sum_i^m \theta_i] * [\sum_i^m \frac{L_{C_i}}{L_{X_i}}]]}{L_c * m * m} \right] \tag{2.31}$$

Tortuosity based on vessel wall thickness

This is proposed by Hind Azegrouz et al. [5] and extended by Emanuele Trucco and Hind Azegrouz [29]. It combines curvature and thickness. It is defined as a weighted Minkowski norm of the curvatures along the vessel boundaries, and is an increasing function of vessel diameter (Thickness), see Equation 2.32 where C_b1 and Cb_2 are, respectively, the local curvatures of the two vessel boundary points ($b1$ and $b2$), and p is a strictly positive integer.

$$TW = \left(\sum_{n=3}^{N} \frac{|K_{B_{1(n)}}| + |K_{B_{2(n)}}|}{2} \right)^{\frac{1}{P}} \tag{2.32}$$

Automatic tortuosity image classifier

This algorithm can automatically classify images as tortuous or non-tortuous, where n_{i_c} and L are the number of inflection points and arc length respectively. This measure evaluates vessel tortuosity by summing curvature at every pixel of vessel and also considers the number of inflection point at each sub-vessel. This formula has a dimension of $1 = L$ and thus may be interpreted as a tortuosity density, so it can be compared in vessels that have a different length. The advantage of this formula is that it does not depend on segmentation of the vessel tree [20, 88].

2.9 Review of Fourier transform analysis

It is clear that FT is not a novel technique when it comes to tortuosity evaluation. In this study the FT of the vessel signed curvature, displacement distances, (which are the distances from each point along the blood vessel segment and the vessel chord), and the first and second derivatives of the vessel segment were all investigated to estimate tortuosity in an attempt to accurately evaluate tortuosity using 2D images.

Fourier Transform is the process in which a signal or a function of time or space is processed expressed in the form of frequencies of the sine and cosine waves that make up the signal or the function. The concept of Fourier transform was introduced by Baron Fourier after 20 years after introducing the Fourier series, which is effective in the representation of periodic, continuous and discrete signals or functions, as an extension of, and in order to solve, what the Fourier series

failed to represent, which is non periodic signals. In this study the blood vessel segments are represented as functions of space, which are aperiodic and discrete, therefore Discrete Fourier Transform of aperiodic signals Discrete Fourier Transform of aperiodic signals (DTFT) can be efficiently computed using the Fast Fourier Transform.

The input or the signal to be analysed using FT, is normally either a function of space or time. The signal in time domain, can simply be described as if a signal has been viewed while its amplitudes are going up and down in an erratic manner with the time progressing to the right. With FT analysis, any arbitrary wave or signal can be broke down into its harmonic components and then their contents(amplitudes) can easily be identified.

The output of FT analysis is normally in the form of Frequency Domain or Signal Spectrum, which is when the output of the input signal is viewed from the side, along the frequency axis. In this case the constituent frequencies along the frequency axis can be seen, as well as the peak amplitudes of these discrete frequencies. Spectrum has many names in the literature such as: gain, frequency response, rejection, magnitude, power spectrum, power spectral density etc; all these terminologies simply refer to this distribution of signal content over a certain frequency band. The width of the spectrum is known as the bandwidth of the signal and the resolution of the frequencies ($f_{n+1} - f_n$) is called the bin size. The bin size of a spectrum is constant and it is an important parameter in determining how well the signal has been represented. The fundamental frequency is the smallest frequency with the largest amplitude [12, 42].

To analyse the spectrum of a given signal using the Fourier transform, the continuous form of Fourier analysis is normally used with a continuous signal, which is given by Equation 2.33 and the inverse by Equation 2.34, where $F(w)$ represents the spectrum and w is the frequency; $f(x)$ is the signal in time domain where x is the time and i is the $sqrt(-1)$(complex number theory). Finite discrete signals are those signals that are finite in time, and have a discrete set of points. They are also known as sampled signals. As previously noted, analysing a discrete signal using the continuous form of the Fourier analysis, can be achieved by increasing the period of the discrete signal which allows the creation of an aperiodic version of the signal.

To represent a finite signal in time or space mathematically, the infinite borders of the integrals are replaced by finite ones, and the integral symbol will be replaced by a sum as explained in Equations 2.35 and 2.36 for Discrete Fourier Transform (DFT) and its inverse.

$$F(w) = \int_{-\infty}^{\infty} f(x) e^{(-2\pi wix)} dx \tag{2.33}$$

$$F(x) = \int_{-\infty}^{\infty} f(w) e^{(2\pi wix)} dw \tag{2.34}$$

$$Fn = \sum_{k=0}^{N-1} f(k) e^{(-2\pi ink)/N} \tag{2.35}$$

$$Fk = \frac{1}{N} \sum_{n=0}^{N-1} f(2) e^{(2\pi ikn)/N} \tag{2.36}$$

2.10 Data analysis methods

The main aim of most studies in this problem domain, that of grading retinal blood vessels tortuosity, is to find an accurate measure that can precisely evaluate the degree of retinal blood vessels tortuosity. However, objectives to satisfy this aim are varied. Normally, ophthalmologists evaluate the degree of a retinal blood vessel segment tortuosity by considering changes in and around that vessel segment, and then (based on a pre-set number of indicators or signs), the vessel segment is classified as tortuous(abnormal) or non-tortuous(normal). These signs are largely based on the knowledge and expertise of the clinician or the ophthalmologist carrying out the screening or the grading test. On some occasions, more precise, qualitative scales such as mild, moderate, severe and extreme are used.

Analysis techniques vary according to the objectives of the studies and the nature of available datasets. The most commonly used method to test proposed tortuosity measures is the classification of blood vessel segments, or a whole retinal vascular tree, into “tortuous” or “non-tortuous”. For instance [48] used a logit model for the binary classification of individual segments and the classification of whole retinal vascular trees, and Rashmi et al. [88]used three supervised learning techniques (Naive Bayesian classifier, K-Nearest (KNN) classifier and K-mean clustering algorithm) for tortuosity classification. Random Forests (RF) and Artificial

Neural Network (ANN) are used in this study to evaluate the proposed framework. [background Details of these methods and their implementations can be found in sections 2.10 and 2.10]. Other studies, used more than the basic two class classification. For example Trucco, Emanuele et al. used a logistic regression model to assign vessels to one of three tortuosity classes [29].

On the other hand, there are other studies that went on to classify a number of tortuous vessels by reference to the manner of increased tortuosity, for example utilising datasets such as the RVTDS, which consists of retinal blood vessel segments that are ranked in increased tortuosity from 1 (representing non-tortuous) to 30 (representing severely tortuous) by an expert ophthalmologist.

Furthermore, there are more innovative analysis methods used to test proposed tortuosity measures, such as a study done by Hathout and Do [50] which used a mathematical model of non-tortuous or normal vessels by extracting the parameters of the shape of the non-tortuous vessels. Using those parameters the model was then tested by using normal vessels to test the accuracy of the developed model. A similar model was introduced in the 1960s for analysing the meandering of rivers as cited in [50].

Machine learning

Arthur Samuel defined Machine Learning (ML) as the field of study that "gives computers the ability to learn without being explicitly programmed" [81]. Tom Mitchell provided a more logically detailed definition as follows: " A computer program is said to learn from experience E with respect to some task T and some performance measure P, if its performance on T, as measured by P, improves with experience E" [68].

The simplest basic approach in machine learning is to test multiple algorithms until the best algorithm is found based on performance. However, this approach has been found to be very time-consuming. Machine learning can be classified into two classes of learning approaches, supervised/ unsupervised and reinforcement learning.

In reinforcement learning the parameters of an artificial neural network are normally fixed and where data is usually not given, but generated by interactions

with the environment. Reinforcement learning is suitable for problems which include a long-term versus short-term reward trade-off, such as robot control, telecommunications, and games such as chess and other sequential decision making tasks [55].

In unsupervised learning, data are grouped based on characteristics or similarity, and interpreted only based on the input data. The algorithms used on this occasion are called Clustering algorithms such as k-means, Gaussian mixture and neural networks, etc. As can clearly be noted there are overlapping characteristics between regression and clustering analysis in techniques such as decision trees, neural network, linear regression and ensemble methods.

In supervised learning a model will be developed based on the input data, which is the processed raw data that needs to be analysed; and the output or the response variable. This also known as the desired output. If the desired output is discrete in nature, classification techniques can be used such as support vector machines and Naive Bayes. However, if it is continuous, then regression methods should be utilised such as linear regression, artificial neural networks and decision trees.

With all that being said, machine learning is not entirely free from challenges and obstacles. These problems range from the amount of data; predictors, and their degree of complexity, to the significant technical expertise needed in order that the fundamentals of the methods are understood and correctly followed.

Neural networks ANN represents a type of computing that is loosely based on the way that the brain, or the central nervous systems of mammalians in general, perform complex computations, such as an approximation of functions that depend on a large number of data or variables [46]. Artificial neural networks are typically organised in layers, which normally consist of one or more interconnected nodes, which themselves contain activation or cost functions. The inputs are introduced to the neural network through the input layer, which is connected to one or more hidden layers that carry out the processing or the computations. The result of these computations is subsequently passed through the output layer. Artificial neural networks, in general, have some form of learning rule, which modifies the connection weights according to the inputs that are presented to the neuron through the input layer. There are different kinds of learning methods which can modify the connection

weights in order to obtain the desired output.

A logistic neuron, which is a non-linear neuron, was utilised to learn the degree of the retinal blood vessels tortuosity from the various types of features that were encompassed in the proposed tortuosity evaluation framework in order to provide gradings that are close to or match that of the clinical ones provided with the data. First of all, the neuron computes the logit z, which is the bias, b, plus the sum of the total inputs (features) , x_i, multiplied by the weights, w_i. [See Figure 2.37]. The neuron then provides an output y which is a smooth non- linear function of the logit. The function is approximately equal to zero when z, the logit, is big and negative, and it is approximately equal to one if z is big and positive. In between the function changes non-linearly as shown in Figure 2.7. The function is shown in equation 2.38. The smooth continuous change gives the logistic function

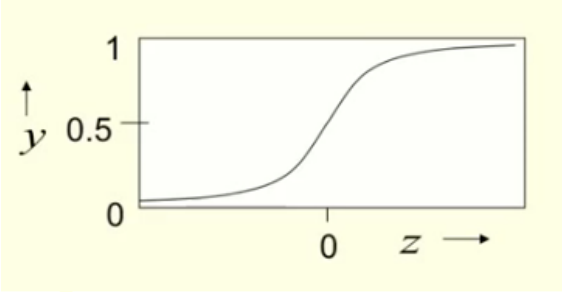

Figure 2.7: This graph shows a logistic function

nice derivatives which make the learning of the neuron easier.

In order to obtain the derivatives of a logistic function with respect to the weight (which is what is needed for the learning process), the derivative of the logit z itself needs to be computed, as the bias plus the sum of the inputs (features) multiplied by the weights. When this is differentiated with respect to w_i, which represents the weights, the result is x_i. Following the same manner, the derivative of the logit with respect to x_i is w_i, as shown in Equations 2.39 and 2.40. The derivative of the output y with respect to the logit can also easily be calculated if y is expressed in terms of the output which is as seen in equation 2.38; to equal $y(1-y)$. [See the proof in Equation 2.41]. The chain rule is then used to get the derivatives needed for the weight learning of the logistic unit. To learn the weight the derivative of the output with respect to each weight is needed see equation 2.42,

which is the gradient descent learning rule, where E represents the error.

$$Z = b + \sum_{i=1}^{N} x_i w_i \tag{2.37}$$

$$y = \frac{1}{1 + e^{-Z}} \tag{2.38}$$

$$\frac{\partial z}{\partial w_i} = x_i \tag{2.39}$$

$$\frac{\partial z}{\partial x_i} = w_i \tag{2.40}$$

$$\begin{aligned} &\frac{dy}{dz} = y(1-y), \\ &\qquad y = \frac{1}{1+e^{-z}} = (1+e^{-z})^{-1}, \\ &\frac{dy}{dz} = \frac{-1(-e^{-z})}{(1+e^{-z})^2} = \frac{1}{1+e^{-z}}\frac{e^{-z}}{1+e^{-z}} = y(1-y) \\ &\qquad\qquad because: \\ &\frac{e^{-z}}{1+e^{-z}} = \frac{(1+e^{-z})-1}{1+e^{-z}} = \frac{1+e^{-z}}{1+e^{-z}}\frac{-1}{1+e^{-z}} = 1-y \end{aligned} \tag{2.41}$$

$$\begin{aligned} &\frac{\partial y}{\partial w_i} = \frac{\partial z}{\partial w_i}\frac{\partial y}{\partial z}, \\ &\frac{\partial E}{\partial w_i} = \sum_n \frac{\partial y^n}{\partial w_i}\frac{\partial E}{\partial y^n} = -\sum_n (x_i)^n y^n (1-y^n)(t^n - y^n) \end{aligned} \tag{2.42}$$

Random forests Random Forests (RF) is one of the most powerful, fully automated machine learning techniques [10]. It is an ensemble learning method for classification and regression, in which a number of decision trees are generated at one time and their final outputs are combined for the final output or prediction. The concept and technique was originally developed by UC Berkeley visionary, Leo Breiman in a paper that was published in 1999 [9], and he continued to perfect it with his student and collaborator Adele Cutler to develop the final form of Random Forests [85].

RF can be used to predict different types of variable, such as continuous, as well as an estimation of the probability of the occurrence of a particular outcomes. Ensembles are normally used as a divide and conquer technique to improve the performance of classifiers. The main idea behind using Ensembles is that a group of individual weak variables or features can be grouped to form a strong variable or learner.

Random Forests analysis usually starts with an input of a group of variables, to which the concept of decision trees is applied. Flowing from top to bottom these features start to bracket together in smaller sets of group of features as they traverse down the tree. The results of RF analysis is either an average or weighted average of the terminal nodes or a voting majority in the case of categorical variables. In RF analysis of a large number of predictors, the eligible predictor group will be different from one node to another. With the increment of the rate of intra-correlation, The RF error will also increase, therefore uncorrelated trees in RF models are essential. The decrement of the selected group of features, normally indicates the decrement of both intra-tree correlation and the strength of individual trees, so an optimal number of features is advised. Among the biggest advantages of RF are that it characterises by speed, and its ability to cope with unbalanced and missing data. However when used for regression RF are not able to predict beyond the range that is set in the training data, and might over-fit datasets that are particularly noisy [85]. Several methods of testing or validating classifiers can be used such as threshold, cross-validation, mean precision and so on.

2.11 Conclusion

With the strong correlation found between the tortuosity of retinal blood vessels and a number of vascular diseases together with the advancement in image processing technologies, many attempts have been made to find an accurate evaluation tool to measure the degree of retinal blood vessels tortuosity. In these attempts various methods have been proposed and evaluated on datasets of different pathologies, sizes and shapes. The tortuosity evaluation methods have been analysed and critically evaluated in terms of accuracy and suitability. They can be placed into three main

groups: a distance approach; a curvature approach and combined methods. The next chapter details the process of building our proposed tortuosity evaluation framework and why these group of features are incorporated along with our new proposed features into one tortuosity evaluation framework.

Chapter 3

Building tortuosity datasets

This chapter details the building process of three new tortuosity datasets. It starts by inspecting currently available tortuosity datasets, discusses their advantages and drawbacks and identifies the benefits of building new ones. The chapter proceeds to outline the actual process of building the proposed datasets, including the image segmentation, segments labelling (as veins and arteries), through to stage of vessels grading which was carried out by volunteer graders. This chapter also includes a description of the grading systems used and the actual manual grading process. The chapter concludes by discussing the manual grading results in terms of reliability, and analyses the observers' agreement on both grading types and the final proposed gold standard datasets.

3.1 Introduction

The strong correlation found to exist between the retinal blood vessels tortuosity and the presence and progression of diseases, has encouraged a great number of researchers to investigate and evaluate this phenomenon. Most of the existing tortuosity evaluation measures were tested on private datasets with segments that were preprocessed using various methods in terms of vessels segmentations, labelling, etc. Whether these datasets were private or public, they differ in their sizes, pathologies, segment types and the tortuosity validation methods. Validation methods such as classification of segments as tortuous or non-tortuous, or ranking in case of the use of datasets with manual clinical order, etc.

As previously indicated in this document, researchers have started to focus on investigating the underlying causes of tortuosity and the suitable methods of quantifying them. In particular, ophthalmologists suggested that segments used in the evaluation of the tortuosity should have specific properties, such as the type of vessels in terms of size, segment cut and location. Our new tortuosity dataset segments were taken from seventeen retinal images of patients with diabetic and hypertensive retinopathy. Two pathology sub-datasets were also generated from these segments of diabetic and hypertension.

3.2 Tortuosity datasets

There is a great number of tortuosity evaluation datasets, however the majority are private. [See table 3.1 for some of the tortuosity datasets used in the literature]. The BioImLab Retinal vessel tortuosity dataset appears to be the only publicly available one, which is proposed by [44], and discussed in great detail in section 3.3. Both public and private datasets differ in size, types of segments, segment length, segmentation techniques and pathologies. They also vary in their evaluation methods, such as using a manual clinical order of the datasets segments in increased or decreased order, or using a simple classification in two or more classes similar to the subjective clinical evaluation. Thus comparative tortuosity studies and providing feasible accurate results prove to be quite difficult. In addition, researches in this field focus on perfecting tortuosity evaluation measures, and ignore datasets. I believe that datasets need to be improved and revised as a number of ophthalmologists noted that the segments used in tortuosity estimation, should be one of the following: A) a segment that extends from the optic disc to the peripheral without bifurcation; B) a segment that extends from the optic disc to the first major bifurcation; C) a segment that lies between two major bifurcations. Therefore new robust datasets for evaluating retinal blood vessels tortuosity are crucial, especially when it comes to comparative tortuosity studies between different diseases. In summary most of the tortuosity datasets reviewed in the literature, are not available publicly, are relatively small in size and there are no specialized datasets for specific diseases such as diabetic and hypertensive retinopathy and with the same processing methods such

as vessel segmentation, labelling and marking.

In this study specialised tortuosity datasets from images of diabetic and hypertensive patients were built to aid in the process of quantifying retinal blood vessels tortuosity. The datasets consist of three subsets: 1) a general tortuosity dataset with vein and artery segments and two manual grading (segments are from diabetic and hypertensive patients); 2) hypertensive retinopathy dataset with vein and artery segment sets; 3) diabetic retinopathy dataset with vein and artery segment sets. Details of these datasets will be found in the next sections.

Author	**Pathology /feature measured**	**Availability**	**Nature of the dataset**
Kagan et al. (1976)	ROP/Tortuosity (segments and whole tree)	Private	Not available
William E. Hart (1997,1999)	Not particular(segments and whole tree)	Private	20 retinal images
Geoffrey Dougherty (2000)	Abdominal Arterial/ Tortuosity	Private	Aortograms of 82 patients
Conor Henghen (2002)	ROP/Width and tortuosity	Private	23 subjects
Elizabeth Bullitt (2003),	Brain tumours/vessels Tortuosity	Private	11 normal and 6 patients
Elizabeth Bullitt (2005)	Brain tumours/vessels Tortuosity	Private	34 Healthy subjects and 30 patients
Enrico Grisan (2003,2006,2008)	Not particular/Tortuosity	Public	Retinal Vessel Tortuosity Data
Christopher G. Owen (2008)	Diabetes/Tortuosity	Private	53 patients and 60 controls
Sodi A (2013)	Fabry disease/Tortuosity + width	Private	35 patients
Susannah Q. Longmuir, et al(2010)	FSHD /Tortuosity	Private	7 patients
Amir Mohsenin (2013)	ROP/Tortuosity	Private	9 patients and 7 healthy

Table 3.1: This table shows some of the tortuosity datasets used in the literature

3.3 The retinal vessel tortuosity dataset

The RVTDS is a dataset of retinal vessels segments from normal and hypertensive patients and their manually estimated tortuosity degrees [33]. It consists of 30 images of retinal arteries and 30 retinal veins segments with similar length and calibre, and 30 images of the same arteries as well as 30 images of the same veins, all preprocessed by a normalization algorithm. The dataset also contains Matlab data structures that consist of records. Each record includes the name of the image, the X and Y samples of the manually drawn vessel centreline in addition to the ordinal position of the vessel in the manual order, which is the increasing tortuosity order list, as provided by a retinal specialist (Dr. S. Piermaracocchi, Department of Ophthalmology, University of Padova).

The images were acquired with a 50° fundus camera (TRC 50, Topcon, Japan) and digitized with a scanner at 1100 x 1300 pixels. To sum up, the dominant

properties of the RVTDS as the ground truth (gold standard) of a tortuosity dataset are:

1) Artery and vein segments in this dataset have similar length and calibre.

2) The centreline points of these segments are preprocessed by a normalization algorithm.

3) Vessels are manually ordered by a single retinal specialist in increased degree of tortuosity.

4) The dataset also falls on the small size side, since it consists of just 60 vein and artery segments.

5) These segments are taken from images of hypertensive and normal patients.

3.4 Proposed dataset

One of the main objectives of this study is to build a relativity larger tortuosity dataset to help grade retinal blood vessels tortuosity, and specialized datasets for hypertensive and diabetic retinal vessels to identify differences or similarities in tortuosities the way in which retinal blood vessels change to cope with the effects of those diseases on the retinal vascular system.

Our general dataset consists of 109 retinal blood vessel segments, extracted from seventeen retinal images. The number of segments extracted per image, were ranged between 1 to 20 segments. The seventeen retinal images used in this dataset were of patients who underwent retinal screening due to diabetic and hypertension retinopathy in UK, Denmark and Greece. Six of the images are of diabetic patients and were taken as part of the screening system in the United Kingdom in Sunderland Eye Infirmary, as provided by doctor Majed Habeeb. The other eight images are of diabetic patients, were from Denmark provided by doctor Toke Bek, and the last three images are of hypertensive patients and provided by doctor Areti Triantafyllou, research fellow of Internal Medicine, Papageorgiou Hospital, Aristotle University of Thessaloniki, Greece. The general dataset was then divided, based on pathology, into two subsets, diabetic and hypertension each of which has vein and artery groups.

3.4.1 Image dataset

Retinal vessels segmentation

The retinal blood vessels of the retinal images were segmented using the segmentation method described in [3], which uses two pairs of contours to capture each vessel edge, while maintaining width consistency. The segmentation stage produced some fragmented segments due to overlapped vessels, bifurcations and the poor quality of some images. A semi-automated program was built to connect these fragmented segments which involves manual selection of the fragmented segments ends to be connected. [Refer to figure 3.1 for an example of these fragmented and then connected segments].

Since there were no clear, standard rules to identify the types, locations or parts of retinal blood vessel segments that are appropriate for the process of tortuosity evaluation, the segments used were chosen based on a number of those rules which expert ophthalmologists normally use during naked eye inspection in clinical settings, as previously indicated. Such rules for example that the vessels are of a certain size and extend from the optic disc to the peripheral without bifurcation, or a segment that lies between two major bifurcations or first major bifurcation, are the best suited segments for tortuosity evaluation. Therefore the selection process of the vessels were formally based on these rules. This stage involved separation or dividing of what appear to be unified longer segments into smaller segments due to bifurcations. 131 segments were produced at this stage. The next section provides the details of labelling these segments as veins and arteries.

Retinal vessels segments labelling

Vein segments in general can be distinguished from arteries in the retina through a well known set of medical properties. For instance arteries are characterised by thick muscular walls, to withstand the high pressure of blood pumped out of the heart, whereas veins on the other hand have thin walls and relatively darker colour when compared to arteries, [see section 2.5.1]. That been said, the labelling of retinal segments as veins and arteries through eye inspection is not an easy task. The labelling of segments has been carried out by an expert ophthalmologist and

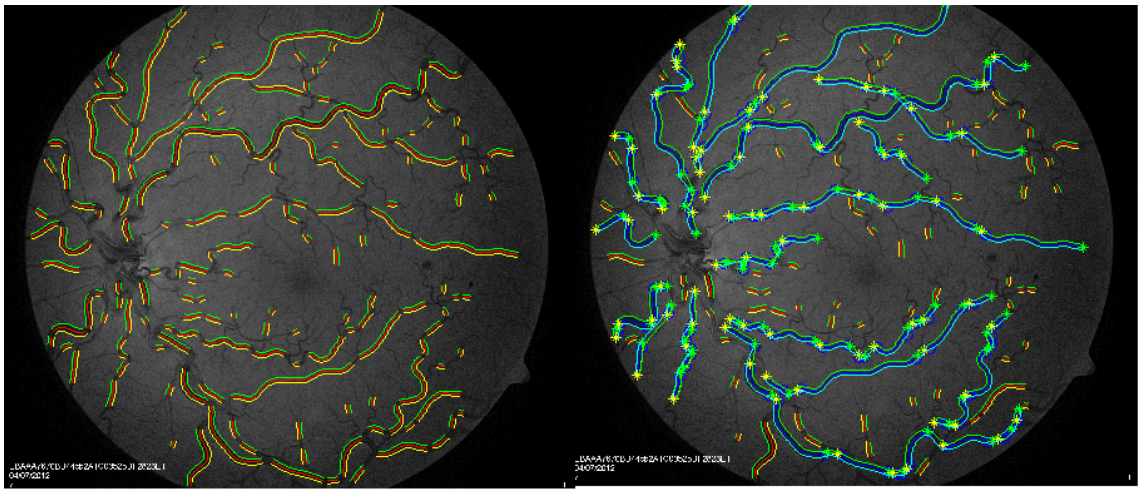

Figure 3.1: This graph shows the vessel segmentation stage and the fragmented vessels connection stage

two expert researchers in retinal image processing. Another researcher was also consulted in cases of conflict. At the end of this stage, 74 segments were labelled as vein and 57 segments were labelled as artery.

3.4.2 Graders

Three doctors volunteered to assist in the process of grading the retinal blood segments. The first grader was doctor Majed Habeeb, who is a consultant ophthalmologist, from Sunderland Eye Infirmary in the United Kingdom. The second grader was Doctor Michelle Teoailing, a senior house officer in Lincoln County Hospital. The third and final grader was Doctor Bakhit Digry, an emergency consultant doctor in Lincoln County Hospital. Those three graders were randomly chosen and they graded the segmented retinal segment independently. The grading was performed manually, then the final grades were fed to the system.

3.4.3 Grading systems

Two grading systems were used in the new tortuosity dataset: The order, i.e. ordering the retinal vessel segments in increased or decreased tortuosity; and classification i.e. the classification of retinal vessel segments into groups based on the degree of tortuosity. The next sections provide more details of these grading systems.

Order

Using the order grading system, the segments in the general tortuosity dataset were ordered in increased positive tortuosity, from least to most tortuous, for each group (artery, vein) independently. For the arteries, the grading was from 1 to 57 and for the veins the grading was from 1 to 74. The grading was performed by the graders mentioned in Section 3.4.2. The grading process was carried out separately and independently by each grader. This grading was based on the grading of the free public tortuosity dataset RVTD, which is found in section 3.3; in which the segments were ordered in increased tortuosity from 1 to 30, which is the number of instances for each of the artery and vein groups, 1 representing non tortuous, and 30 the most tortuous. The blood segments in the RVTDS were all presented in a position showing them traversing in the horizontal plane. However, the number of the instances in the proposed dataset is large compared with the number of segments in the RVTD, also the order in the RVTD was conducted by a single ophthalmologist. The manual grading reliability and the agreement between the observers (graders), of this grading, were analysed, in order to validate the order based graded segments as a new gold standard tortuosity dataset. [See section 3.5 for the analysis results.]

Group classification

The previous order grading system works well with small datasets, however it becomes complicated, especially with large datasets that have larger instances. Consequently, we introduced the group classification grading system. This grading is an extended version of the subjective tortuosity scale, normally used by ophthalmologists, to evaluate retinal vessels tortuosity as mild, moderate and severe in a clinical setting. The group classification includes seven classes: non tortuous; tortuous to mild; mild; mild to moderate; moderate; moderate to severe; and severe. They are represented by numbers from 1 to 7. Similar to the previous grading, the volunteer graders grouped the datasets arteries and vein segments into seven classes based on the degree of tortuosity with class one being non tortuous and class seven representing severe tortuous. The final group classifications were analysed to validate the graders agreement. [See section 3.5 for the analysis results.]

3.5 Manual grading analysis

At the grading stage, an initial grading was carried out by the researcher and one of the three volunteer experts, to rule out any errors or mistakes in the segmented, marked and labelled blood vessels. This involved checking the clarity of the images of the segments, and that they were correctly labelled and marked before the final grading. The grading of the retinal blood vessels tortuosity, within the new tortuosity dataset, was then conducted in two stages. The first stage was the task of grading the segments using the order grading system. The graders were asked to grade a number of blood vessels' segments, manually, in increased tortuosity from 1 being non tortuous to the last segment which represents the most tortuous. The second stage was to group the segments into classes using the group classification grading system. In this task the graders were asked to group all segments into seven groups: group one for non-tortuous; two for tortuous to mild tortuous; three for mild tortuous; four for mild to moderate tortuous; five for moderate tortuous; six for moderate to severe tortuous and seven for severe tortuous.

The average of the graded segments, using the order grading, of the veins were varied between 34 and 37 tortuosity among the three graders, and between 22.5 and 29 tortuosity for the arteries. [See the following tables 3.2 and 3.3 for the veins and arteries gradings descriptive statistics respectively.] Whereas the average

Descriptive Statistics

	N	Mean	Std. Deviation	Variance
Grades by Dr. M, H	68	34.50	19.774	391.000
Grades by Dr. B, D	73	37.03	21.264	452.166
Grades by Dr. M, T	69	35.39	20.527	421.359
Valid N (listwise)	63			

Figure 3.2: This graph shows the descriptive statistics of the three grades order of the veins segments

of the classification of the veins into tortuosity degree groups were varied between

Descriptive Statistics

	N	Mean	Std. Deviation	Variance
Grade by Dr. M, H	44	22.50	12.845	165.000
Grades by Dr. B, D	57	29.00	16.598	275.500
Grade by Dr. M, T	55	28.00	16.021	256.667
Valid N (listwise)	43			

Figure 3.3: This graph shows the descriptive statistics of the three grades order of the arteries segments

3.67 and 4.36 tortuosity group, among the three graders and between 2.18 and 4.35 tortuosity group for the arteries. [See the following figures 3.4 and 3.5 for the veins and arteries group classification descriptive statistics respectively.]

Descriptive Statistics

	N	Minimum	Maximum	Mean	Std. Deviation	Variance
Class M, T	69	1	7	3.67	1.892	3.578
Class M, H	68	1	7	4.01	2.440	5.955
Class B, D	73	1	7	4.36	1.813	3.288
Valid N (listwise)	63					

Figure 3.4: This graph shows the descriptive statistics of the graders tortuosity group classification of the veins segments

3.5.1 Inter observers agreement

Inter observer error represents the differences between the interpretations of a number of observations of the same phenomena carried out by different observers at different times using the same measure. Intraclass Correlation Coefficient is a measurement normally used to measure the reliability of such ratings or measurements. When it comes to a model in which each subject is graded by the same grader, a choice can be made between two types of statistical analysis: Consistency, which is

Descriptive Statistics

	N	Minimum	Maximum	Mean	Std. Deviation	Variance
Class M, T	55	1	7	3.16	1.844	3.399
class M, H	44	1	7	2.18	1.795	3.222
Class B, D	57	1	7	4.35	1.876	3.518
Valid N (listwise)	43					

Figure 3.5: This graph shows the descriptive statistics of the graders tortuosity group classification of the arteries segments

when systematic differences between graders are irrelevant; and absolute agreement in which systematic differences are relevant. However in this study each subject (vessel segment) was graded by a different grader, therefore in this case the measure will be a measure of absolute agreement [80].

ICC is normally calculated by taking the ratio between the sums of various variance component estimates, and it is defined to be within the interval [0, 1]. The labels "single" or "average" in the ICC output refer to the grade whose reliability is to be measured. The "average measures" give the reliability of a grade that is made up as the average of the different observed grades. Conversely, the "single measure" is the appropriate statistic to quantify inter-observer reliability. It gives the reliability of a grade that is scored by just one of several observes. The interpretation of alpha values according to the Streiner and Norman [84] is: if the values > 0.9, then it implies some possible redundancy, values between 0.7 and 0.9 are usually acceptable and values < 0.7 indicate that the items do not correlate very well with one another.

On the other hand, for non-numerical items for example qualitative or categorical, the inter observer agreement analysis is normally measured by Cohen's kappa coefficient analysis. Landis and Koch [57] for Kappa coefficients suggest that: values of 0.01 indicates "poor" agreement, values from 0.01 to 0.20 indicate "slight" agreement, values from 0.21 to 0.40 indicate "fair" agreement, values from 0.41 to .60 indicate "moderate" agreement, values from 0.61 to 0.80 indicate "substantial" agreement and values from 0.81 to 1.00 indicate "almost perfect" agreement. These categories are probably also reasonable for intraclass correlation coefficients. Since

Cohen's kappa was built to be used for two observers, an extended version introduced by Light [61] was used to estimate the observers' agreement by calculating the average kappa for all observer pairs.

The next sections provide a detailed ICC and Kappa analysis of both grading methods by the three graders and the new proposed gold standard tortuosity dataset.

ICC analysis of the order grading

The interclass correlation coefficient conducted between the order gradings of the veins segments (from least to most tortuous) by grader one, two and three showed a high degree of reliability between those graders measurements. The single measures of ICC for the veins was .760 with 95% confidence interval from .663 to .837 ($F(62, 124) = 10.578$, $p < .001$). [See the details in figure 3.6]. The ICC of the arteries showed a high degree of reliability between the three graders measurements, the single measures of ICC was .736 with 95% confidence interval from .607 to .836 ($F(42, 84) = 9.737$, $p < .001$). [See the details in figure 3.7.]

Intraclass Correlation Coefficient

	Intraclass Correlation[b]	95% Confidence Interval		F Test with True Value 0			
		Lower Bound	Upper Bound	Value	df1	df2	Sig
Single Measures	.760[a]	.663	.837	10.578	62	124	.0000000000001
Average Measures	.905	.855	.939	10.578	62	124	.0000000000001

Two-way random effects model where both people effects and measures effects are random.

a. The estimator is the same, whether the interaction effect is present or not.

b. Type A intraclass correlation coefficients using an absolute agreement definition.

Figure 3.6: This table shows the ICC of the graders order of the veins segments

Kappa analysis of the group classification grading

An inter observer reliability analysis using the Kappa statistic was performed between the graders pairs, to determine consistency among the three graders. The inter observer reliability of the pairs of the graders, (B, D and M, H), (B, D and M, T) and (M, H and M, T), on the veins, were found to be Kappa = 0.237 (p =0.000), Kappa = 0.079 (p =.08) and Kappa = 0.125 (p = 0.004) respectively, with average

Intraclass Correlation Coefficient

	Intraclass Correlation[b]	95% Confidence Interval		F Test with True Value 0			
		Lower Bound	Upper Bound	Value	df1	df2	Sig
Single Measures	.736[a]	.607	.836	9.737	42	84	.0000000000001
Average Measures	.893	.823	.939	9.737	42	84	.0000000000001

Two-way random effects model where both people effects and measures effects are random.

a. The estimator is the same, whether the interaction effect is present or not.

b. Type A intraclass correlation coefficients using an absolute agreement definition.

Figure 3.7: This table shows the ICC of the graders order of the arteries segments

Kappa = 0.192 [61]. [See details in Figures 3.8, 3.9 and 3.10]. On the other hand,

Symmetric Measures

		Value	Asymp. Std. Error[a]	Approx. T[b]	Approx. Sig.
Measure of Agreement	Kappa	.125	.051	2.845	.004
N of Valid Cases		68			

a. Not assuming the null hypothesis.

b. Using the asymptotic standard error assuming the null hypothesis.

Figure 3.8: This graph shows Kappa analysis of (B, K and M, H) of the group classification of the veins segments

the Kappa analysis conducted between the graders pairs, of the artery group were found to be Kappa = 0.03 (p = 0.4), Kappa= 0.107 (p = .03) and Kappa = 0.191 (p = 0.001) for (B, D and M, H), (B, D and M, T) and (M, H and M, T) respectively, with average Kappa = 0.23. [See details in Figures 3.11, 3.12 and 3.13.]

3.5.2 Ordered and classified tortuosity dataset

The ICC and Kappa analysis of the order and classification gradings showed a high to moderate degree of reliability, and slight agreement between the graders' grading for both tests respectively, but are not close to a complete agreement. Consequently a voting system was used, which considers the first grader grades in conflicted cases, due to his expertise in this field compared to the other graders. The gold standard tortuosity dataset using tortuosity order and classification was formed as follows:

Symmetric Measures

		Value	Asymp. Std. Error[a]	Approx. T[b]	Approx. Sig.
Measure of Agreement	Kappa	.079	.054	1.703	.089
N of Valid Cases		68			

a. Not assuming the null hypothesis.

b. Using the asymptotic standard error assuming the null hypothesis.

Figure 3.9: This graph shows Kappa analysis of (B, K and M, T) of the group classification of the veins segments

Symmetric Measures

		Value	Asymp. Std. Error[a]	Approx. T[b]	Approx. Sig.
Measure of Agreement	Kappa	.237	.059	5.292	.000
N of Valid Cases		63			

a. Not assuming the null hypothesis.

b. Using the asymptotic standard error assuming the null hypothesis.

Figure 3.10: This graph shows Kappa analysis of (M, H and M, T) of the group classification of the veins segments

It consists of 43 artery and 63 veins taken from hypertensive and diabetic patients, and their manually estimated tortuosity. Some segments were eliminated because they either graded in the wrong group or were overlooked by one of the graders. The dataset includes Matlab R2014a data structures that consist of records. Each record includes the name of the image, the coordinates of the vessel walls, the ordinal position of the vessel segment in the manual order, manual class, disease type and where the image is from.

3.5.3 Diabetic and hypertension datasets

The ordered and classified tortuosity dataset has been divided, based on disease, to hypertension and diabetic datasets, as follows:

Symmetric Measures

		Value	Asymp. Std. Error[a]	Approx. T[b]	Approx. Sig.
Measure of Agreement	Kappa	.036	.045	.729	.466
N of Valid Cases		44			

a. Not assuming the null hypothesis.

b. Using the asymptotic standard error assuming the null hypothesis.

Figure 3.11: This graph shows Kappa analysis of (B, K and M, H) of the group classification of the artery segments

Symmetric Measures

		Value	Asymp. Std. Error[a]	Approx. T[b]	Approx. Sig.
Measure of Agreement	Kappa	.107	.064	2.176	.030
N of Valid Cases		55			

a. Not assuming the null hypothesis.

b. Using the asymptotic standard error assuming the null hypothesis.

Figure 3.12: This graph shows Kappa analysis of (B, K and M, T) of the group classification of the artery segments

Diabetic dataset

The diabetic dataset consist of 53 retinal blood vessel segments segments divided to 34 vein and 19 artery segments. Similar to the ordered and classified tortuosity dataset it include Matlab data structures that consist of records; each record include the name of the image, the coordinates of the vessel walls, the ordinal position of the vessel segment in the manual order, manual class, disease type and where the image is from.

Hypertension dataset

The hypertension dataset consist of 77 retinal blood vessel segments, 39 vein and 38 artery segments. As with the previous datasets, it includes Matlab data structures that consist of records, each of which includes the name of the image, the coordinates of the vessel walls, the ordinal position of the vessel segment in the manual order, manual class, disease type and where the image is from.

Symmetric Measures

		Value	Asymp. Std. Error[a]	Approx. T[b]	Approx. Sig.
Measure of Agreement	Kappa	.191	.076	3.042	.002
N of Valid Cases		43			

a. Not assuming the null hypothesis.

b. Using the asymptotic standard error assuming the null hypothesis.

Figure 3.13: This graph shows Kappa analysis of (M, H and M, T) of the group classification of the artery segments

3.6 Conclusion

One of the main problems involved in carrying out tortuosity evaluation is the availability of free public datasets characterised by decent size and variety in pathology suitable to be used for tortuosity evaluation. In this study we propose a general tortuosity dataset that includes 130 segments of diabetic and hypertensive patients in addition to two pathology based datasets of hypertension and diabetic retinopathy. Although the ICC of the gradings carried out by the three graders showed a degree of high to moderate agreement, it was expected that it would be difficult to reach a complete agreement between the three graders specially in the order grading. Likewise, the Kappa tests performed between the graders pairs showed slight agreement. Tortuosity evaluation, even if it conducted by an expert ophthalmologist, is a subjective evaluation and largely relies upon the clinician's experience. To sum up, the dominant properties of the proposed retinal vessels tortuosity datasets from the standpoint of a new improved tortuosity dataset are:

1) The first disease based tortuosity datasets.

2) The vessel segments in these datasets are not of similar length or calibre.

3) They include two manual grading systems, with order and classification based on tortuosity

4) In addition to the vessel center line, the segments walls coordinates are also included.

5) Relatively large in size, the general dataset consists of 130 vein and artery segments.

Chapter 4

My framework

This chapter documents the development of the proposed tortuosity evaluation framework and its analytic processes, in addition it details the proposition of our new tortuosity features. It starts by an introduction to highlight the rationale behind building this evaluation tool. It describes all the tortuosity parameters included in the framework, as well as providing their logical grouping arrangements. The chapter proceeds to list and subsequently review the implementation stages, of both new and existing features, and presents the analysis of the resulting data. The framework is implemented on two tortuosity datasets. (The statistical analysis, classification and machine learning analysis are found in sections 4.3 and 4.4). The chapter concludes with a discussion of the statistical analysis results of the outlined problems and provides plans and recommendations for future work.

4.1 Introduction

One of the main objectives of this study is to develop an evaluation tool that is accurately able to estimate the degree of retinal blood vessels tortuosity, in view of the fact that huge benefits ensue from early identification of these retinal changes. In the course of the literature review it became clear that ophthalmologists have failed to agree on a single medical definition of the word "tortuosity". As a result various fundamentally different descriptions have been published and this has led to confusion as to what to measure in order to quantify the degree of abnormal vessel tortuosity.

A number of factors need to be considered in order to quantify the degree of retinal blood vessel curvature accurately and this is often overlooked. More importantly, some of these factors need to be applied first before the evaluation process is commenced, which is often overlooked. For example, structural properties such as the number of sub-curves and the degree and types of curves along the blood vessel segment need to be considered in the evaluation process. This requires a standard description of retinal vessels tortuosity. In discussions with ophthalmologists it was highlighted that the blood vessel segments to be measured for tortuosity should either be a single segment that extends from the optic disc to the periphery of the retina without bifurcations or a segment that lies between two major bifurcations.

Furthermore, most of the proposed tortuosity measures are constructed of a combination of a limited number of features, such as the estimate of the curvature of the segment, segment length, etc. Although some of these measures reported good results, the majority have been found to capture only partial aspects of this condition. For example, distance approach measures only capture the relative length increase of the vessel arc by comparing it with its chord. They give the same results for a segment with a smooth curved vessel, as they do to visually more curved segment of the same length. Consequently, these measures were deemed unable to capture the twists of the blood vessel segments, [see Figure 4.1]. On the other hand, despite ability of curvature measures to pick up on where distance based measures failed, this approach was also found unable to capture some of the important aspects related to blood vessels walls or boundaries such as aneurysms [5].

Based on the above, I propose a tortuosity evaluation framework that takes into consideration most of the structural changes in retinal blood vessel structures. This framework also includes various tortuosity evaluation methods, taken from some of the best proposed in the literature, as well as a group of new features proposed in this study. The next section provides an insight to this evaluation tool.

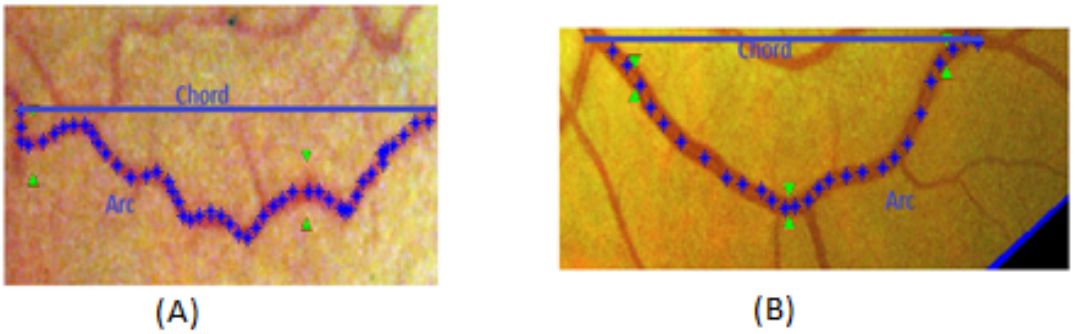

Figure 4.1: Two different vessels with the same tortuosity value using Arc over Chord tortuosity measure, (A): Vessel segment tortuosity =1.6, (B): Vessel segment tortuosity =1.6

4.2 Methodology

4.2.1 My new features

As previously indicated that, up until now their is no universally accepted tortuosity estimation measure. In addition, through the course of the literature review it become clear that one of the main reasons for that is the ambiguity of tortuosity definition and the subjective clinical tortuosity estimation without standardised descriptions. Therefore, I propose a suite of thirty five tortuosity estimation features, which can be classified into three groups as follow: A) Vessel structural properties (five features) B) Constructed features (six features), C) Features based on signal processing (twenty four features). The next sections describe and list some of these features.

Vessel structural properties:

This group of features provides number of properties along a blood vessel segment in terms of its structure. The group include five features (S1, S2, S3, S4, S5), these features are:

S1 (Sub-curves number), in case of a tortuous segment, this represent the number of sub-curves exist along a single segment.

S2 (Number of maximum points), this is the number of high points along a blood

vessel segment.

S3 (Number of minimum points), this is the number of low points along a blood vessel segment.

S4 (Sum of spaces under sub-curves), this is the sum of areas under sub-curves along a single blood vessel segment.

S5 (Sum of sub-curves Heights), this is the sum of all individual heights of sub-curves along a single blood vessel segment.

Constructed features:

Features in this group resulted from combining between some of the existing and new features, specially features of the previous feature group(Structural properties) with the aim of finding a robust feature with high tortuosity estimation capability. This group include six features(C1, C2, C3, C4, C5, C6). Descriptions of these features are as follow:

C1 (Vessel profile 1), this features results from the addition of the path over chord tortuosity measure (L5) and the sum of the spaces under sub-curves (S4).

C2 (Vessel profile 2), this feature results from the addition of the path over chord (L5) and the sum of the heights of sun-curves along a single blood vessel segment (S5).

C3 (Path over chord times maximum points), this feature results from the multiplication of the path over chord tortuosity measure (L5) and the number of maximum points (S2).

C4 (Arc over chord times maximum points), this feature results from the multiplication of the arc over chord tortuosity measure () and the number of maximum points (S2) along a blood vessel segment.

C5 (Path length added to sub-curves numbers), this results from the addition of the path length (L3) of a blood vessel segment and the numbers of sub-curves (S1) along that segment.

C6 (Absolute of slopes differences and unsigned curvature), this feature results from the addition of the unsigned curvature (L24) and the absolute slope differences at each point along a blood vessel segment.

Features based on signal processing:

These twenty four features were derived from Fourier transform analysis. Four forms of values along the blood vessel segments, represented as functions of spaces, were used as an input in this analysis. For each of these four forms, six features of the frequency domain or signal spectrum elements were derived. Some of these features were derived by combining other features. The functions of space representing blood vessel segments, which was used as an input to the Discrete Fourier analyses were as follows:

1) The displacement distances between the blood vessel segment and its underlining chord, which are the distances that resulted from the differences between each point along the blood vessel segment and the equivalent point in the underlining chord of the same segment; given that the blood vessel segments were all horizontally positioned in a 2D plane. See Figure 4.3 for an example of the calculated displacement points, and figure 4.2 for Fourier transform analysis.

2) The first derivatives of the x axis of the segment centreline points.

3) The second derivatives of the x axis of the segment centreline points

4) The signed curvature at each point along the blood vessel segment, which is calculated by equation 2.8.

The built in Matlab Discrete Fourier Transform function was used to analyse these functions of spaces, which represent the same retinal blood vessel segments, but in different ways. The DFT of a vector x of length n is another vector y of length n and is given by equation 4.1.

The output features of the conducted Fourier analysis are as follow:

1) The power of the signal or function in the place of analysis.

2) The sum of magnitudes of the resulted sine/cosine waves.

3) The sum of the signal spectrum phases normalised by the path length of the blood vessel segment.

4) The sum of the magnitudes of the resulted sine/cosine waves normalised by the path length of the segment;

5) The ratio between the segment's chord and path lengths multiplied by the sum of the resulted magnitudes.

6) The unsigned total curvature multiplied by the sum of resulted magnitudes.

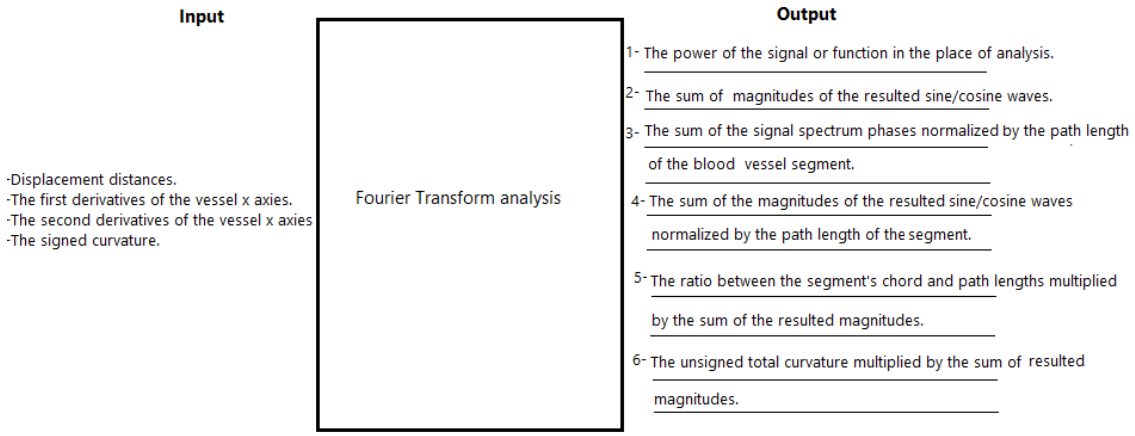

Figure 4.2: A diagram shows Fourier transform analysis

$$y_{p+1} = \sum_{j=0}^{n-1} w^{jp_{x(j+1)}} \tag{4.1}$$

Where w is a complex nth root of unity: $w = e^{-2\pi i/n}$ Here i refers to the imaginary unit, and p and j are for the indices that run from 0 to n–1. The indices $p+1$ and $j+1$ run from 1 to n, corresponding to ranges associated with Matlab vectors. The features of this group are as follow:

F1 (DFT measures and path over chord using displacement points), this is the sum of the magnitudes of the DFT analysis of the displacement points, then multiplied by the length difference between the path and chord lengths (L7).

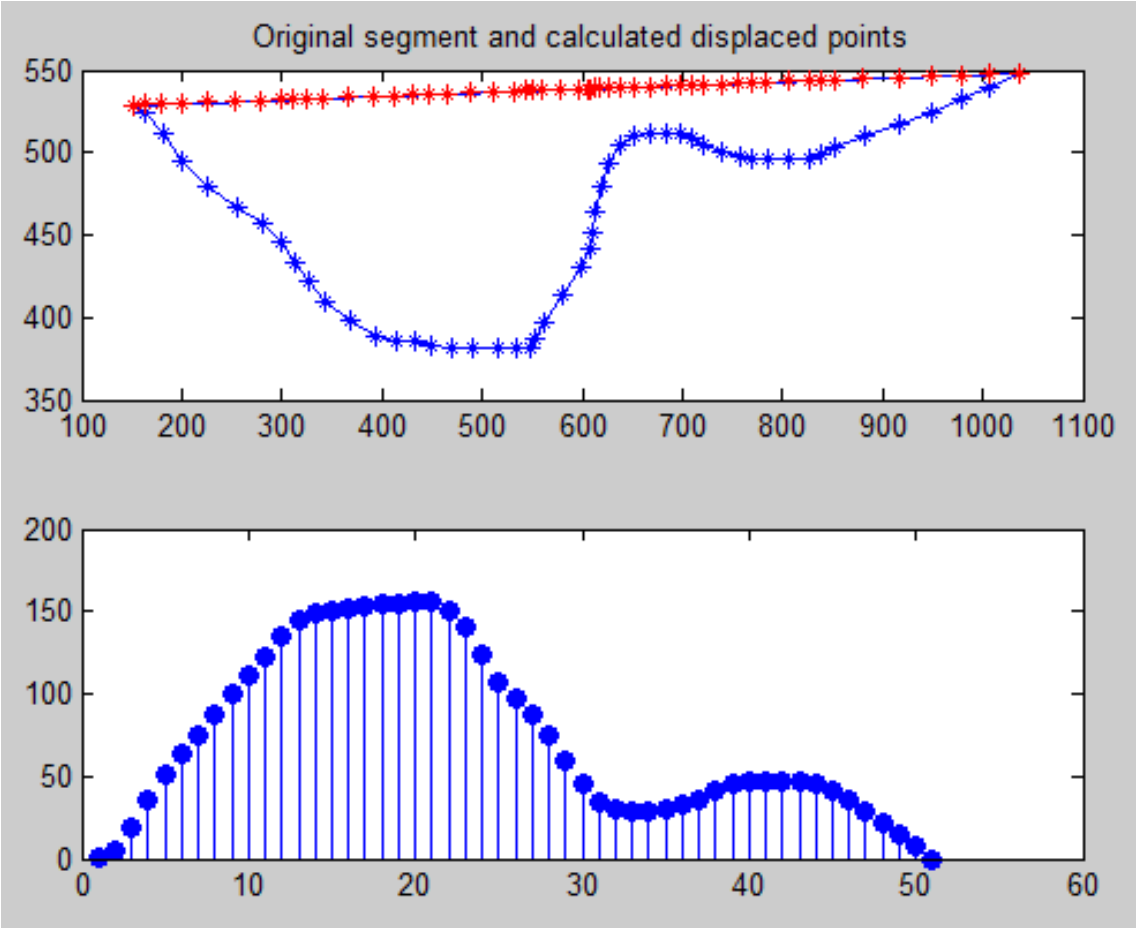

Figure 4.3: Example of a blood vessel segment and its calculated displacement points

F2 (DFT measures and curvature using points displacement), this is the sum of the magnitudes of the DFT analysis of the displacement points, then multiplied by the unsigned total curvature (L24).

F3 (DFT Measure using path over chord and xPrime), this is the sum of the magnitudes of the DFT analysis of the first derivatives of the X axis, then multiplied by the length difference between the path and chord lengths (L7).

F4 (DFT Measures and curvature using xPrime), this is the sum of the magnitudes of the DFT analysis of the first derivatives of the X axis of the blood vessel segment, then multiplied by the unsigned total curvature (L24).

F5 (DFT Measures and path over chord using xsec), this is the sum of the magnitudes of the DFT analysis of the second derivatives of the X axis of the blood vessel segment, then multiplied by the length difference between the path and chord lengths (L7).

F6 (DFT Measures curvature using xsec), this is the sum of the magnitudes of the DFT analysis of the second derivatives of the X axis of the blood vessel segment, then multiplied by the length difference between the path and chord lengths (L7).

F7 (DFT Measures and path over chord using curvature), this is the sum of the magnitudes of the DFT analysis of the curvature at each point along the blood vessel segment, then multiplied by the length difference between the path and chord lengths (L7).

F8 (DFT measures and curvature using curvature), this is the sum of the magnitudes of the DFT analysis of the curvature at each point along the blood vessel segment, then multiplied by the curvature calculated by the length difference between the path and chord lengths (L7).

F9 (Sum of DFT Mag using points displacement), this is the sum of the magnitudes of the Discreet Fourier Transform of the displacement points along the blood vessel segment.

F10 (The sum of DFT Mag normalised By path length using displacement points), this is the sum of the magnitudes of the Discreet Fourier Transform of the displacement points along the blood vessel segment, then normalised by the path length (L3).

F11 (DFT Power norm by path length using displacement points), this is the power of the DFT analysis of the displacement points along the blood vessel segment.

F12 (DFT Power using xprime), this is the power of the DFT analysis of the first derivatives of the X axis points along the blood vessel segment.

F13 (DFT Mag using xprime), this is the sum of the magnitudes of the Discreet Fourier Transform of the first derivatives of the X axis points along the blood vessel segment.

F14 (DFT Power using xsec), this is the power of the DFT analysis of the second derivatives of the X axis points along the blood vessel segment.

F15 (DFT Mag xsec), this is the sum of the magnitudes of the DFT analysis of the second derivatives of the X axis points along the blood vessel segment.

F16 (DFT Power using curvature), this is the power of the Discreet Fourier Transform of the curvature at each single point along the blood vessel segment.

F17 (DFT Mag using curvature), this is the sum of the magnitudes of the DFT analysis of the curvature values at each single point along the blood vessel segment.

F18 (Sum of signal phases norm by path length using displacement points), this is the sum of frequency phases of the DFT analysis of the displacement points, then normalised by the path length (L3).

F19 (Sum of the signal phases norm by path length using xPrime), this is the sum of frequency phases of the DFT analysis of the first derivatives of the X axis points along the blood vessel segment, then normalised by the path length (L3).

F20 (Sum of Mag norm by path Length using xPrime), this is the sum of the magnitudes of the DFT analysis of the first derivatives of the X axis points along the blood vessel segment, then normalised by by the path length (L3).

F21 (Sum of phases norm by path length using xsec), this is the sum of frequency phases of the DFT analysis of the second derivatives of the X axis points along the blood vessel segment, then normalised by the path length (L3).

F22 (Sum of Mag norm by path length using xsec), this is the sum of the magnitudes of the DFT analysis of the second derivatives of the X axis points along the blood vessel segment.

F23 (Sum of signal phases norm by path length using curvature), this is the sum of frequency phases of the DFT analysis of the curvature at each single point along the blood vessel segment, then normalised by the path length (L3).

F24 (Sum of Mag norm by path length using curvature), this is the sum of the magnitudes of the DFT analysis of the curvature values at each single point along the blood vessel segment, then normalised by the path length (L3).

4.2.2 Features derived from the literature

This section highlights the most frequently used tortuosity estimation features in the literature. This group include thirty one features (from L1 to L31) chosen to be incorporated in the proposed tortuosity evaluation framework. Detailed description of these features and references are found in Section 4.2.4 These features are:

L1 Segment chord length.

L2 Segment arc length.

L3 Segment path length.

L4 Arc over chord.

L5 Path over chord.

L6 Length difference between arc and chord.

L7 Length difference between path and chord.

L8 Grisan's tortuosity measure.

L9 Rashmi's tortuosity measure.

L10 Tortuosity coefficient.

L11 Unsigned tortuosity slope.

L12 Signed tortuosity slope.

L13 Mean direction angle change.

L14 Inflection count metric using arc length.

L15 Inflection count metric using path length.

L16 Total signed curvature.

L17 Total signed curvature over path length.

L18 Total signed curvature over arc length.

L19 Total signed curvature over chord length.

L20 Total squared signed curvature.

L21 Total squared signed curvature over arc length.

L22 Total squared signed curvature over path length.

L23 Total squared signed curvature over chord length.

L24 Total unsigned curvature.

L25 Total unsigned curvature over path length.

L26 Total unsigned curvature over arc length.

L27 Total unsigned curvature over chord length.

L28 Total squared unsigned curvature.

L29 Total squared unsigned curvature over path length.

L30 Total squared unsigned curvature over arc length.

L31 Total squared unsigned curvature over chord length.

4.2.3 My proposed framework

some researchers found that some of the tortuosity estimation features are not able to capture all forms of tortuosity. For instance, distance measures, which are the measures that based on taking the ratio between the chord and curve lengths, were found not able to capture tight coils and curves [29, 48]. Likewise, curvature measures, which are the measures that estimate curvature at each single point along a curve, were found unable to capture some of the important aspects related to blood vessels walls or boundaries such as aneurysms [5]. Consequently, since their is no universally accepted tortuosity measure with suitable combination of tortuosity features that are able to capture all forms of tortuosity with high accuracy, I propose a tortuosity estimation framework that include 66 features, which cover a broad range of vessels structural changes. The framework originally consisted of 74 features. Eight were later excluded, due to fundamental flaws and redundancy. The selection criteria of the framework's features were mainly based on three aspects:

A) The features should reflect various aspects of structural changes in blood vessels, in particular changes due to pathologies or their complications such as diabetes and hypertension retinopathy. B) The characteristics of the dataset to be used in the features evaluation, plays a significant role in the types of chosen features, in terms of vessel segment types and the available data about these segments. If the width of the segments are needed, characteristics such as the availability of the coordinates within points of blood vessel segments' walls are required. C) The feasibility of the implementation of the measures and properties is related to given available resources, such as 2D images or 3D images. Sections 4.2.2 and 4.2.1 provides list of the features that were selected from the literature as well as a list of the new ones.

4.2.4 Framework features' grouping and implementation

This section provides an overview of the implementation of the 66 features of the proposed framework. These features are organised into five groups: 1) Structural properties, 2) Distance approach features, 3) Curvature approach features, 4) Combined approach features, 5) Signal approach features. The grouping is mainly based on similarities. Implementations in this section were carried out, on the RVTDS using Matlab R2014a, for all feature groups except signal features which are already discussed in section 4.2.1.

Structural properties features

This includes five features, which represent some aspects that describe the structural nature of blood vessels. The greater are the values produced by these features, the more tortuous the segment would be and vice versa. These features are implemented as follows:

Maximum and minimum points along a blood vessel segment (S2, S3) These are the highest and lowest points along a blood vessel segment. If a blood vessel segment S is represented as a function of x, $f(x)$, where $x = [0, 1, ..., N]$, then the minimum and maximum points along this segment can be identified by using the derivatives rules of: if $f'(x_i) > 0$ and $f'(t_{x+1}) < 0$, which checks if the function is increasing to the left side of x_i and decreasing to the right side of x_i; if true, then

f has a local maximum point at x, and if $f'(x_i) < 0$ and $f'(t_{i+1}) > 0$, which checks that if the function is decreasing to the left side of x_i and increasing to the right side of x_i; if true in this case the function has a local minimum at x_i,nsee Figure 4.4. As shown in the figure, after applying these rules along a blood vessel segment, the points that satisfy the conditions are shown, in this case, two close maximum or minimum points can be produced. However, this can be resolved by checking the distances between those points and ignoring one of these points if they are found to be too close.

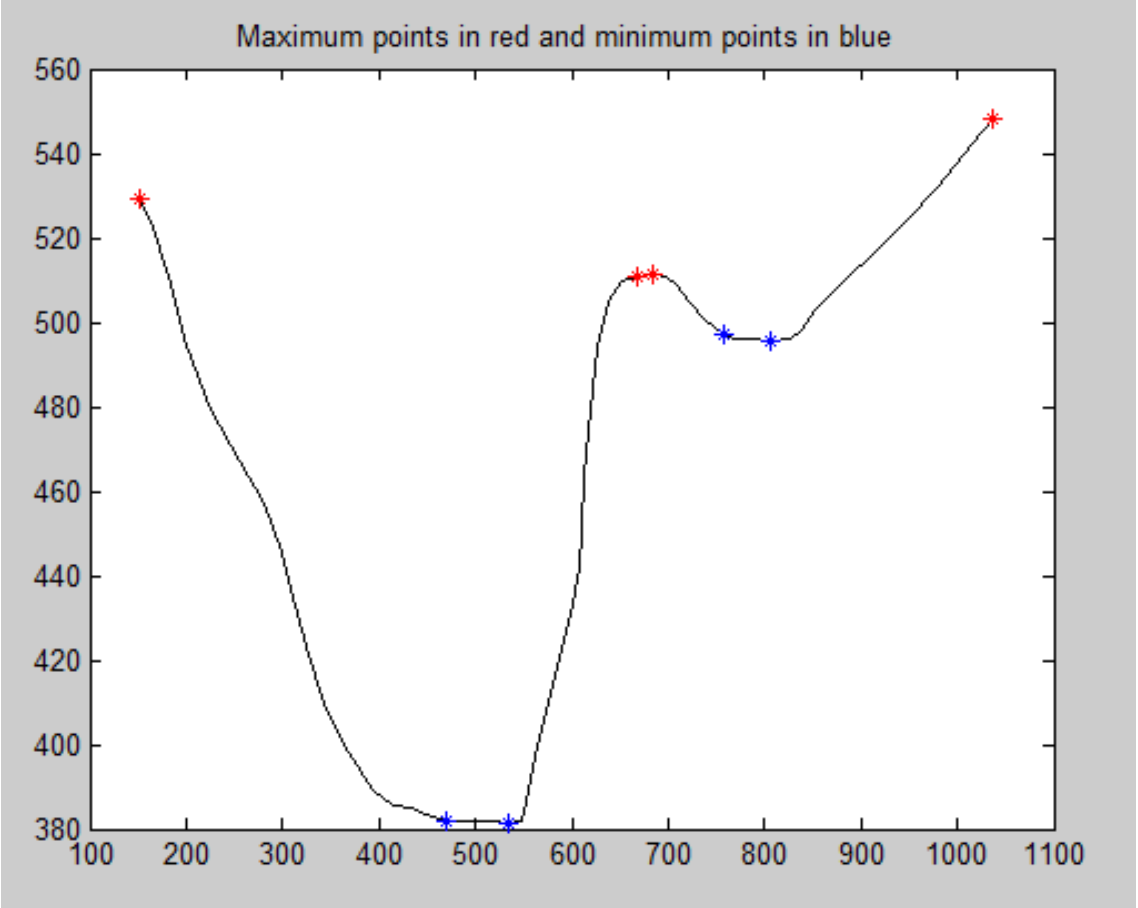

Figure 4.4: Minimum and maximum points along a blood vessel segment

Sub-curves number (S1) This can be identified by an algorithm that inspects the high and low points along the vessel segment. Using these points sub-curves can be identified by each of two or three consecutive points along a blood segment. For example, a minimum, maximum and minimum sequence will indicate a concave down sub-curve, and a maximum, minimum and maximum sequence will indicate

and a concave up sub-curve whereas two points indicate a half sub-curve.

The sub-curves heights (S5) The heights of sub-curve segments were calculated by measuring the length between the sub-curve highest or lowest point and the underling chord, which is the straight distance between the two end points of the sub-curve.

The sum of areas under sub-curves (S4) The spaces under the sub curves were calculated through integration as shown in figure4.5.

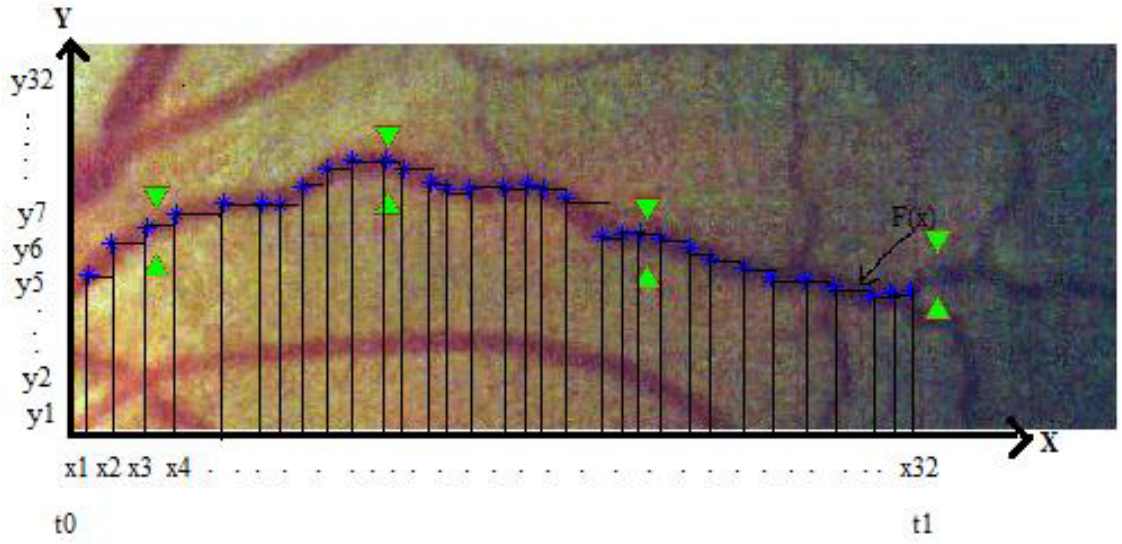

Figure 4.5: Estimation of the area under curve

Distance approach features

These are seven length related features. With this group, the blood vessel segments are measured by two different methods: The segment path length measure (L3) 2.5, and the segment curve or arc length measure (L2) 2.6. Most of these features' ways of evaluating tortuosity are based on the ratio between the curve/path lengths and the chord length, which is the length between the two end points of the blood vessel segment. Since the proposed tortuosity evaluation framework in this project is an automated system, the measures which should be included under this category have to be automated too. Therefore, the relative length variation has been excluded from the evaluation framework. Most of the mathematical implementations examples

shown in this section were carried out on two vessel segments (an artery and a vein) from the Retinal Vessels Tortuosity Dataset described in chapter 3. Figure 4.6 shows a JPG image of the artery and vein segments used (as an example). The distance features were as follow:

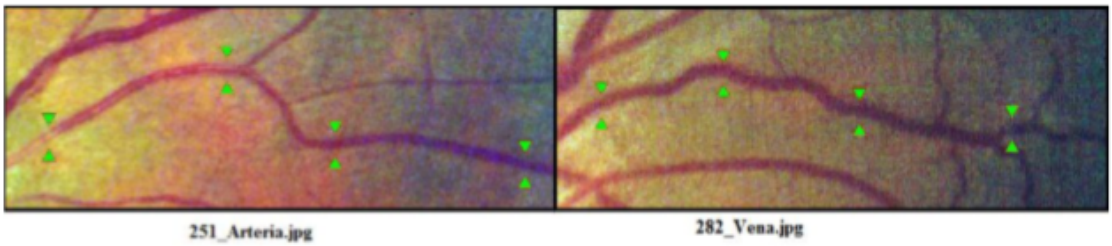

Figure 4.6: A marked artery segment on the left, and a marked vein segment on the right

Segment arc length and Segment path length (L2, L3) Segment path length is simply the measurement of the length of the blood vessel segment. The path length Equation 2.5 was used to estimate this length, which calculates the length of the blood vessel segment using the vessels' centreline points x_n, y_n. Where $n \subset R$, by summing the geodesic distances along the curve or the vessel segment.

Segment arc length is another method of measuring the segment length. The segment arc length is calculated, using Pythagoras theory, by estimating the integral of the differential distance of all points along the blood vessel segment, $\triangle$x, and $\triangle$y, see Equation 2.6.

These methods produce measurements with relatively small variations when implemented on the same blood vessel segment. This is considered to some extent a useful aspect, since variance between blood vessels segments measurements is seen as an important aspect, when it comes to the process of vessels classification given that the gold standard dataset segments have the same length and calibre, See Figure 4.7, which shows an artery segment and its calculated length using both methods. The implementation code is in Appendix .2, section .2.1.

Chord length (L1) This is the measurement of the length between the two end points of a blood vessel segment, as in Equation 2.7. The Pythagorean theorem is

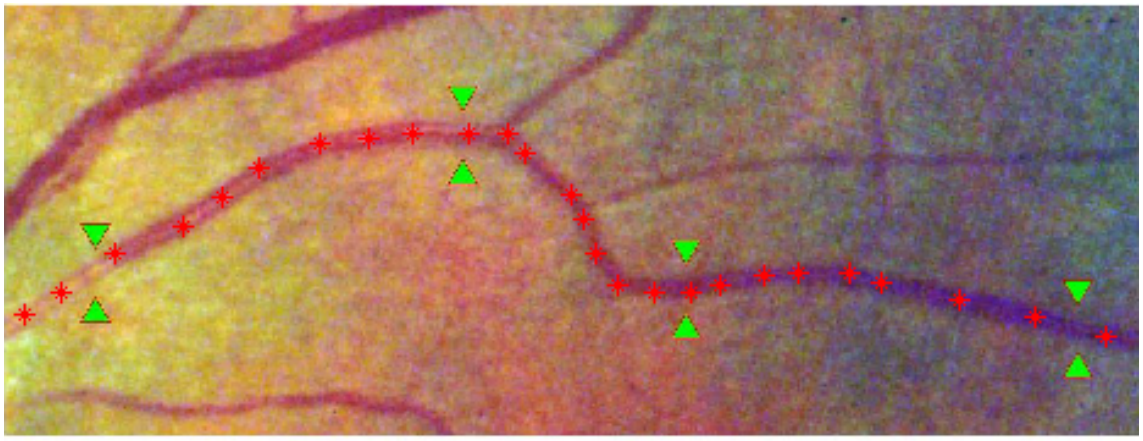

Figure 4.7: An artery segment normalised length measurements; path length = 0.204 and Arc length = 0.230

used to calculate this length using the two end points of each segment, see code in Appendix .2, section .2.1.

The ratio of arc and chord length Features (L4, L5, L6, L7) These are a group of four similar features. These features are:1) The ratio of the arc length and the chord length minus one. 2) The ratio of the path length and the chord length minus one. 3) The ratio of the arc length and the chord length 3) The ratio of the path length and the chord length. The first two features are as in equations 2.3 and equation 2.4 respectively. They should give a value of zero if the segment is straight and a positive increasing value if it is tortuous. Whereas Features 3 and 4 will give a value of one if the segment is straight and positive increasing value if tortuous. These were used with other features to generate new ones, refer to section 4.2.4.

Curvature approach features

This group includes twenty two features. For implementation purposes features of this group were grouped into smaller subgroups based on their similarity and overlapping mathematical implementations. See all implementation code of this group in Appendix .2, section .2.2. These features are as follow:

1) Group A: This group includes four features: 1) The total signed curvature. 2) The total unsigned curvature. 3) The total squared signed curvature. 4) The total squared unsigned curvature. Most of the curvature measures were imple-

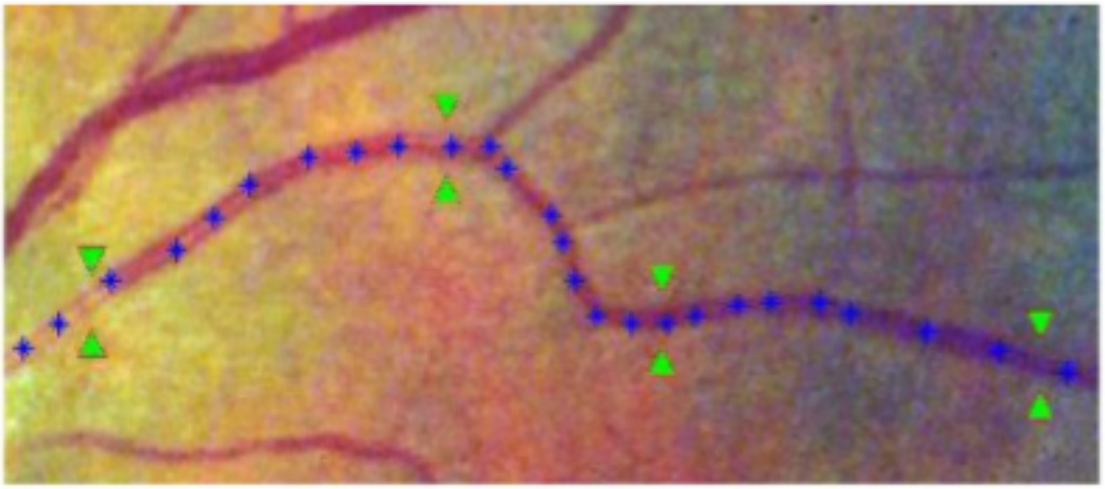

Figure 4.8: An example of an artery with centreline points

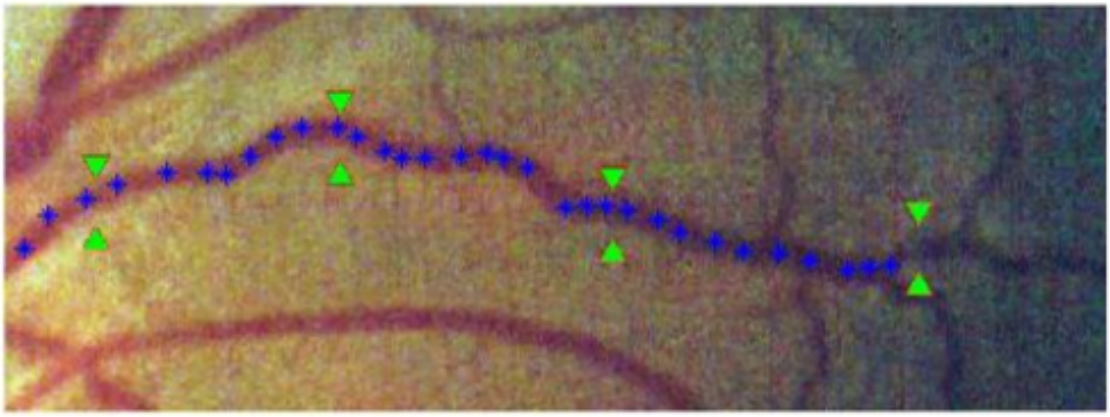

Figure 4.9: An example of a vein with centreline points

mented using numerical differentiation. The first and the second derivatives at each point along the blood vessels were calculated. Backward differentiation was used to calculate the derivatives of end points in vessel segments.

The signed curvature of blood vessels segments were calculated at each point along the blood vessels using the first and the second derivatives as in Equation 2.8, and shown in figure 4.10, which shows the signed curvature values at each point along a blood vessel segment. The unsigned curvature was calculated by taking the absolute values of the signed curvature, as in Equation 2.9. The sum of the signed and unsigned values of curvature along vessels segments provided the total signed and unsigned curvature of each segment, as given by Equations 2.10 and 2.11. These totals were then doubled to calculate the

total squared signed curvature and the total squared unsigned curvature.

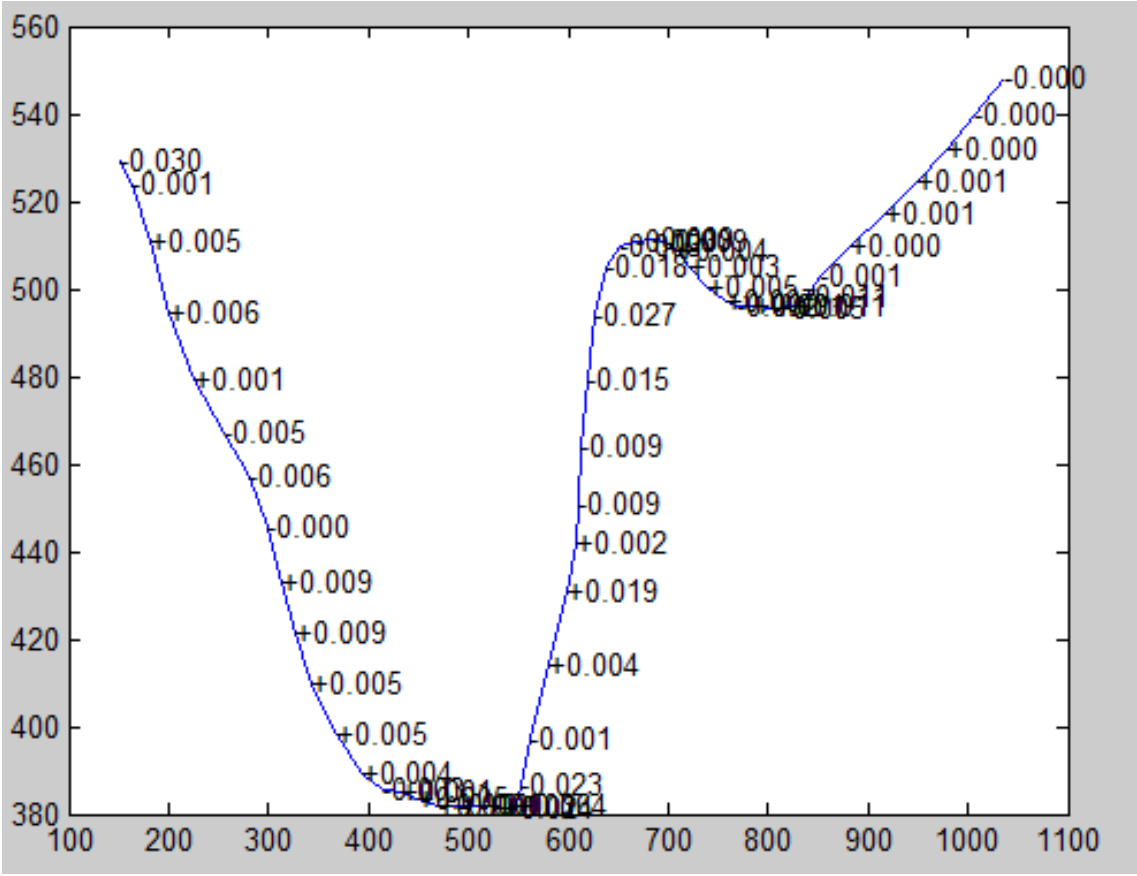

Figure 4.10: Signed curvature at each point along blood vessel segment

2) Group B: This group includes twelve features: 1) The total signed curvature normalised by the segment chord length. 2) The total signed curvature normalised by the curve length. 3) The total signed curvature normalised by the path length 4) The total unsigned curvature normalised by the segment chord length. 5) The total unsigned curvature normalised by the curve length. 6) The total unsigned curvature normalised by the path length.7) The total squared signed curvature normalised by the segment chord length. 8) The total squared signed curvature normalised by the curve length. 9) The total squared signed curvature normalised by the path length. 10) The total squared unsigned curvature normalised by the segment chord length. 11) The total squared unsigned curvature normalised by the curve length. 12) The total squared unsigned curvature normalised by the path length. These features were generated by normalizing the previous curvature groups' features,

each by the chord, curve and path lengths respectively, equation are in section 2.8.2, and implementation code in Appendix .2, section .2.2.

3) Group C: This group includes five features: 1) Tortuosity coefficient. 2) The signed tortuosity using the gradients along blood vessel segment. 3) The unsigned tortuosity using the gradients along blood vessel segment. 4) Rashmi's measure of tortuosity. 5) Mean direction angle change. The implementation of the Tortuosity coefficient feature was based on the second differences of the coordinates of the vessel mid-line. After calculating the differences between each of two successive gradients, the absolute sum of these differences were calculated and then divided by the sampling interval since the measure depends on the vessel length or the segment sampling interval P, see equation 2.18. The signed and unsigned tortuosity features were estimated by calculating the slopes or the gradients along each blood vessel segment. The sum of the absolute slopes differences were taken to estimate the unsigned tortuosity, and the sum of the slopes differences to estimate the signed tortuosity.

   Rashmi's measure of tortuosity is similar, in implementation, to the previous feature. The tortuosity here is calculated by taking the differences of the slopes along the blood vessel segment, see equation 2.17.

   In the execution of the Mean direction angle change (MDAC) feature, for each point p, along the blood vessel segment two vectors $[p+step]$ and $[p-step]$ were formed. The step value is governed by the length of the segment. Then, each vector is normalised by its norm. Consequently, the angle theta (θ) between those two vectors is computed using the dot products, $\theta = arccos(v1.v2)$, Then tortuosity can be calculated using Equation 2.22.

4) Group D: This group includes one feature, which is the total sum of the combined unsigned curvature along blood vessel segment and the absolute differences of gradients along blood segment. This feature results from the combination of the previous measure, Rashmi's measure of tortuosity, and the unsigned curvature. In this measure the absolute values of the slopes differences along a blood vessel segment were added to the equivalent curvature values at each point, then the sum of those values were calculated.

Combined features

These features were built with the intention of capturing more of the vessels curvature. Various features and evaluation techniques were included in this group. Some blood vessels features were thoughtfully combined with other features to form, as indicated by their proposers, powerful tortuosity measures. This category includes eight features. Five features were from the literature and the rest are proposed in this study. See code in Appendix .2, section .2.4. This group features are as follow:

1) Grisan's tortuosity measure: This was proposed by Grisan et al. [43, 28, 44]. Their methods used spline interpolation to estimate the curvature of retinal blood segments. Although their own techniques, code and dataset were used, their results were unreproducible. Consequently, a similar approach was followed using their own theory, which is a tortuosity estimation algorithm that calculates the number of sub-curves in the blood vessel segment, and its tortuosity estimation. In addition to the length of the segment. Numerical differentiation and derivatives rules were used to identify the sub-curves in each blood vessel segment, as described in detail in section 4.2.4, then the ratio between each sub-curve and its underlining chord was calculated, which represents the tortuosity value of that particular sub segment. Finally, the integrals of these sub-curves tortuosities were calculated to estimate the tortuosity of the blood vessel segment as in Equation 2.30.

2) Inflection count metric one and two: Inflection count metric is proposed by Smedby [83] and extended by Elizabeth Bullitt [13, 27]. The measure originally counts the inflection points along each space, plane or curve and multiplies this number, plus one, and the total segment curve length divided by the chord length as in equation 2.26. The number of sub-curves were used, as they indicate the turning points along blood vessels segments. There were two tortuosity features produced by this measure because there were two methods of estimating the curve length.

3) Arc over chord combined with the number of maximum points along a blood vessel segment, and the Path over chord combined with the number of maximum points along a blood vessel segment: These are examples of the new

features, which resulted from the combination (multiplication) of each of the path length and the arc length of the blood vessel segment, and the number of the maximum points along the blood vessel segment plus one.

4) Path length combined with the sub-curves numbers along blood vessel segment: This estimates the curvature of the blood vessel segment by adding up the segment path length and the number of sub-curves or segments in a single segment. The code is found in Appendix .2, section .2.4.

5) Vessel profile features one and two: Vessel profile feature one is formed by adding up the path over chord feature, discussed in section 2.8.1 and the sum of all sub-curves under spaces, which is one of the structural properties features. Vessel profile feature two is constructed by adding the path over chord to the sum of the sub-curves heights. The main reason behind the construction of these features is to capture more aspects of the vessel tortuosity. The code is in Appendix .2, section .2.4.

4.3 Data analysis using the retinal vessel tortuosity dataset

Several statistical analyses were used to analyse the framework features. IBM SPSS (21) and Matlab R2014a software were used interchangeably in these processes. This section starts by analysing the proposed tortuosity evaluation framework features using basic descriptive statistics. This is to identify any differences and similarities between the set of artery and vein segments and to monitor the range and distribution measurements of individual features. These are important factors especially in classification. Correlation analysis was then conducted to examine the strength of the relationship between the framework features and the clinical order of the segments. This was followed by regression analysis to identify the best set of features that could accurately predict the clinical order. In addition, further analyses methods from machine learning were utilised in an attempt to obtain higher performance level of grading blood vessel segments' tortuosity. The next sections provide an overview of the implementation of these statistical methods and the results analysis

Table 4.1: This table shows the descriptive statistical analysis of the structural properties features of the arteries

Descriptive Statistics

Feature	N	Minimum	Maximum	Mean	Std. Deviation	Variance
S1	30	.000	1.000	.36250	.235232	.055
S2	30	.000	1.000	.44545	.275689	.076
S3	30	.000	1.000	.43939	.271243	.074
S4	30	.000	1.000	.43411	.229984	.053
S5	30	.000	1.000	.37146	.259718	.067
Valid N (listwise)	30					

using RVTDS, described in section 3.3, and the new tortuosity dataset built in chapter 3.

4.3.1 Descriptive statistical analysis

Descriptive statistical analysis of the structural properties features on artery and vein segments

The descriptive analysis results of the five structural properties features of the vein and artery segments groups, revealed that there is no significant variances when it come to the structural properties between the two groups. However the arteries group showed a small increase in variability compared to veins. The standard deviations of the two groups also showed small differences between the veins and arteries segments, See Tables 4.1 and 4.2 for the veins and arteries descriptive analysis respectively.

Descriptive statistical analysis of the distance approach features on artery and vein segments

The basic descriptive analysis results of these seven features, revealed that most means of the features of the arteries were slightly higher than those in the veins. This observation supports the fact that the arteries are more elastic and flexible in nature compared to veins, as discussed in details in Sections 2.5.1 and 2.6, hence the segments tend to become tortuous in a smooth manner. The variability of the two groups' tortuosity grades appeared increasingly different especially with Arc

Table 4.2: This table shows the descriptive statistical analysis of the structural properties features of the veins

Descriptive Statistics

Feature	**N**	**Minimum**	**Maximum**	**Mean**	**Std. Deviation**	**Variance**
S1	30	.000	1.000	.47043	.219015	.048
S2	30	.000	1.000	.48118	.216997	.047
S3	30	.000	1.000	.39817	.218649	.048
S4	30	.000	1.000	.45072	.260388	0.68
S5	30	.000	1.000	.42839	.295839	.088
Valid N (listwise)	30					

Table 4.3: This table shows the descriptive statistical analysis of the distance approach features for arteries

Descriptive Statistics

Feature	**N**	**Minimum**	**Maximum**	**Mean**	**Std. Deviation**	**Variance**
L1	30	.000	1.000	.72805	.243215	.059
L2	30	.000	1.000	.39726	.275272	.076
L3	30	.000	1.000	.38930	.276223	.076
L4	30	.000	1.000	.36028	.285869	.082
L5	30	.000	1.000	.37073	.277549	.077
L6	30	.000	1.000	.6028	.285869	.082
L7	30	.000	1.000	.37073	.277549	.077
Valid N (listwise)	30					

over chord (L4), Path over chord (L5) and the length differences using the ratios of the path and Arc lengths to chord length features (L6, L7) in the arteries group. However, the veins showed little variation between the sample data, which indicated the closeness of the tortuosity grades of this group. The standard deviations of the two groups also showed small variation between the vein and artery groups, See Tables 4.8 and 4.4 for the artery and vein segments respectively.

Descriptive statistical analysis of curvature approach features on artery and vein segments

Examining descriptive results of the twenty two curvature features, of the arteries and veins showed that the means of the vein segments, especially the signed cur-

Table 4.4: This table shows the descriptive statistical analysis of distance based approach features for veins

Descriptive Statistics

Feature	N	Minimum	Maximum	Mean	Std. Deviation	Variance
L1	30	.000	1.000	.71165	.232865	.054
L2	30	.000	1.000	.37925	.236962	.056
L3	30	.000	1.000	.36372	.236436	.056
L4	30	.000	1.000	.25901	.240999	.058
L5	30	.000	1.000	.23326	.244366	.060
L6	30	.000	1.000	.07282	.218917	.048
L7	30	.000	1.000	.25901	.240999	.58
Valid N (listwise)	30					

vature (L16) and the unsigned tortuosity measure combined with the slope (L11), were slightly higher than those in the arteries. Both groups' features' showed small variations. See Tables 4.5 and 4.6 for the descriptive analysis of the artery and vein segments respectively.

Descriptive statistical analysis of the combined features on artery and vein segments

The statistical analysis of the eight combined features showed that, in general, the means of the veins segments were slightly higher than those in the arteries group. Both groups showed small standard deviation values, which indicated the closeness of these groups' features to their means values; this is also supported by small variations values reported between the values of both groups' tortuosities grades, with the vessel profile 2 (C2) feature reporting the highest variance value of 0.078 in the veins group. Refer to Table 4.7 for the descriptive analysis of this group.

Descriptive statistical analysis of Fourier Transform based features on artery and vein segments

The statistical analysis revealed that the variance among the artery segments' measurements was higher than that in the veins. This was to some extent, backed up by the standard deviation values which showed a slight increment among these groups,

Table 4.5: This table shows the descriptive statistical analysis of curvature based approach features of arteries

Descriptive Statistics

Feature	N	Minimum	Maximum	Mean	Std. Deviation	Variance
C6	30	.000	1.000	.27875	.197663	.039
L9	30	.000	1.000	.13996	.240689	.058
L10	30	.000	1.000	.35111	.201801	.041
L11	30	.000	1.000	.39413	.219804	.048
L12	30	.000	1.000	.49125	.183666	.034
L13	30	.000	1.000	.57299	.232864	.054
L16	30	.000	1.000	.37631	.230296	.053
L17	30	.000	1.000	.38261	.212677	.045
L18	30	.000	1.000	.38384	.213556	.046
L19	30	.000	1.000	.38524	.225672	.051
L20	30	.000	1.000	.11746	.230892	.053
L21	30	.000	1.000	.11076	.218684	.048
L22	30	.000	1.000	.11014	.217918	.047
L23	30	.000	1.000	.11682	.228682	.052
L24	30	.000	1.000	.32583	.236547	.056
L25	30	.000	1.000	.35217	.246913	.061
L26	30	.000	1.000	.35120	.246639	.061
L27	30	.000	1.000	.33425	.239573	.057
L28	30	.000	1.000	.17101	.210083	.044
L29	30	.000	1.000	.18233	.217231	.047
L30	30	.000	1.000	.18191	.216848	.047
L31	30	.000	1.000	.17455	.211717	.045
Valid N (listwise)	30					

whereas there were no significant differences between the means values of the two groups. See Table 4.9 and Table 4.10 for the descriptive analysis of the artery and vein segments respectively.

Descriptive statistics results

The descriptive statistical analysis, in general, showed that the means of the artery segments of the Fourier Transform, and the distance approach features were slightly higher than those in the vein segments. However, the means of the structural,

Table 4.6: This table shows the descriptive statistical analysis of the curvature based approach features of veins

Descriptive Statistics

Feature	**N**	**Minimum**	**Maximum**	**Mean**	**Std. Deviation**	**Variance**
C6	30	.000	1.000	.15922	.208878	.044
L9	30	.000	1.000	.10273	.272136	.074
L10	30	.000	1.000	.36152	.243251	.059
L11	30	.000	1.000	.48108	.240448	.058
L12	30	.000	1.000	.24323	.185960	.035
L13	30	.000	1.000	.59759	.259724	.067
L16	30	.000	1.000	.57023	.228564	.052
L17	30	.000	1.000	.57401	.225507	.051
L18	30	.000	1.000	.58064	.224314	.050
L19	30	.000	1.000	.56841	.239255	.057
L20	30	.000	1.000	.13512	.249541	.062
L21	30	.000	1.000	.14121	.255229	.065
L22	30	.000	1.000	.14315	.257881	.067
L23	30	.000	1.000	.14092	.258454	.067
L24	30	.000	1.000	.28933	.269886	.073
L25	30	.000	1.000	.29097	.258172	.067
L26	30	.000	1.000	.29218	.260825	.068
L27	30	.000	1.000	.27967	.270718	.073
L28	30	.000	1.000	.16695	.259324	.067
L29	30	.000	1.000	.16810	.249723	.062
L30	30	.000	1.000	.16610	.245823	.060
L31	30	.000	1.000	.16479	.257662	.066
Valid N (listwise)	30					

curvature and combined approach features, of the veins, were all higher than the means of the artery segments. This indicates that, in this sample, the vein segments are more tortuous than the arteries.

In terms of the distribution of individual values in feature groups, the standard deviation of the distance and the structural approach features, of the artery segments, were slightly higher than those in the veins. On the contrary, the standard deviation of the curvature approach features, of the veins, were higher than those in the arteries. However both Fourier Transform and combined approach features

Table 4.7: This table shows the descriptive statistical analysis of the combined approach features of the artery segments

Descriptive Statistics

Feature	N	Minimum	Maximum	Mean	Std. Deviation	Variance
C1	30	.000	1.000	.43411	.229985	.053
C2	30	.000	1.000	.37149	.259729	.067
C3	30	.000	1.000	.22970	.228617	.052
C4	30	.000	1.000	.37585	.245740	.060
C5	30	.000	1.000	.38716	.274516	.075
L8	30	.000	1.000	.28582	.233175	.054
L14	30	.000	1.000	.33706	.226965	.052
L15	30	.000	1.000	.33417	.225131	.051
Valid N (listwise)	30					

Table 4.8: This table shows the descriptive statistical analysis of the combined approach features of the vein segments

Descriptive Statistics

Feature	N	Minimum	Maximum	Mean	Std. Deviation	Variance
C1	30	.000	1.000	.45750	.261814	.069
C2	30	.000	1.000	.41753	.279961	.078
C3	30	.000	1.000	.21133	.244939	.060
C4	30	.000	1.000	.53641	.238824	.057
C5	30	.000	1.000	.36878	.230261	.053
L8	30	.000	1.000	.29044	.283506	.080
L14	30	.000	1.000	.45677	.206628	.043
L15	30	.000	1.000	.43133	.222297	.049
Valid N (listwise)	30					

showed small variance in standard deviation between arteries and veins.

4.3.2 Correlation analysis

Correlation analysis, as defined by Gosling [39] is concerned with determining the extent to which the variables of interest are related. It is a procedure that provides a measure of the relative strength of the relationship between features. The most popular correlations are: Pearson's Correlation Coefficient, which is a measure of

Table 4.9: This table shows the descriptive statistical analysis of the Fourier Transform analysis features of the artery segments

Descriptive Statistics

Feature	**N**	**Minimum**	**Maximum**	**Mean**	**Std. Deviation**	**Variance**
F1	30	.000	1.000	.354	.248	.061
F2	30	.000	1.000	.208	.221	.049
F3	30	.000	1.000	.195	.185	.034
F4	30	.000	1.000	.246	.242	.059
F5	30	.000	1.000	.134	.176	.031
F6	30	.000	1.000	.155	.200	.040
F7	30	.000	1.000	.212	.199	.040
F8	30	.000	1.000	.214	.200	.040
F9	30	.000	1.000	.385	.246	.060
F10	30	.000	1.000	.430	.242	.059
F11	30	.000	1.000	.319	.385	.031
F12	30	.000	1.000	.353	.257	.066
F13	30	.000	1.000	.207	.180	.033
F14	30	.000	1.000	.068	.180	.032
F15	30	.000	1.000	.133	.176	.031
F16	30	.000	1.000	.105	.181	.033
F17	30	.000	1.000	.214	.201	.041
F18	30	.000	1.000	.265	.413	.171
F19	30	.000	1.000	.659	.205	.042
F20	30	.000	1.000	.227	.175	.030
F21	30	.000	1.000	.603	.438	.192
F22	30	.000	1.000	.147	.175	.031
F23	30	.000	1.000	.270	.421	.177
F24	30	.000	1.000	.203	.194	.038
Valid N (listwise)	30					

the tendency of two variables to rise and fall in relation to each other; and Spearman's Correlation Coefficient, in which the rank of data is calculated, and then the correlation is taken from the ranked data instead of the real data. Since the tortuosity grading is ranked from non to most tortuous, the latter analysis was used. The next sections detail the Spearman's Rank Correlation Coefficient analysis between the groups' features and the clinical order of tortuosity.

Table 4.10: This table shows the descriptive statistical analysis of the Fourier Transform analysis features of the vein segments

Descriptive Statistics

Feature	N	Minimum	Maximum	Mean	Std. Deviation	Variance
F1	30	.000	1.000	.281	.247	.061
F2	30	.000	1.000	.160	.241	.058
F3	30	.000	1.000	.273	.253	.064
F4	30	.000	1.000	.217	.261	.068
F5	30	.000	1.000	.271	.231	.054
F6	30	.000	1.000	.203	.257	.066
F7	30	.000	1.000	.260	.276	.076
F8	30	.000	1.000	.256	.273	.075
F9	30	.000	1.000	.312	.250	.063
F10	30	.000	1.000	.375	.272	.074
F11	30	.000	1.000	.205	.258	.067
F12	30	.000	1.000	.448	.282	.080
F13	30	.000	1.000	.416	.254	.065
F14	30	.000	1.000	.291	.242	.058
F15	30	.000	1.000	.341	.252	.064
F16	30	.000	1.000	.161	.237	.056
F17	30	.000	1.000	.263	.274	.075
F18	30	.000	1.000	.583	.424	.179
F19	30	.000	1.000	.551	.199	.039
F20	30	.000	1.000	.460	.265	.070
F21	30	.000	1.000	.415	.454	.207
F22	30	.000	1.000	.371	.260	.068
F23	30	.000	1.000	.552	.432	.187
F24	30	.000	1.000	.237	.246	.061
Valid N (listwise)	30					

Spearman's rank correlation coefficient of the structural properties features and the clinical order

This is the Spearman's Rank Correlation Coefficient of the structural properties features of the arteries and veins segments, and the clinical order. It reveals that the arteries group were more correlated to the clinical order values, than the veins. The sum of the sub-curves heights (S5) was the highest positive correlated feature

Table 4.11: Spearman's rank correlation coefficient of the structural properties features of the artery and vein segments

Measure	**Arteries**	**Veins**
Sub-curves numbers (S1)	.550	.478
Number of maximum points (S2)	.615	.494
Number of minimum points (S3)	.597	.355
Sum of sub-curves under spaces (S4)	-.466	-.309
The sum of sub-curves heights (S5)	.826	.589

in both groups with $RHO = .826$ ($p < .05$) and $RHO = .589$ ($p < .05$) for the artery and vein groups respectively. The number of the maximum points along a blood vessel segment was also highly, positively correlated with the clinical order in the arteries. However it was moderately correlated in the veins group. See Table 4.11 for the Spearman's Rank Correlation Coefficient of this group and the clinical order.

Spearman's rank correlation coefficient of the distance approach features and the clinical order

In general, the arteries measures were more correlated to the clinical order, compared to the veins. In the arteries group the following features: length differences between path and chord length (L7), length differences between arc and chord length (L6), Arc over chord length (L4), path over chord length (L5), segment arc length (L2) and segment path length (L3), were highly positively correlated with the clinical order with $RHO = .853$ ($p < .05$), $RHO = .816$ ($p < .05$), $RHO = .816$ ($p < .05$), $RHO = .853$ ($p < .05$), $RHO = .729$ ($p < .05$) and $RHO = .739$ ($p < .05$) respectively. Whereas the same features analysed using the veins' measurements, showed weak to moderate correlations except of the length difference between the path length and the chord length (L7) with $RHO = .608$ ($p < .05$), see Table 4.12 for the Spearman's coefficient rank correlation between the distance based features and the clinical order.

Table 4.12: Spearman's rank correlation coefficient of the distance approach features and the clinical order of the artery and vein segments

.

Measure	**Arteries**	**Veins**
Segment chord length (L1)	-.478	-.233
Segment arc length (L2)	.729	.265
Segment path length (L3)	.739	.266
Arc over chord length (L4)	.816	.608
Path over chord length (L5)	.853	.630
Length differences between arc and chord length (L6)	.816	.761
Length differences between path and chord length (L7)	.853	.608

Spearman's rank correlation coefficient of the curvature approach features and the clinical order

Both groups were found to be correlated to the clinical order. In the artery group, Rashmi's Tortuosity measure (L9), total squared unsigned curvature over chord length (31), total squared unsigned curvature (L28), mean direction angle change (13) and the total unsigned curvature over chord length (27) were highly correlated to the clinical order with $RHO = .898$ ($p < .05$), $RHO = .736$ ($p = .44$), $RHO = .731$ ($p < .05$), $RHO = -.707$ ($p < .05$) and $RHO = .724$ ($p < .05$) respectively. The remaining features showed moderate to weak correlations with the clinical order. On the other hand, the Abs slope difference and unsigned curvature (C6), total squared unsigned curvature over the chord length (31) and Rashmi's Tortuosity measure (L9) were the highest correlated features in the vein group with $RHO = .810$ ($p < .05$), $RHO = .793$ ($p < .05$) and $RHO = .800$ ($p < .05$) respectively, [for more details see Table 4.13].

Spearman's rank correlation coefficient of the combined approach features and the clinical order

Both groups showed various strength of correlations, however the path over chord times number of maximum points feature (C3) reported the highest correlation value in the artery group with $RHO = .920$ ($p < .05$). Whereas, the path length and sub-

Table 4.13: Spearman's rank correlation coefficient of the curvature approach features and the clinical order of the artery and vein segments

.

Measure	**Arteries**	**Veins**
Total signed curvature (L16)	.144	-.145
Total squared signed curvature (L20)	.230	.126
Total unsigned curvature (L24)	.731	.789
Total unsigned curvature over Path length (L25)	.659	.766
Total squared signed curvature over arc length (L21)	.212	.117
Total unsigned curvature over arc length (L26)	.673	.765
Total squared signed curvature over path length (L22)	.212	.177
Total unsigned curvature over chord Length (L27)	.724	.797
Total squared signed curvature over chord Length (L23)	.230	.139
Tortuosity coefficient (L10)	.506	.399
Unsigned tortuosity slope (L11)	.485	.028
Signed tortuosity slope (L12)	-.257	.391
Mean direction angle change (L13)	-.707	-.727
Rashmi's Tortuosity measure (L9)	.898	.800
Total signed curvature over Path length (L17)	.134	-.140
Total signed curvature over Arc length (L18)	.134	-.147
Total squared unsigned curvature (L28)	.731	.788
Total squared unsigned curvature over path length (L29)	.710	.778
Total squared unsigned curvature over arc length (L30)	.704	.780
Total signed curvature over chord length (L19)	.144	-.154
Total squared unsigned curvature over chord length (L31)	.736	.793
Abs slope difference and unsigned curvature (C6)	.385	.810

curves number (C5) reported the highest correlation in vein group with $RHO = .739$ ($p < .05$). C3 is the highest correlated feature, to the clinical order, among all other tortuosity evaluation approaches for the artery segments. [For more details see Table 4.14].

Table 4.14: Spearman's rank correlation coefficient of the combined approach features and the clinical order of the artery and vein segments

.

Measure	**Arteries**	**Veins**
Tortuosity measure by Grisan (L8)	.752	-.233
Inflection Count Metric using arc length (L14)	.406	.265
Inflection Count Metric using path length (L15)	.405	.266
Vessel profile 2 (C2)	.826	.608
Arc over chord times number of maximum points (C4)	.651	.630
Path length and sub-curves number (C5)	.743	.761
vessel profile 1 (C1)	-.466	.608
Path over chord times number of maximum points (C3)	.920	.608

Spearman's rank correlation coefficient of the Fourier Transform approach features and the clinical order

Both group showed various strength of negative and positive correlations to the clinical order. The highest correlated features in both groups were the DFT measures and curvature using points displacement (F2) with $RHO = .804$ ($p < .05$) for the arteries and the DFT Measures and curvature using xPrime (F6) with $RHO = .752 (p < .05)$. [For more details see Table 4.15].

Spearman's correlation results

The Spearman's correlation analysis revealed a number of strong features, that were able to predict the clinical order with very high performances. At the level of the features groups, the combined approach features included the highest performed for the arteries, with feature C3 reporting 92%. On the other hand, the curvature approach features included the highest performed feature for the veins, C6 reporting .81%. During the course of this statistical analysis, it has been observed that most of the framework features did not perform equally for arteries and veins. In particular, most features reported high performances with the arteries, however, they drastically underperformed with the veins. This is also has been noticed with previous studies in the literature, refer to Section 2.7. I believe this is very interesting marker that

Table 4.15: Spearman's Rank correlation coefficient of the Fourier Transform features and the clinical order for the artery and vein segments. DFT: Discrete Fourier Transform, Mag: Magnitude, xPrime: The first derivatives of the x axis, xSec: The second derivatives of the x axis, Norm: Normalised

Measure	**Arteries**	**Veins**
DFT Measures and Path Over Chord using displacement points (F1)	.747	.600
DFT measures and curvature using points displacement(F2)	.804	.728
DFT Measure using Path Over Chord and xPrime (F3)	.740	.538
DFT Measures and curvature using xPrime (F4)	.749	.729
DFT Measures and Path Over Chord using xsec (F5)	.607	.673
DFT Measures curvature using xsec (F6)	.751	.752
DFT Measures and Path Over Chord using curvature (F7)	.599	.667
DFT Measures and curvature using curvature (F8)	.600	.661
Sum of DFT Mag using points displacement (F9)	.711	.597
The sum of DFT Mag norm By Path Length using displacement points (F10)	.661	.606
DFT Power norm by path length using displacement points (F11)	.333	.482
DFT Power using xprime (F12)	-.502	-.725
DFT Mag using xprime (F13)	.649	.492
DFT Power using xsec (F14)	.005	-.071
DFT Mag xsec (F15)	.527	.656
DFT Power using curvature (F16)	.635	.619
DFT Mag using curvature (F17)	.612	.666
Sum of signal phases norm by path length using displacement points (F18)	.042	-.414
Sum of the signal phases norm by Path Length using xPrime (F19)	-.189	.220
Sum of Mag norm by path Length using xPrime (F20)	.426	.442
Sum of phases norm by path length using xsec (F21)	-.298	-.051
Sum of Mag norm by path length using xsec (F22)	.652	.386
Sum of signal phases norm by path length using curvature (F23)	-.107	-.297
Sum of Mag norm by path length using curvature (F24)	.547	.673

leads to the fact that, there are differences with the arteries and veins, especially in tortuosity. In conclusion, comparing my proposed features' performances to the literature ones, four out of five best performed features, for the veins, were proposed in this study (S5, C6, C5, F6), and three out of five best performed, for the arteries, were also proposed in this study (F2, C3, S5).

4.3.3 Regression analysis

In statistics, regression is a technique for estimating the relationship between two or more variables. It is used to examine the nature of a relationship between a dependent and an independent variable. It can also be used to predict the dependent variable when the independent variable is known.

Linear regression is normally used to model the relationship between two continuous variables. This relationship might be positive, negative or non-relational. The strength of the relationship is usually reported as weak, moderate or strong. However, in multiple regressions as described by [34] a number of independent variables are used to predict the dependent variable. In this study, all the tortuosity framework's features were used to predict the clinical order of vessels tortuosity; the regression analyses methods used were stepwise, backward and forward feed analysis. These analyses were conducted separately for the artery and vein groups as following:

Stepwise analysis

A multiple linear regression using stepwise analysis was run for both arteries and veins groups to predict the clinical order, using the proposed framework features, which consists of over 60 features. The arteries test revealed that the path over chord ($\beta = .836$, $p = 0.00$), DFT power using xprime ($\beta = -.329$, $p = .001$) and the tortuosity coefficient ($\beta = 0.324$, $p = .009$) were the only significant predictors. The stepwise analysis of this group produced three models, which showed a strong multiple correlation of $R = .836$, $R = .893$ and $R = .919$; and coefficient of determination of $R^2 = .698$, $R^2 = .797$ and $R^2 = .844$ by model one, two and three respectively. Model three indicated that around 84% of the variation in the clinical order (the ophthalmologist grading order), could be accounted for or predicted by combining the three significant predictors. [See figure 4.11 for the model summary]. Whereas the mean direction angle change and the sum of sub-curves under spaces with ($\beta = -.710$, $p = 0.00$) and ($\beta = -.327$, $p = 0.009$) were the only significant predictors in the veins group. The overall models fit of the veins segments were $R^2 = 0.533$, and $R^2 = 0.639$, and multiple correlation of $R = .730$, $R = .800$ for resulted models one and two respectively. [See Figure 4.12 for the model summary

].

Model Summary

Model	R	R Square	Adjusted R Square	Std. Error of the Estimate
1	.836[a]	.698	.687	.169711
2	.893[b]	.797	.781	.141902
3	.919[c]	.844	.826	.126700

a. Predictors: (Constant), 'Path over chord15'

b. Predictors: (Constant), 'Path over chord15', 'DFT Power using xprime64'

c. Predictors: (Constant), 'Path over chord15', 'DFT Power using xprime64', 'Tortuosity coefficient16'

Figure 4.11: Model summary of a multiple linear regression stepwise analysis-arteries

Model Summary

Model	R	R Square	Adjusted R Square	Std. Error of the Estimate
1	.730[a]	.533	.516	.211423
2	.800[b]	.639	.613	.189185

a. Predictors: (Constant), 'Mean direction angle change20'

b. Predictors: (Constant), 'Mean direction angle change20', 'Sum of sub-curves under spaces25'

Figure 4.12: Model summary of a multiple linear regression stepwise analysis-veins

Forward feed analysis

The model summary of the multiple linear regression using forward feed analysis, on the framework, of the arteries segments showed a strong multiple correlation; three models were produced of $R = 0.836$, $R = 0.893$ and $R = 0.919$; and coefficient of determination of $R^2 = .698$, $R^2 = .797$ and $R^2 = .844$ respectively. The third summary indicated that around 84% of the variation in the clinical order (the ophthalmologist grading order), could be accounted for or predicted by each of the path over chord feature, ($beta = .495$, $p = 0.00$), DFT power using xprime ($beta = -.472$, $p = .000$) and the tortuosity coefficient ($beta = .324$, $p = .009$) which were the only

significant predictors. [See figure 4.13 for the model summary]. The forward feed analysis of the veins segments produced two models; the first model consisted of a single feature, which is the mean direction angle change, whereas the other model included the mean direction angle change combined with the sum of sub-cures under spaces as the only significant predictors. The overall models fit of the veins segments were $R^2 = .533$, and $R^2 = .639$ and multiple correlation of $R = .730$ and $R = .800$ for model one and two respectively. [See Figure 4.14 for the model summary].

Model Summary

Model	R	R Square	Adjusted R Square	Std. Error of the Estimate
1	.836[a]	.698	.687	.169711
2	.893[b]	.797	.781	.141902
3	.919[c]	.844	.826	.126700

a. Predictors: (Constant), 'Path over chord15'

b. Predictors: (Constant), 'Path over chord15', 'DFT Power using xprime64'

c. Predictors: (Constant), 'Path over chord15', 'DFT Power using xprime64', 'Tortuosity coefficient16'

Figure 4.13: Model summary of a multiple linear regression forward feed analysis-arteries

Backward feed analysis

Multiple linear regression using backward feed analysis applied to the proposed tortuosity evaluation framework, to predict the clinical order, revealed that there are twenty nine significant predictors in the arteries group. The model summary of the arteries showed a strong multiple correlation of $R = 1.000$; and coefficient of determination of $R^2 = .698$. The model summary indicated that 100% of the variation in the clinical order (the ophthalmologist grading order) could be accounted for or predicted by combining the twenty nine identified significant predictors from

Model Summary

Model	R	R Square	Adjusted R Square	Std. Error of the Estimate
1	.730[a]	.533	.516	.211423
2	.800[b]	.639	.613	.189185

a. Predictors: (Constant), 'Mean direction angle change20'

b. Predictors: (Constant), 'Mean direction angle change20', 'Sum of sub-curves under spaces25'

Figure 4.14: Model summary of a multiple linear regression forward feed analysis-veins

the proposed framework. See figure 4.15 for the model summary. In the vein group a different set of twenty nine features were also identified as significant predictors using backward feed analysis. The overall model fit of the veins segments was $R^2 = 1.000$, and multiple correlation of $R = 1.000$. See Figure 4.16 for the model summary.

4.3.4 Machine learning analysis

Introduction

The issue is to predict the order of number of blood vessels that have been previously ordered, in increased tortuosity, by an expert ophthalmologist, given a number of blood vessels features. In other words, is to predict some output y (the clinical order) given an input x (the framework features) The objective of this, is to identify best feature/features that are good at estimating tortuosity.

Data

Data is very important factor when it comes to models training in various machine learning approaches. In this analysis, 66 tortuosity estimation features of 30 artery and 30 vein segments (RVTDS) were used to train the ANN and RF models. Since the input (66 features) and the output (Clinical order) are known, this is considered

Model Summary

Model	R	R Square	Adjusted R Square	Std. Error of the Estimate
1	1.000[a]	1.000	.	.

a. Predictors: (Constant), 'DFT Mag using curvature69', 'DFTPower norm by path length uing displacement points61', 'Signed tortuosity slope18', 'Tortuosity coefficient16', 'vessel profile1-path over chord add the sum of sub-curves space46', 'Rashmis Tortuosity measure29', 'Tortyosity by Grisan21', 'DFT Power using xsec66', 'Toatl signed curvature over Arc length33', 'Segments chord length2', 'DFT Power using xprime64', 'Iflection Count Metric using path length27', 'Unnsigned tortuosity slope17', 'The sum of subcurves Heights43', 'Total squared unsigned curvature over arc length36', 'Total squared signed curvature4', 'Number of maximum points on a segment23', 'The sum of DFT Mag norm By Path Length using displacement points 60', 'DFT Mag using xprime65', 'DFT Power using curvature68', 'Number of minimum points on a segment24', 'DFT measures and curvture using points displacement 51', 'DFT Measures curvture using xsec55', 'DFT Mag xsec67', 'length difference between Path and chord31', 'Path over chord times maximapoints47', 'length difference between Arc and Chord30', 'Mean direction angle change20', 'Total unsigend curvture over chord Length12'

Figure 4.15: Model summary of a multiple linear regression using backward analysis-arteries

as a supervised classification problem. Most of the classification attempts in the literature, whether were supervised or unsupervised learning, were based on two or three class classification, such as tortuous and non-tortuous. [See Section 2.10 for data analysis methods used to grade and test tortuosity]. The features are scaled to take values between 0 and 1. The next sections detail the building of the ANN and RF models.

ANN analysis

ANN structure The following are the elements of the ANN structure: A) The ANN used was constructed of an input layer, that includes 66 inputs x_i. B) an output layer that include 30 outputs $\widehat{y_i}$, which is an estimate of y. C) a single hidden layer that include 30 hidden units. D) neurons are activated by a logistic

Model Summary

Model	R	R Square	Adjusted R Square	Std. Error of the Estimate
1	1.000[a]	1.000	.	.

a. Predictors: (Constant), 'DFT Mag using curvature69', 'DFT Power using xsec66', 'Unnsigned tortuosity slope17', 'DFTPower norm by path length uing displacement points61', 'Sum of sub-curves under spaces25', 'Total signed curvature over Path length32', 'Rashmis Tortuosity measure29', 'Tortuosity coefficient16', 'Iflection Count Metric using arc length26', 'Tortyosity by Grisan21', 'DFT Mag using xprime65', 'Total squared signed curvature4', 'DFT Power using xprime64', 'Segments chord length2', 'The sum of subcurves Heights43', 'length difference between Path and chord31', 'Number of minimum points on a segment24', 'DFT measures and curvture using points displacement 51', 'Signed tortuosity slope18', 'DFT Mag xsec67', 'Arc over chord times Maximum points44', 'The sum of DFT Mag norm By Path Length using displacement points 60', 'DFT Power using curvature68', 'Mean direction angle change20', 'Total unsigned curvature over arc length10', 'Path over chord times maximapoints47', 'DFT Measures and curvture using slope49', 'length difference between Arc and Chord30', 'DFT Measures curvture using xsec55'

Figure 4.16: Model summary of a multiple linear regression using backward analysis-veins

activation function. [See Figure 4.17 for an example of a neuron].

ANN model analysis At the input layer the neurons take the weighted sum of the inputs x_i, which are the blood vessel segments' measurements $30x66$. These are then passed into the activation function to produce a predicted grade of these segments. In order to obtain an accurate tortuosity prediction for the blood vessels segments, a learning algorithm is needed. This algorithm will modify the weights of the connections according to the input patterns which the neuron is presented with. Backpropagation with the gradient descent learning rule, as an optimization method, is used in the learning of the neuron. Given the type of the dataset, the learning was supervised. Generally, in artificial neural networks, there are two different approaches to models training. 1) On-line training mode; here the weights are optimized in each case and in each epoch. On-line training mode characterised

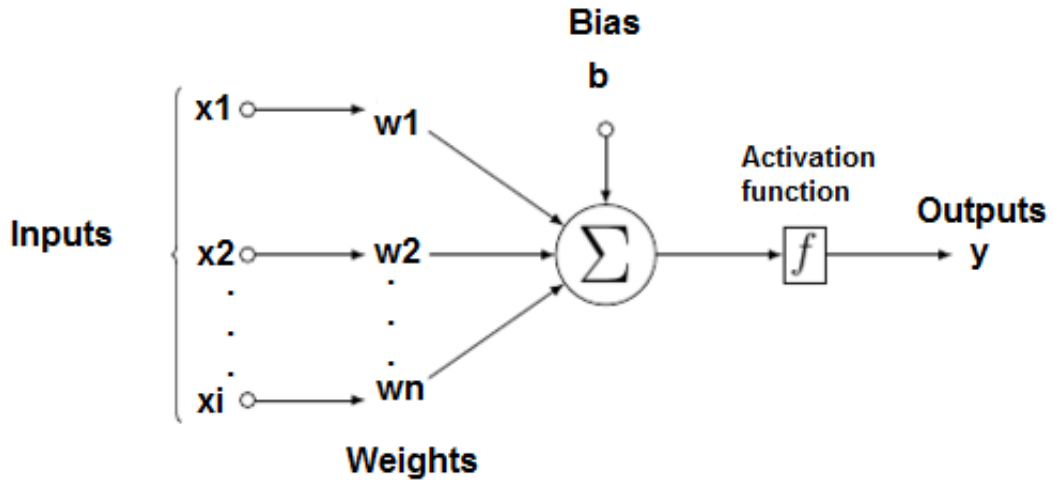

Figure 4.17: This graph shows a single node structure

by its speed and also found to be less prone to local minima. 2) Patch mode, in which at each epoch the weights are adjusted once at the end of the epoch. Given the nature of the available dataset, patch mode was used in the learning of the neuron (Training testing and validation are in section 4.3.4). As previously indicated the backwards propagation of error (BACKPROPAGATION) algorithm was used in the neuron learning. This performs a gradient descent within the solution's vector space, which is the clinical order, towards a minimum error. Initially, the learning of the neuron starts with initial random weights for each input. Since the target output (The manual clinical grading) is ranked the Spearman's Rank Correlation Coefficient was used to test the performance of the neuron. Spearman's Rank correlation analysis was conducted between the first predicted output, which is calculated using the initial random weights, and the targeted or desired output (the clinical grading) to assess the initial performance of the neuron. Subsequently, the predicted output is passed through the optimization algorithm (the gradient descent learning rule) to minimize the error, which is the difference between the desired and predicted output. The neuron learning continues, with optimizing the weights to reduce the error.

Leave-One-Out cross validation (L-O-OUT) method was used to test and validate the model. This approach was adopted because of the small size of the

used dataset, which is not sufficient for training and testing. By doing so, model over-fitting can be avoided. Over fitting is the case when the whole data is used to fit the model and used at the same time to assess the model. Therefore, since the number of the cases (segments) in the dataset for each group (veins and arteries) are thirty segments; the training and testing using leave-one-out cross validation was conducted as follows: It starts by; isolating one of the thirty segments to be used at the end of the training for testing. The remaining twenty nine segments are used for learning or training of the neuron. The training runs through n number of epochs, in which the gradient descent, learning algorithm, runs for 29 times, on the 29 segments. At each cycle (epoch) a learning rate was used. Twenty nine weights are produced by this stage. These weights are then averaged and saved to be used as initial weights for the next cycle of training. These average weights are also used to calculate the predicted output of the left out input (segment) by taking Spearman's Rank Correlation between the desired output of the isolated segment and its calculated predicted output. The average weights and the Spearman's Rank Correlation results (RHO) of all the epochs cycles for the segment were saved, to be used at the final testing phase. The learning rate is reset at the end of each epoch. At the end of the epoch cycles the maximum reported RHO is identified as well as its equivalent weights, which are then used in the testing of the left-out case to calculate the predicted output. This process continues until all the left-out segments are tested, by using the produced best weights in the training process. Finally, all of the predicted output of the left-out cases will be tested with regard to their desired outputs using Spearman's Rank Correlation Coefficient to produce the final performance of the neuron. See Appendix .3, section .3.2 for the learning algorithm.

ANN analysis results The proposed framework was trained and tested using leave-one-out cross validation. The analysis initially was performed on the five feature groups discussed above. The combined and distance approach features of the arteries group, reported the highest performance of $RHo = .8611$, $Error = .0297$ and $RHo = .8611$, $Error = .0328$ respectively. Whereas the Fourier Transform features reported the lowest performance of $RHo = .7076$ and $Error = .057$. See figures **??** and 4.19 for the combined and distance approach features analysis using

Leave-One-out. On the other hand, in the veins group the curvature approach features and the proposed features reported the highest performance of $RHo = .7307$ with $Error = .0467$, and $RHo = .7124$ with $Error = .0.0683$, respectively; whereas the distance approach measures reported the lowest performance of $RHo = .5754$ with $Error = .0676$, (refer to table 4.16 for more details).

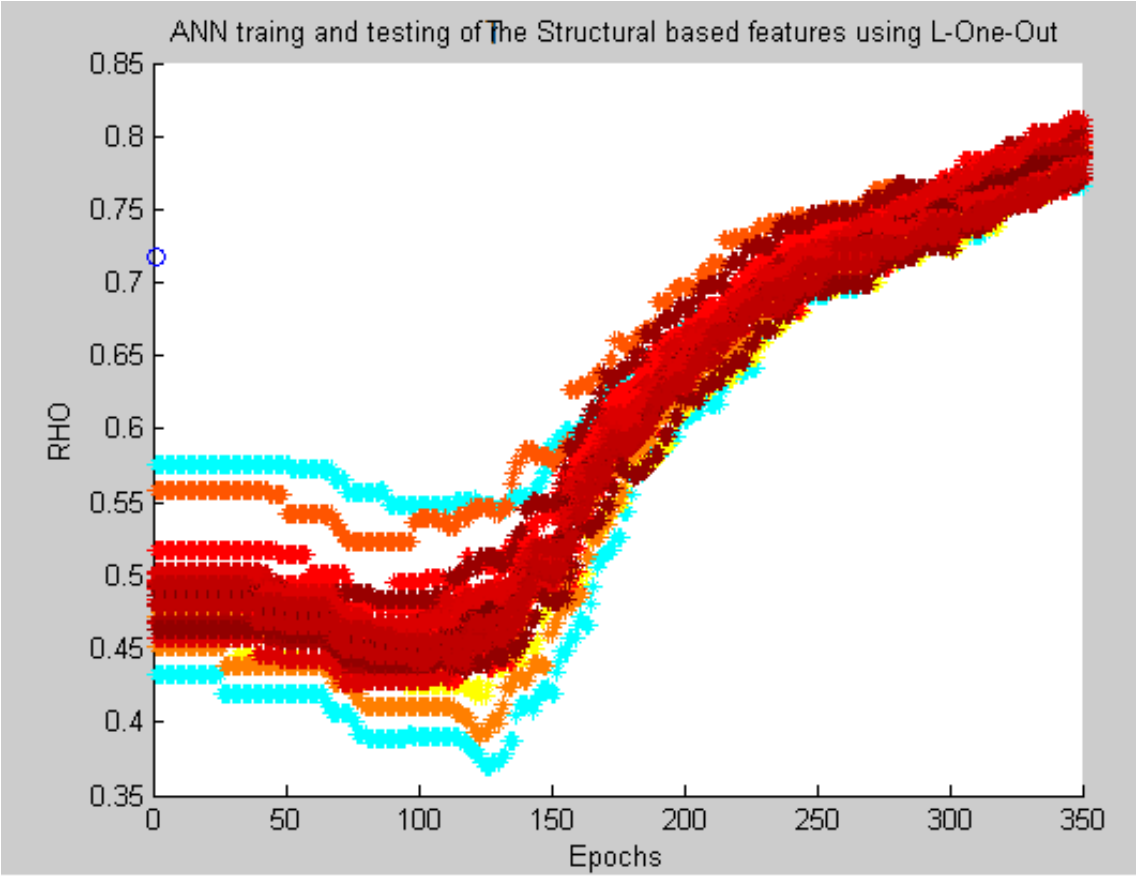

Figure 4.18: This graph shows ANN training and testing using the leave one out cross validation of the structural properties features: Coloured lines represent segments, and stars represent performances on training cycles.

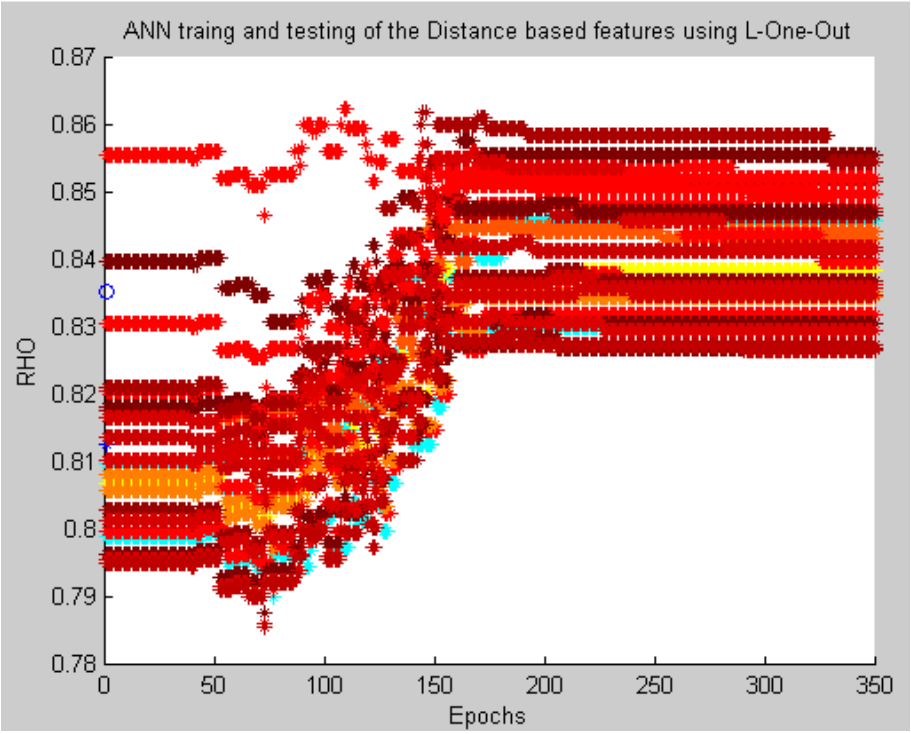

Figure 4.19: This graph shows ANN training and testing using the leave one out cross validation of the distance approach features: Coloured lines represent segments, and stars represent performances on training cycles.

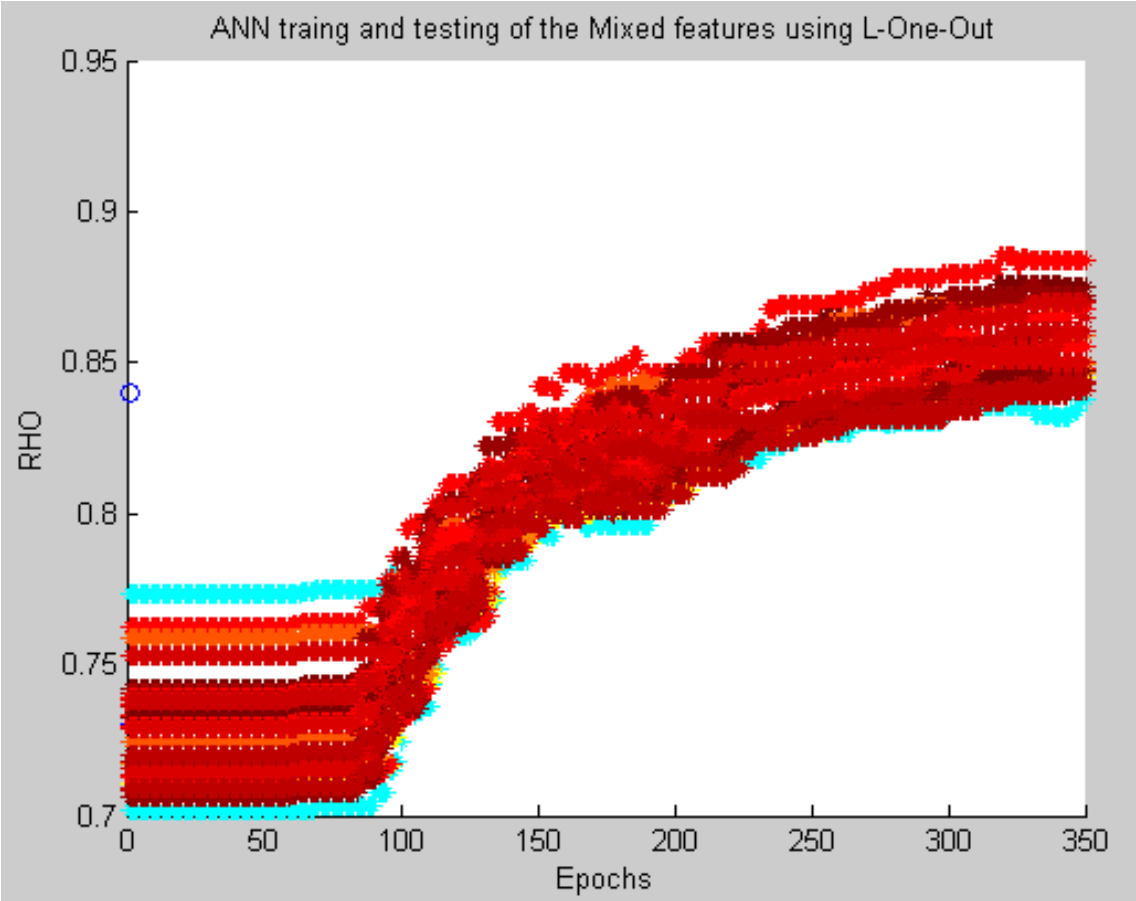

Figure 4.20: This graph shows ANN training and testing using the leave one out cross validation of the combined approach features: Coloured lines represent segments, and stars represent performances on training cycles.

Table 4.16: The artificial neural network analysis of the proposed tortuosity evaluation framework features groups

Feature group	Arteries	Error	Veins	Error
Structural Properties	0.765	0.0531	0.5818	0.0699
Distance approach	0.861	0.0328	0.5754	0.0676
Curvature approach	0.738	0.0446	0.7307	0.0497
Combined approach methods	0.861	0.0297	0.6241	0.6241
Fourier Transform features	0.707	0.057	0.7124	0.0683

Random Forests analysis

RF structure and analysis Random Forests analysis for regression was conducted using Matlab *fitensemble* function. The function takes the input features x_i, desired outputs y_n, the method of classification, learning cycles and trees specifications. Random number of trees were used to analyse the proposed tortuosity framework features to assess their ability to accurately estimate the degree of retinal blood vessel segments increased tortuosity. similar to ANN, at the end of training and testing Spearman's rank correlation is conducted between the predicted and desired output.

RF analysis results The analysis was conducted first for all feature groups in the proposed tortuosity framework. Then, Random Forests analysis was carried out on best feature subsets that are selected through feature selections from the proposed framework. In both groups (Arteries and Veins) the combined approach methods reported the highest performance among the framework's feature groups with $RHO = .814$. The structural properties reported the highest performance in the veins group with $RHO = .689$, whereas the curvature and the Fourier Transform features were among the highest performers in the arteries group with $RHO = .748$ and $RHO = .780$ respectively. [See figures 4.21 and 4.22]. On the other hand, the distance approach measures reported the lowest performance in both groups with $RHO = .664$ for the arteries, $RHO = .285$ for the veins. [Refer to table 4.17 for more details].

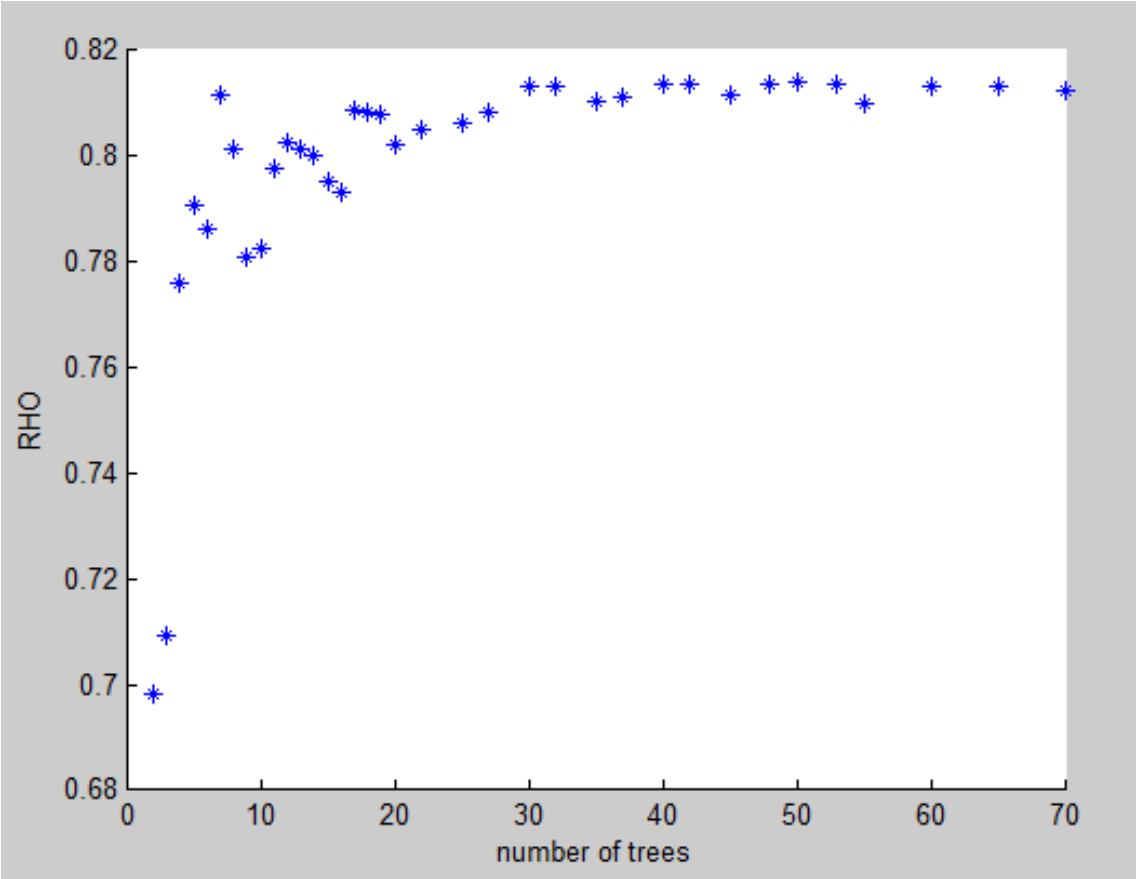

Figure 4.21: This graph shows RF training and testing using the leave one out cross validation of the combined approach features of the arteries

Table 4.17: Randome forest analysis of the proposed tortuosity evaluation framework's features

Features group	**Arteries**	**Veins**
Structural properties features	0.7059	0.689
Distance approach features	.664	.285
Curvature approach features	.748	.507
Combined approach features	.814	.517
Fourier Transform features	.780	.536

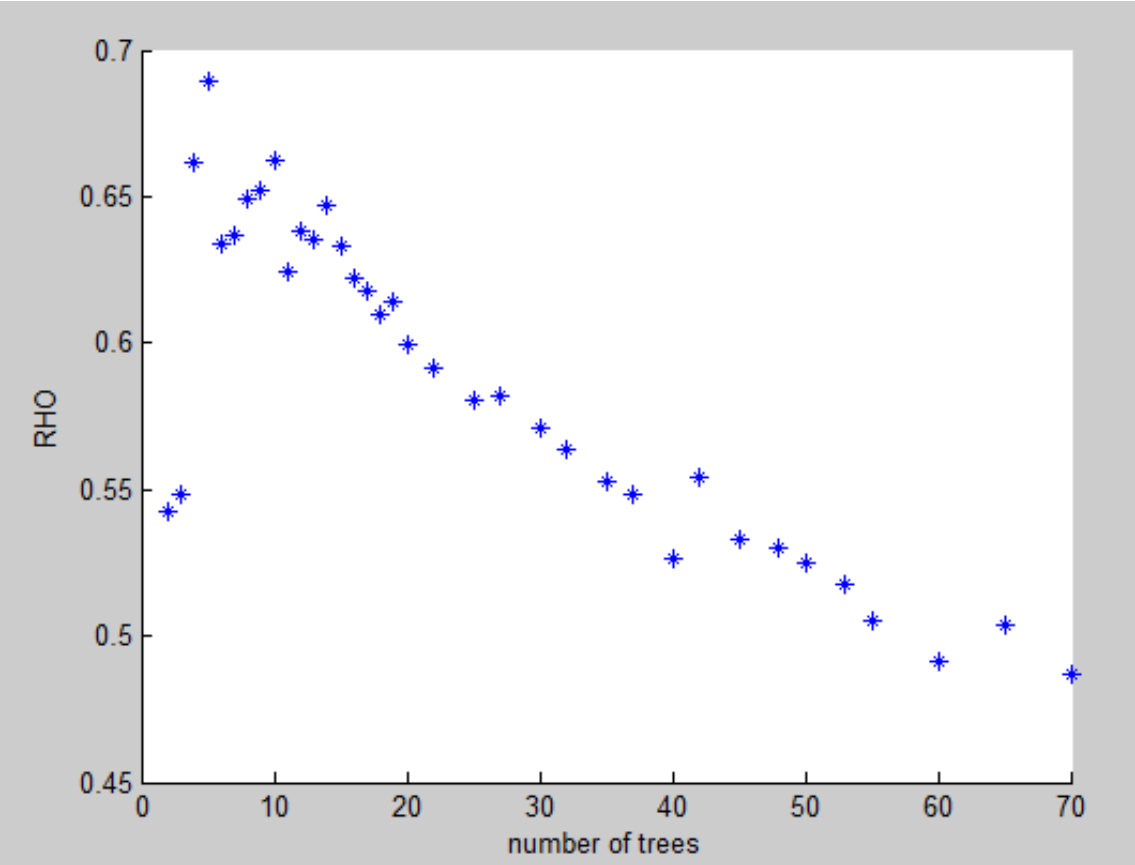

Figure 4.22: This graph shows RF training and testing using the leave one out cross validation of the structural properties features of the veins

4.3.5 Feature selection

Feature selection, or subset selection, is a process used in machine learning, in which a subset of the whole available data is selected for application of learning algorithm. It is one of the model construction stages in which a subset or subsets are selected for the use of training and testing of the model. The best subset contains the least number of dimensions that mostly contribute to accuracy. The remaining unimportant dimensions are then discarded [78].

Feature selection methods

There are three general approaches in feature selection: Filter methods, Wrapper methods and Embedded methods. 1) Filter methods select subsets of variables or features as a pre-processing step, independently of the chosen predictor. Examples of these methods include Information gain, Chi squares test and Correlation Coefficient

scores. 2) Wrapper methods utilize the learning machine of interest as a black box to score subsets of variables according to their predictive power, such as recursive feature elimination algorithms like forward and backward passes to add and remove features.3) Embedded methods perform variable selection in the process of training and are usually specific to given learning machine. Example of these methods are Ridge Regression and Elastic Net[45].

Feature selection implementation

To take advantage of the different available tortuosity features in an effective way, and to reduce the risk of over fitting the model from the large number of features a feature selection mechanism is needed. This mechanism is intended to sift through features to identify the strongest feature or sets of features, by which features dimensionality can be reduced and classifiers performances (ANN and the Random forest) could be improved. Two approaches of feature selection were used; Forward selection and Backward selection. Forward selection starts with no variables and adds them one by one at each step, adding the one that decreases the error the most, until any further addition does not significantly decrease the error; whereas Backward selection starts with all the variables and removes them one by one, at each step removing the one that decreases the error the most, or increases it only slightly, until any further removal increases the error significantly. To reduce over fitting, the error referred to above is the error on a validation or testing set that is distinct from the training set [78]. SPSS Linear regression using Backward and Forward feed was used to select the feature subsets for the purpose of training and testing classifiers to evaluate tortuosity. To avoid bias in these processes , for example using the whole data to select subset of features, the following steps were followed:

- Using the 30 segments of arteries and 30 segments of veins in the RVTDS dataset; 30 sets of features for each group were selected using Leave-one-out, (this means that a set of features would be selected without one of the segments in each cycle). This has been done to avoid bias in the feature selection.

- These sets of features or variables, were then used to train the ANN and RF, using Leave-one-out cross validation, to test the performances against the

clinical order. These tests were performed by Spearman's Rank Coefficient Correlation. Using artificial neural networks, the training and testing of the feature sets selected through forward feed analysis for the arteries group reported high positive correlation of $RHO = 0.981, Error = 0.193$, whereas, for the veins, it achieved $RHO = 0.904$, $Error = 0.120$. The variable sets selected through backward feed analysis for the arteries and veins showed positive correlation of $RHO = 0.770$, $Error = 0.306$ and $RHO = 0.838$, $Error = 0.283$ for the artery and vein groups respectively. On the other hand, the Random Forests analysis of the selected features reported various strength of positive correlations among both groups. The features of the forward-feed for the arteries reported a positive corroboration of $RHO = 0.707$ and reported $RHO = 0.533$ for the veins, whereas the features of the backward-feed reported a positive correlation of $RHO = 0.761$ for the arteries and $RHO = 0.629$ for the veins. In addition, the most selected features in the artery group among the feed forward features reported a high correlation of $RHO = 0.8750$, $Error = 0.037$ and mean performance of five neurons of $RHO = 0.8633$, $Error = 0.038$; same feature group of the veins reported moderate correlations of $RHO = 0.656$, $Error = 0.070$ and mean performance of five neurons of $RHO = 0.590$, $Error = 0.075$, whereas the most selected features in the backward feed of the artery showed strong to moderate correlations of $RHO = 0.749$, $Error = 0.0419$, which is the best performance of five neurons, and average performance of $RHO = 0.500$, $Error = 0.107$; same features in the vein group reported moderate correlations of $RHO = 0.653$, $Error = 0.050$, the best performance among five neurons and reached average performance of $RHO = 0.519$, $Error = 0.119$. On the other had, using RF analysis, the most selected features of the forward feed of the arteries reported $RHO = 0.870$, which is the best performance for this set, whereas it reported $RHO = 0.571$, as the best performance. The RF analysis of the most selected features of the backward feed reported $RHO = 0.828$ and $RHO = 0.663$ for the arteries and veins respectively, as best performances. [See 4.18 for more details of the classifiers analysis of the selected features sets].

- Another set of features were extracted from these subsets of features, by

Table 4.18: Neural network and Random Forests analysis of the selected sets of features using Linear Regression

.

	ANN				RF	
Features group	**Arteries**	**Error**	**Veins**	**Error**	**Arteries**	**Veins**
Forward Feed	0.981	0.193	0.904	0.120	0.707	0.533
Backward Feed	0.770	0.306	0.838	0.283	0.761	0.629

Table 4.19: Neural network and Random Forests analysis of the intersected features of the selected features using Linear Regression

.

	ANN				RF	
Features group	**Arteries**	**Error**	**Veins**	**Error**	**Arteries**	**Veins**
Forward-Feed(intersected features)	0.853	0.079	0.615	0.075	0.731	0.597
Backward-Feed(intersected features)	0.848	0.047	0.622	0.05	0.724	0.557
Forward-Feed(most selected features)	0.8750	0.0370	0.659	0.070	0.870	0.571
Backward-Feed(most selected features)	0.749	0.041	0.653	0.050	0.828	0.663

identifying the common features among these subsets of features (intersected features), which are in Appendix .3, section .3.3. These features were then analysed using the neural network and random forest. The ANN analyses of the forward-feed intersected features of the arteries and veins group showed positive correlation of $RHO = 0.853$, $Error = 0.079$ and $RHO = 0.615$, $Error = 0.283$, whereas the RF analysis for the same features and groups reported $RHO = 0.731$ and $RHO = 0.597$ for the arteries and veins respectively. On the other hand, the analyses of the intersected features of the backward-feed feature selection reported $RHO = 0.848$, $Error = 0.0471$ and $RHO = 0.622$, $Error = 0.059$. The random forest analysis for this group reported positive correlations of $RHO = 0.724$ and $RHO = 0.557$. [see table 4.19 for details.

Table 4.20: Spearman's rank correlation coefficient of the structural properties features of the artery and vein segments and the clinical order-new datasets

Measure	**Arteries**	**Veins**
Sub-curves numbers (S1)	.3677	.478
Number of maximum points (S2)	.3685	.494
Number of minimum points (S3)	.3685	.355
Sum of sub-curves under spaces (S4)	.1756	-.309
The sum of sub-curves heights (S5)	.3973	.589

4.4 Data analysis using the new tortuosity dataset

This section highlights some of the statistical analysis of the application of the proposed tortuosity evaluation framework to the new tortuosity dataset. It starts by providing the basic statistics, to identify any differences and similarities between the set of artery and vein segments in the dataset, and to monitor the measurements of individual features' measures since this dataset is characterized by segments with different lengths and calibres and to monitor their ranges and distributions. The analysis extends to include artificial neuron analysis and Random Forests. Previously trained classifiers will also be used to analyse the new tortuosity dataset data.

4.4.1 Correlation analysis

Spearman's Rank Correlation Coefficient of the structural properties features and the clinical order-new dataset

The correlation analysis between the group features and the manual clinical order, in general, was weak. The sum of sub-curves heights reported the highest correlation score in both groups with $RHO = .589$ and $RHO = .3973$ for the veins and arteries, respectively. [See table 4.20].

Table 4.21: Spearman's rank correlation coefficient of the distance based features of the artery and vein segments-new datasets

Measure	**Arteries**	**Veins**
Segment chord length (L1)	0.176	-0.073
Segment arc length (L2)	0.244	0.083
Segment path length (L3)	0.237	0.086
Arc over chord length (L4)	0.697	0.793
Path over chord length (L5)	0.676	0.800
Length differences between arc and chord length (L6)	0.6971	0.793
Length differences between path and chord length (L7)	0.676	0.800

Spearman's Rank Correlation Coefficient of the distance approach features and the clinical order-new dataset

This group showed a number of strong correlations with the manual clinical order. The Arc over chord length, Path over chord length, Length differences between arc and chord length and Length differences between path and chord length of the vein group were the highest correlated features with $RHO = 0.793$, $RHO = 0.800$, $RHO = 0.793$, $RHO = 0.800$ respectively, whereas the Arc over chord length and the Length differences between arc and chord length were the highest correlated for the arteries with $RHO = 0.697$ for both. [see table 4.21]

Spearman's Rank Correlation Coefficient of the curvature approach features and the clinical order-new dataset

The correlations of this group features were noticeably weaker compared to the same group performance on the RVTDS. The Total unsigned curvature over chord Length recorded the highest performance for the veins reaching $RHO = 0.450$ and the Total unsigned curvature reporting $RHO = 0.458$, which was the highest correlation in the artery group. [See table 4.22].

Table 4.22: Spearman's rank correlation coefficient of the curvature approach features - of the new tortuosity dataset

.

Measure	**Arteries**	**Veins**
Total signed curvature (L16)	0.139	0.044
Total squared signed curvature (L20)	0.338	0.280
Total unsigned curvature (L24)	0.458	0.406
Total unsigned curvature over Path length (L25)	0.418	0.397
Total squared signed curvature over arc length (L21)	0.328	0.275
Total unsigned curvature over arc length (L26)	0.419	0.398
Total squared signed curvature over path length (L22)	0.331	0.305
Total unsigned curvature over chord Length (L27)	0.445	0.450
Total squared signed curvature over chord Length (L23)	0.331	0.305
Tortuosity coefficient (L10)	0.203	0.209
Unsigned tortuosity slope (L11)	0.286	0.175
Signed tortuosity slope (L12)	-0.1433	-0.002
Mean direction angle change (L13)	-0.179	-0.041
Rashmi's Tortuosity measure (L9)	0.300	0.339
Total signed curvature over Path length (L17)	0.128	0.025
Total signed curvature over Arc length (L18)	0.128	0.025
Total squared unsigned curvature (L28)	0.4582	0.406
Total squared unsigned curvature over path length (L29)	0.434	0.423
Total squared unsigned curvature over arc length (L30)	0.434	0.423
Total signed curvature over chord length (L9)	0.123	0.038
Total squared unsigned curvature over chord length (L31)	0.447	0.452
Abs Slops Difference and unsigned curvature (C6)	0.418	0.318

Spearman's Rank Correlation Coefficient of the combined approach features and the clinical order-new dataset

This group features also revealed weak correlations with the clinical order. In the artery group the Path over chord times number of maximum points feature showed the highest correlation of $RHO = 0.673$, whereas it reported 0.633 for the vein. [See

Table 4.23: Spearman's rank correlation coefficient of the combined approach features and the clinical order of the artery and vein segments of the new tortuosity dataset

.

Measure	Arteries	Veins
Tortuosity measure by Grisan (L8)	0.435	0.54
Inflection Count Metric using arc length (L14)	0.240	0.088
Inflection Count Metric using path length (L15)	0.248	0.088
Vessel profile 2 (C2)	0.464	0.477
Arc over chord times number of maximum points (C4)	0.352	0.244
Path length and sub-curves number (C5)	0.244	0.086
vessel profile 1 (C1)	0.248	0.107
Path over chord times number of maximum points (C3)	0.633	0.673

table 4.23].

Spearman's Rank Correlation Coefficient of the Fourier Transform features and the clinical order-new dataset

This group also revealed large number of features with weak correlations to the clinical order, with DFT measures and curvature combined with the displacement points feature reporting $RHO = 0.470$, which is the highest correlation score in both artery and vein segments. [See table 4.24].

4.4.2 Artificial neural network analysis

The framework features were applied on the new dataset. The machine learning analysis results of the resulted data on the ANN built in section 4.3.4 were as follow: The performances of the all groups on the new dataset were noticeably weaker compared to the RVTDS. The distance approach features reported the highest performance in both groups of $RHo = .0.775$, $Error = .044$ and $RHo = .0.641$, $Error = .057$ for the arteries and veins respectively, refer to table 4.25 for detailed results.

Table 4.24: Spearman's rank correlation coefficient of the Fourier transform features and the clinical order for the artery and vein segments of the new dataset. DFT: Discrete Fourier transform, Mag: Magnitude, xPrime: The first derivatives of the x axis, xSec: The second derivatives of the x axis, Norm: Normalised

.

Measure	**Arteries**	**Veins**
DFT Measures and Path Over Chord using displacement points (F1)	0.386	0.299
DFT measures and curvature using displacement points (F2)	0.470	0.393
DFT Measures using Path Over Chord and xPrime (F3)	0.325	0.302
DFT Measures and curvature using xPrime (F4)	0.421	0.356
DFT Measures and Path Over Chord using xsec (F5)	0.324	0.302
DFT Measures of curvature using xsec (F6)	0.420	0.352
DFT Measures and Path Over Chord using curvature (F7)	0.428	0.422
DFT Measures and curvature using curvature (F8)	0.422	0.422
Sum of DFT Mag using points displacement (F9)	0.381	0.319
The sum of DFT Mag norm By Path Length using displacement points (F10)	0.381	0.319
DFT Power norm by path length using displacement points (F11)	0.264	0.175
DFT Power using xprime (F12)	0.298	0.245
DFT Mag using xprime (F13)	0.295	0.250
DFT Power using xsec (F14)	0.292	0.268
DFT Mag using xsec (F15)	0.292	0.250
DFT Power using curvature (F16)	0.412	0.372
DFT Mag using curvature (F17)	0.411	0.341
Sum of signal phases norm by path length using displacement points (F18)	-0.204	-0.024
Sum of the signal phases norm by Path Length using xPrime (F19)	-0.263	0.0183
20 Sum of Mag norm by path Length using xPrime (F20)	0.282	0.275
Sum of phases norm by path length using xsec (F21)	-0.204	-0.035
Sum of Mag norm by path length using xsec (F22)	0.271	0.267
Sum of signal phases norm by path length using curvature (F23)	-0.130	0.167
Sum of Mag norm by path length using curvature (F24)	0.400	0.377

Table 4.25: The mean performance of five artificial neurons analysis of the proposed tortuosity evaluation framework features groups on the new general dataset

.

Feature group	**Arteries**	**Error**	**Veins**	**Error**
Structural properties features	0.252	0.0921	0.363	0.13
Distance approach features	0.641	0.057	0.775	0.044
Curvature approach features	0.369	0.076	0.348	0.225
Combined approach features	0.375	0.073	0.457	0.065
Fourier Transform features	0.321	0.0807	0.362	0.0805

Table 4.26: Classifiers performances on the new dataset

.

Classifier	**Performance**
Intersected features Feed forward-arteries	0.676
Intersected features Backward-Feed arteries	0.434
Intersected features Feed-forward-veins	0.0413
Intersected features Backward-Feed-veins	0.408

4.4.3 Classifiers performances

The classifiers in section 4.3.5 were evaluated using the new tortuosity dataset. The resulted weights from the trained neurons were used to calculate the predicted output of the new dataset segments. The intersected features using forward feed of the arteries reported the highest correlation performance between the predicted output and the manual clinical order of $RHO = 0.676$, whereas the intersected features using feed forward of the veins reported the lowest performance of $RHO = 0.0413$. [See table 4.26]. On the other hand, there were a number of high positive correlations when the classifiers were tested on the RVTDS. The most selected features of the feed forward reported $RHO = 0.911$ for the arteries, and the most selected features of the backward feed reported $RHO = 0.805$ as the highest performance for the veins. [See table 4.27 for more details].

Table 4.27: Classifiers performances on the Retinal Vessel Tortuosity Dataset

.

Classifier	**Performance**
Intersected features Feed forward-arteries	0.853
Intersected features Backward-Feed arteries	0.885
Intersected features Feed-forward-veins	0.691
Intersected features Backward-Feed-veins	0.758
Most selected features Backward-Feed arteries	0.805
Most selected features Feed-forward-arteries	0.911
Most selected features Backward-Feed veins	0.805

4.5 Results and discussion

Broadly, there were variances between the framework features in terms of tortuosity evaluation performance against the clinical evaluation. The Spearman's correlation coefficient exposed a number of strong features across all feature groups. In the structural properties, the sum of sub-curves heights (S5) was the highest performed feature in both arteries and vein segments with $RHO = .826$ and $RHO = .589$ respectively, whereas in the distance approach features the path over chord ratio (L5) and the length differences between path and chord length (L7) reported the highest performance accuracy for the arteries with $RHO = .853$ for both features. However, the length differences between the arc and chord length feature (L6) reported the highest performance among the vein features with $RHO = .761$. Here, It has been observed that the measurement method of the segments length plays a significant role in tortuosity estimation accuracy, especially with the use of arc length, as found in equation 2.6. It has been noted that the performance has increased for the veins while it decreased for the arteries, and by using the path length measure the opposite occurred, [see Equation 2.5]. In the curvature approach features Rashmi's tortuosity measure (L9) [88], showed a noticeably high correlation to the clinical order in both artery and vein groups with $RHO = .898$ and $RHO = .800$ respectively. However, the absolute slopes differences and the unsigned curvature feature (C6) reported the

highest positive correlation among all the framework features with $RHO = .810$ in the vein group. This is a new feature proposed in this study, which is generated by combining the absolute differences of the slope along the blood vessel segment and the unsigned curvature at each single point. The Fourier Transform approach features have performed relatively well with the highest correlated feature for the arteries, which is the path over chord times the number of maximum points (C3) reporting $RHO = .920$, and the veins by the absolute slopes differences and the unsigned curvature (C6) with $RHO = .810$ both being from the new proposed features. The group of the Fourier transform analysis was slightly low compared with the other group, with the DFT measures and curvature using displacement points feature (F2) reporting $RHO = .804$ for the arteries and the DFT measures and curvature using the second derivatives of the x axis feature (F4) reporting $RHO = .729$.

The highest prediction accuracy reported with the multiple linear regression analysis on the framework, was with the backward feed analysis. The model summary of both groups showed that 100% of the variations in both groups can be accounted for or predicted with a different set of 29 features for each group. However, those results were biased since the same dataset (segments) were used for feature selection and testing.

With the machine learning, in general the ANN performed better than the RF analysis. With the individual groups, the distance approach features and the combined approach features reported the highest performances for the arteries, whereas with the RF the combined features and the Fourier Transform features were the highest performers. For the veins in the ANN the curvature approach features were the highest, whereas the structural properties were the highest with RF. However with feature selection, these performances were significantly improved especially with ANN.

Based on our observations, the statistical analysis on the RVTDS revealed some differences between the tortuosity estimation accuracy results of the arteries and veins. In other words, most of the tortuosity evaluation features tend to work better on grading the tortuosity of the arteries group, as opposed to veins. In addition, most of the distance approach and the combined approach features showed

the highest tortuosity evaluation accuracy compared to the rest of the feature groups. The curvature approach features and, to some extent, the combined measure showed relatively high tortuosity estimation accuracy for the vein segments.

Looking closely, it has been noticed that the veins and arteries have different types of tortuosities.By examining the structural properties measurements of the arteries and veins it has been observed that the means of the vein sub-curves numbers and the sum of these sub-curves under spaces and their heights are slightly higher than those in the arteries. [See tables 4.1, and 4.2]. Bearing that in mind, it appears that both types of blood vessels have different degrees of tortuosity. In other respects, based on conducted analysis, the veins are slightly more tortuous than the arteries and they tend to be tortuous in a rigid way since the only high performance feature reported for this group is the curvature features group which is characterised by measuring the local curvature of each point along the blood vessel segment. In contrast the arteries become tortuous in a smooth manner, which can easily be estimated by the distance measures, such as arc over chord ratio, as proven in figure 4.1. Consequently, I believe these differences can be attributed to the anatomical structures of both blood vessel segments, given that the arteries are more elastic and flexible than the vein. [See section 2.5.1]. I also consider these differences are possibly related to the causes of disease which I believe, has not been investigated before. The analysis conducted on the new tortuosity dataset showed noticeably poor correlations results in almost all aspects of the analysis. From the researcher's point of view, that is due to the grading system used and the large number of instances in the new dataset.

4.6 Conclusion

A tortuosity evaluation framework is proposed. It consists of over 60 features, which are classified in five groups (Structural properties; Distance approach features; Curvature approach features; Combined approach features; Fourier Transform features). The framework includes some of the strongest tortuosity estimation features that were proposed in the literature, as well as those proposed in this study. The statistical analysis of the proposed framework revealed some strong features that were

highly correlated to the clinical order, such as the path over chord times the number of maximum points (C3) with RHO=92% for the arteries and the absolute slopes difference and unsigned curvature (C6) with 81% for the veins. Both of these features were proposed in this study. Using feature selection methods, the best set of features were selected. Consequently, improved performances were recorded, for example the ANN analysis of the forward-feed of the most selected features reported RHO=87% for both arteries and veins, and the forward feed group features reported RHO=98% and RHO=90% for the arteries and veins respectively.

Differences in tortuosities between the arteries and veins were unexpectedly observed during the course of the research. Veins proved to be slightly difficult to accurately estimate their tortuosity in order to match the clinical order. The structural properties of the veins showed that those segments are slightly more tortuous than the arteries. These differences in tortuosity were clearly shown in the correlation analysis, which showed that the majority of the framework features were able to pick up the tortuosity in arteries.

Chapter 5

Investigating tortuosity differences in hypertensive and diabetic retinopathy

This chapter investigates the tortuosity differences between diabetic and hypertension retinopathy, in terms of retinal vessels morphological changes. The first section provides an introduction about the two vascular diseases under investigation, and description of their clinical examination and diagnosis methods. The following sections detail the methodology used in the investigation, followed by the statistical analysis and results. The chapter concludes by discussing the obtained results and reflects on main findings of this chapter.

5.1 Introduction

Hypertension and diabetic retinopathy are diseases that affect the retina, and they can lead to devastating outcomes, such as losing eye sight. (Discussions about the association between these diseases and retinal vessels tortuosity are found in sections 2.6 and 2.6). Thought-provoking facts regarding how these diseases affect the retina occur frequently in reviewing the literature. In clinical examinations, retinal arterial attenuation is one of the major indicators of hypertensive retinopathy. Whereas, retinal venous dilation or tortuosity in general are the common signs of diabetic retinopathy [54]. This indicates that the retinal structure, especially retinal blood

vessels, reacts differently to these diseases. As a result, I strongly believe that, there are differences in tortuosity patterns between diabetic and hypertensive retinopathy. To demonstrate this I have applied the framework to the pathology datasets, to detect any of these differences. The next sections details these steps.

5.2 Method

5.2.1 Hypothesis

The Hypothesis is, is there any tortuosity or structural differences between blood vessels in diabetic and hypertensive retinopathy?

5.2.2 Features identification

The type of features used in the investigation were derived from the symptoms of these diseases. In the case of hypertensive retinopathy, symptoms include decrement in the arterial width. This suggests that there will be minor changes in the structure of arteries. However, in diabetic retinopathy, venous dilation and tortuosity are the major symptoms. This indicates that the vessels should have a form of tortuosity beside veins structural changes. Based on that, the structural properties feature group in our proposed framework has been used to see if there are any significant changes in vessels structures in these conditions.

5.2.3 Analysis

The independent sample t-test was used to test the hypothesis. It compares the means of two independent groups by reference to the same continuous, dependent variable to determine whether there is statistical evidence that the associated population means are significantly different. It is a parametric test, [32]. There certain assumptions which have to be met before commencing the test. These assumptions are:

1) The dependent variable should be continuous.

2) The independent variable should be categorical.

3) The cases should have values on both the dependent and independent variables.

4) The samples or groups be independent.

5) The sample of data has to be randomly taken from the population.

6) Normal distributions of the dependent variable for each group.

7) Homogeneity of the dependent variable for each group.

8) No outliers.

One hundred and thirty one segments from 17 images of diabetic and hypertensive retinopathy patients were used in this analysis. The dependent variables are the structural properties features. IBM SPSS (21) software was used to analyse the measurements of the two groups in two stages, firstly all segments (all veins and arteries) grouped by disease (hypertension and diabetes) and secondly all segments grouped by disease and vessel type as vein and artery.

5.3 Results

5.3.1 Sample characteristics

Sample (All segments grouped by disease) A Shapiro-Wilk's test ($p < .05$) [79] and a visual inspection of their histograms, normal Q-Q plots and box plots, showed that the sum of sub-curves heights were not normally distributed for both hypertensive and diabetic retinopathy, with skewness of 1.053 (SE = .274) and kurtosis of .071 (SE = .541) for hypertensive retinopathy, and skewness of .356 (SE = .327) and a kurtosis of -1.326 (SE = .644) for the diabetic retinopath, [18] and [24]. The test also showed that most features in this group are not normally distributed, refer to Figure 5.1 for the normality test results of this group's features.

Sample (All segments grouped by disease and vessel type) A Shapiro-Wilk's test ($p > .05$) [79] and a visual inspection of their histograms, normal Q-Q plots and box plots showed that the sum of sub-curves heights and the sum of sub curves under spaces were not normally distributed for both arteries and veins, with skewness of .056 (SE= .316) and a kurtosis of -1.296 (SE = .623) for arteries and

Tests of Normality

	Disease	Kolmogorov-Smirnov[a]			Shapiro-Wilk		
		Statistic	df	Sig.	Statistic	df	Sig.
Sub-curves numbers	Hypertension	.235	77	.000	.815	77	.000
	Diabetes	.194	53	.000	.851	53	.000
Number of maximum points	Hypertension	.230	77	.000	.799	77	.000
	Diabetes	.182	53	.000	.840	53	.000
Number of minimum points	Hypertension	.230	77	.000	.799	77	.000
	Diabetes	.182	53	.000	.840	53	.000
Sum of sub-curves under spaces	Hypertension	.147	77	.000	.939	77	.001
	Diabetes	.174	53	.000	.893	53	.000
Sum of sub-curves heights	Hypertension	.226	77	.000	.815	77	.000
	Diabetes	.230	53	.000	.862	53	.000

a. Lilliefors Significance Correction

Figure 5.1: Normality test of the structural features: All segments grouped by disease

1.137 (SE= .281) and a kurtosis of .233 (SE=.555) for the veins [18] and [24]. refer to Figure 5.2 for the normality test results of this group's features.

Tests of Normality

	vesseltype	Kolmogorov-Smirnov[a]			Shapiro-Wilk		
		Statistic	df	Sig.	Statistic	df	Sig.
Sub-curves number	Artery	.195	57	.000	.838	57	.000
	Vein	.242	73	.000	.832	73	.000
Number of max points	Artery	.203	57	.000	.818	57	.000
	Vein	.197	73	.000	.820	73	.000
Number of min points	Artery	.203	57	.000	.818	57	.000
	Vein	.197	73	.000	.820	73	.000
Sum of sub-curves under spaces	Artery	.190	57	.000	.943	57	.010
	Vein	.180	73	.000	.908	73	.000
Sum of sub-curves heights	Artery	.219	57	.000	.864	57	.000
	Vein	.231	73	.000	.802	73	.000

a. Lilliefors Significance Correction

Figure 5.2: Normality test of the structural features: All segments grouped by disease and vessel type

5.3.2 All segments grouped by disease

The hypertension retinopathy segment group ($N = 77$) was associated with a sum of sub-curves heights along blood segments ($M = .236$, $SD = .284$). By compari-

son, the diabetic retinopathy group ($N = 53$) was associated with numerically larger sub-curves heights ($M = .369$, $SD = .351$). To test the hypothesis that diabetic and hypertensive retinopathy are associated with statistically different mean sub-curves heights along blood vessels segments, a t-test was performed. As can be seen in 5.3, diabetic and hypertensive distributions were sufficiently normal for the purposes of conducting a t-test (i.e., $skew < |.752|$ and $kurtosis < |-.730|$ [77]. Additionally, the assumption of homogeneity of variance was tested and satisfied via Levene's F test, $F(128) = 5.497, P = .021$, normality test was also conducted as described in Section 5.3.1. The Mann-Whitney test was associated with statistically significant effect; (U=1566.0, $P < 0.05$). Thus diabetic retinopathy was associated with statistically larger mean sub-curves heights than hypertensive retinopathy. The test also revealed that the sum of sub-curves under spaces in hypertensive retinopathy patients were significantly higher than those in the diabetic retinopathy (U=1566.0, n_1=77, n_2 =53, $p < 0.05$). [See Tables 5.4, 5.5 and 5.6].

Statistics

Sum of sub-curves Heights

N	Valid	130
	Missing	0
Skewness		.752
Std. Error of Skewness		.212
Kurtosis		-.730
Std. Error of Kurtosis		.422

Figure 5.3: Distribution test of the sum of sub-curves heights feature

5.3.3 All segments grouped by disease then by vessel type

Mann-Whitney test was conducted to test the hypothesis that diabetic and hypertension retinopathy are associated with statistically different sub-curves heights in vein segments ($N = 34$) and ($N = 39$) respectively. There was a significant difference in the measurements of the sub-curves heights in diabetic retinopathy patients ($M = .346$, $SD = .330$) and hypertensive patients ($M = .157$, $SD = .242$);

Group Statistics

	Disease	N	Mean	Std. Deviation	Std. Error Mean
Sub-curves numbers	Hypertension	77	.256	.296	.034
	Diabetes	53	.274	.281	.039
Number of maximum points	Hypertension	77	.236	.289	.033
	Diabetes	53	.255	.281	.039
Number of minimum points	Hypertension	77	.236	.289	.033
	Diabetes	53	.255	.281	.039
Sum of sub-curves under spaces	Hypertension	77	.541	.211	.024
	Diabetes	53	.490	.204	.028
Sum of sub-curves Heights	Hypertension	77	.236	.284	.032
	Diabetes	53	.369	.351	.048

Figure 5.4: Independent t-test of group means

Test Statistics[a]

	Sub-curves numbers	Number of maximum points	Number of minimum points	Sum of sub-curves under spaces	Sum of sub-curves heights
Mann-Whitney U	1897.500	1924.000	1924.000	1566.000	1637.500
Wilcoxon W	4900.500	4927.000	4927.000	2997.000	4640.500
Z	-.701	-.567	-.567	-2.254	-1.974
Asymp. Sig. (2-tailed)	.483	.571	.571	.024	.048

a. Grouping Variable: Disease

Figure 5.5: This figure shows the Mann-Whitney test statistics

(U = 429.500,p ¡ 0.05). These results suggest that retinal veins of patients with diabetic retinopathy really do structurally differ compared to hypertensive patients. Specifically, our results suggest that when veins in diabetic patients become tortuous, it will be shown in the increment of sub-curves heights. [See Tables 5.7, 5.8 and 5.9]. The test also revealed that the veins in hypertensive retinopathy were associated with statistically larger sum of sub-curves under spaces and sub-curves numbers with (U = 303.00, $p < 0.05$), and (U = 480.00, $p < 0.05$) respectively.

5.4 Discussion

The non-parametric t-test was applied to the new tortuosity dataset. Features of the structural properties were chosen based on the hypothesis, that the retinal vessels in hypertensive patients are different in structure compared to diabetic patients.

Ranks

	Diseases	N	Mean Rank	Sum of Ranks
Sub-curves numbers	Hypertension	77	63.64	4900.50
	Diabetes	53	68.20	3614.50
	Total	130		
Number of maximum points	Hypertension	77	63.99	4927.00
	Diabetes	53	67.70	3588.00
	Total	130		
Number of minimum points	Hypertension	77	63.99	4927.00
	Diabetes	53	67.70	3588.00
	Total	130		
Sum of sub-curves under spaces	Hypertension	77	71.66	5518.00
	Diabetes	53	56.55	2997.00
	Total	130		
Sum of sub-curves heights	Hypertension	77	60.27	4640.50
	Diabetes	53	73.10	3874.50
	Total	130		

Figure 5.6: This figure shows the Mann-Whitney test ranks

The results showed that diabetic retinopathy was associated with statistically larger mean sub-curves heights than hypertensive retinopathy, especially in vein segments. The possible justification of these results can be observed from the symptoms of these diseases. As stated earlier, the main diagnostic features of diabetic retinopathy are venous dilation and tortuosity. Higher curves indicate tortuosity, therefore this supports the statistical analysis results. On the other hand, the test revealed that the veins in hypertensive retinopathy characterise with statistically significant sum of sub-curves under spaces and sub-curves numbers comparing to those in diabetic retinopathey. Given the main diagnostic feature of hypertensive retinopathy, which is decrement in arterial width, these results are very interesting and further investigations are suggested.

5.5 Conclusion

Based on my observations I suspected that diseases affect retinal structure differently. One of these changes that might affect the retinal vessels are abnormal

Group Statistics[a]

	Disease	N	Mean	Std. Deviation	Std. Error Mean
Sub-curves numbers	Hypertension	39	.197	.266	.043
	Diabetic	34	.319	.285	.049
Number of maximum points	Hypertension	39	.181	.258	.041
	Diabetic	34	.297	.285	.049
Number of minimum points	Hypertension	39	.181	.258	.041
	Diabetic	34	.297	.285	.049
Sum of sub-curves under spaces	Hypertension	39	.601	.209	.034
	Diabetic	34	.474	.171	.029
Sum of sub-curves Heights	Hypertension	39	.157	.242	.039
	Diabetic	34	.346	.330	.057

a. vesseltype = Vein

Figure 5.7: Independent t-test of group means of vein segments

Test Statistics[a]

Vessel type		Sub-curves numbers	Number of maximum points	Number of minimum points	Sum of sub-curves under spaces	Sum of sub-curves heights
Artery	Mann-Whitney U	280.500	282.500	282.500	275.000	315.500
	Wilcoxon W	470.500	472.500	472.500	1016.000	1056.500
	Z	-1.401	-1.359	-1.359	-1.467	-.790
	Asymp. Sig. (2-tailed)	.161	.174	.174	.142	.429
Vein	Mann-Whitney U	480.000	499.000	499.000	303.000	429.500
	Wilcoxon W	1260.000	1279.000	1279.000	898.000	1209.500
	Z	-2.111	-1.868	-1.868	-4.030	-2.687
	Asymp. Sig. (2-tailed)	.035	.062	.062	.000	.007

a. Grouping Variable: Disease

Figure 5.8: This figure shows the Mann-Whitney test statistics of the sample grouped by disease and vessel type

tortuosity. I tested the hypertension retinopathy and diabetic retinopathy on the structural features of blood vessels. The sum of sub-curves heights in the diabetic sample was statistically higher than those in the hypertensive retinopathy. The test also revealed that the sum of sub-curves under spaces in hypertensive retinopathy patients were significantly higher than those in the diabetic retinopathy. Based on these results, there is potential of building an automated tool that can inspect retinal vessels and provide the type of the disease that affect the structure.

Ranks

Vessel type		Disease	N	Mean Rank	Sum of Ranks
Artery	Sub-curves numbers	Hypertension	38	31.12	1182.50
		Diabetes	19	24.76	470.50
		Total	57		
	Number of maximum points	Hypertension	38	31.07	1180.50
		Diabetes	19	24.87	472.50
		Total	57		
	Number of minimum points	Hypertension	38	31.07	1180.50
		Diabetes	19	24.87	472.50
		Total	57		
	Sum of sub-curves under spaces	Hypertension	38	26.74	1016.00
		Diabetes	19	33.53	637.00
		Total	57		
	Sum of sub-curves heights	Hypertension	38	27.80	1056.50
		Diabetes	19	31.39	596.50
		Total	57		
Vein	Sub-curves numbers	Hypertension	39	32.31	1260.00
		Diabetes	34	42.38	1441.00
		Total	73		
	Number of maximum points	Hypertension	39	32.79	1279.00
		Diabetes	34	41.82	1422.00
		Total	73		
	Number of minimum points	Hypertension	39	32.79	1279.00
		Diabetes	34	41.82	1422.00
		Total	73		
	Sum of sub-curves under spaces	Hypertension	39	46.23	1803.00
		Diabetes	34	26.41	898.00
		Total	73		
	Sum of sub-curves heights	Hypertension	39	31.01	1209.50
		Diabetes	34	43.87	1491.50
		Total	73		

Figure 5.9: This figure shows the Mann-Whitney test ranks of the sample that is grouped by disease and vessel type

Chapter 6

Discussion, contribution and future work

This chapter discusses the results obtained, presents plans for future work and outlines the contributions of this research. The chapter starts by an introduction to the main objectives of this thesis and proceeds to provide brief description of each of which and discusses results obtained. The subsequent sections outline the contributions made, and provide plans for future work. The last section concludes this chapter.

6.1 Introduction

In this thesis I have proposed and validated a framework for evaluating the tortuosity of retinal blood vessels. In addition, specialised tortuosity datasets have also been built and tested during the project and a comparative study conducted on the newly built datasets to inspect tortuosity differences between diabetic and hypertensive retinopathy. The following sections provide a summary of the results obtained and a brief discussion of those results.

6.1.1 Tortuosity evaluation framework

Tortuosity properties of retinal vessels, their types and definitions were deeply investigated at the start of this project. Consequently, a framework that consists of over 60 tortuosity features was proposed. The framework was tested first on the RVTDS.

Two of our newly proposed features showed a high correlation with the clinical order with $RHO = .920$ and $RHO = .810$ for the arteries and veins respectively. Using recursive feature elimination algorithms, backward and forward feed, best sets of features were identified. In Random Forest analysis the classification accuracy of the forward feed selection using leave-one-out for feature selection as well as with the classifiers training and testing of the arteries and veins, has achieved RHO = .707 and RHO = .533 and for the backward selection, has achieved $RHO = .761$ and $RHO = .629$, for the arteries and veins respectively. However, using an artificial neuron, the accuracy of the correlation against the doctors order using forward selection has increased to $RHO = .981$ and $RHO = .904$ for the arteries and veins groups respectively, while it achieved $RHO = .770$ and $RHO = .838$ for the arteries and veins groups using the backward feature selection.

Sets of features were selected by performing the union (U) between the thirty sets of features in addition to identifying the most selected features for both groups (arteries and veins). The implementation of these sets using RF and ANN showed promising results. It is believed that the framework includes a good variety of features, so that all that is required is a robust feature selection mechanism to select the best combination of features for optimum performance.

The application of the framework in the context of the new dataset showed a relatively weak performance compared to the RVTD. This, it is believed was due to the ranking grading system used, given the large number of instances in the dataset. Better performances are believed to be achievable if the second grading system is used.

Although our Fourier Transform based features did not record the highest correlations to the clinical order, they were the only group of features that were able to capture the degree of tortuosity of vein segments.

6.1.2 Tortuosity differences in hypertensive and diabetic retinopathy

Various forms of tortuosity have been reported in clinical investigations, most commonly curving/curling, angulation, twisting, looping and kinking [47]. The researcher believes that these morphological changes differ from one disease to another

and that these changes can be more accurately identified and quantified. Consequently tortuosity was investigated from the diabetic and hypertensive point of view searching for these anomalies. The investigations conducted on a sample of retinal vessels segments, revealed that in general the veins of the diabetic patients are the most tortuous. In addition, the independent t-test conducted revealed that diabetic retinopathy is associated with statistically larger mean sub-curves heights compared with hypertensive retinopathy.

6.1.3 Contributions

The major contributions that are presented in this thesis are as follows: 1) The proposition of a number of tortuosity evaluating features. 2) The proposition of tortuosity datasets with two manual grading systems and different pathologies. 3) The investigation of the tortuosity differences in hypertensive and diabetic retinopathy. 4) The proposition of a tortuosity evaluation framework.

All framework features were validated on the gold standard dataset for tortuosity (RVTD) resulting in performances that are to some extent comparable to those achieved by retinal experts. The main advantage of this framework is that it includes a variety of tortuosity features that cover broad aspects of vessels tortuosity. In addition the pathological based dataset provides a window through which to investigate and observe tortuosity forms and types in different diseases.

6.2 Future work

This section highlights areas that need improvement and further development. Plans for future work can be grouped as follows:

6.2.1 Framework

A sophisticated feature selection mechanism is needed to improve the performance of the features of the framework and as a result, build robust classifiers to grade tortuosity of all types of vessels.

6.2.2 Datasets

Desired improvement in this area is mainly in conducting a test on the general dataset using the second grading system (The group classification). In addition, performing another grading on the pathology dataset, because the initial grading was only conducted on the general dataset, which was later divided into two to form the pathology datasets. This separation has led to huge gaps in both grading systems of the pathology datasets.

6.2.3 Tortuosity differences in hypertension and diabetic retinopathy

Improvements suggested in this area include: 1) The investigation of differences based on tortuosity degree. 2) The development of classifiers for retinal vessels based on type of retinopathy disease.

6.3 Conclusion

In conclusion, the main aim of conducting this thesis is to find a tortuosity estimation feature/features that are accurate and robust. However, during the course of the research, the definition of vessel tortuosity and the type of vessels to be measured for tortuosity, were questioned. The literature revealed that there is no universal definition of tortuosity, nor specific rules for types of vessels to be used for tortuosity estimation, and also there is lack of public specialised datasets for tortuosity. Consequently, I propose a tortuosity estimation framework that includes 66 features, some of which were also proposed in this project. These features capture various aspects of vessels tortuosity, such as structural features and different methods of tortuosity estimation features. Prior to that, a number of ophthalmologists, who were consulted throughout this research, indicated that they are certain conditions, regarding vessel types, that should be met before estimating tortuosity such as vessels locations, bifurcations and tributaries. As a result specialised tortuosity dataset was built and proposed in this study. This dataset was used to asses retinal blood vessels structural differences between hypertensive and diabetic retinopathy,

surprisingly conducted tests revealed that their are structural differences between the two retninopathies. As indicated in this chapter the proposed framework and some of the newly proposed features, performed exceptional well compared to those in the literature. However, improvement were suggested for the grading system of the new tortuosity datasets.

Bibliography

[1] *OphthoBook*.

[2] Alireza Akhavan, Seyed-Mohammad-Hadi Shafaatian, and Farshad Rajabipour. Quantifying the effects of crack width, tortuosity, and roughness on water permeability of cracked mortars. *Cement and Concrete Research*, 42(2):313–320, 2012.

[3] Bashir Al-Diri, Andrew Hunter, and David Steel. An active contour model for segmenting and measuring retinal vessels. *Medical Imaging, IEEE Transactions on*, 28(9):1488–1497, 2009.

[4] Dulan Amarasinghe, Upul Sonnadara, Marcus Berg, and Vernon Cooray. Channel tortuosity of long laboratory sparks. *Journal of Electrostatics*, 65(8):521–526, 2007.

[5] Hind Azegrouz, Emanuele Trucco, Baljean Dhillon, Thomas MacGillivray, and IJ MacCormick. Thickness dependent tortuosity estimation for retinal blood vessels. *Engineering in Medicine and Biology Society. EMBS'06. 28th Annual International Conference of the IEEE*, pages 4675–4678, 2006.

[6] Mary Bird. *Medical Terminology and Clinical Procedures*. UK: Redhouse Press Ltd, 2nd edition, 1999.

[7] D Bracher. Changes in peripapillary tortuosity of the central retinal arteries in newborns. *Graefe's Archive for Clinical and Experimental Ophthalmology*, 218(4):211–217, 1982.

[8] D Bracher. Changes in peripapillary tortuosity of the central retinal arteries

in newborns. *Graefe's Archive for Clinical and Experimental Ophthalmology*, 218(4):211–217, 1982.

[9] Leo Breiman. 1 random forests–random features. 1999.

[10] Leo Breiman. Random forests. *Machine learning*, 45(1):5–32, 2001.

[11] Ernesto Bribiesca. A measure of tortuosity based on chain coding. *Pattern Recognition*, 46(3):716–724, 2013.

[12] William L Briggs et al. *The DFT: An Owners' Manual for the Discrete Fourier Transform*. Siam, 1995.

[13] Elizabeth Bullitt, Guido Gerig, Stephen M Pizer, Weili Lin, and Stephen R Aylward. Measuring tortuosity of the intracerebral vasculature from mra images. *Medical Imaging, IEEE Transactions on*, 22(9):1163–1171, 2003.

[14] Joseph J Capowski, Jan A Kylstra, and Sharon F Freedman. A numeric index based on spatial frequency for the tortuosity of retinal vessels and its application to plus disease in retinopathy of prematurity. *Retina*, 15(6):490–500, 1995.

[15] Arunava Chakravarty and Jayanthi Sivaswamy. A novel approach for quantification of retinal vessel tortuosity using quadratic polynomial decomposition. *Medical Informatics and Telemedicine (ICMIT), Indian Conference on IEEE*, Null(Null):7–12, 2013.

[16] KV Chandrinos, M Pilu, RB Fisher, and P Trahanias. Image processing techniques for the quantification of atherosclerotic changes. *DAI Research paper*, 1998.

[17] Crystal SY Cheung, Ziad Butty, Nasrin N Tehrani, and Wai Ching Lam. Computer-assisted image analysis of temporal retinal vessel width and tortuosity in retinopathy of prematurity for the assessment of disease severity and treatment outcome. *Journal of American Association for Pediatric Ophthalmology and Strabismus*, 15(4):374–380, 2011.

[18] Duncan Cramer. *Fundamental statistics for social research: step-by-step calculations and computer techniques using SPSS for Windows*. Psychology Press, 1998.

[19] R Pitts Crick and Peng T Khaw. *A textbook of clinical ophthalmology: a practical guide to disorders of the eyes and their management.* World Scientific, 3rd edition, 2003.

[20] B. Uyyanonvara N. Akinori C. Sinthanayothinl D. Onkaew, R.Turior. Automatic retinal vessel tortuosity measurement using curvature of improved chain code. *Electrical, Control and Computer Engineering (INECCE)International Conference on. IEEE*, pages 183–186, 2011.

[21] Diabetes-UK. Diabetes-key-stats-guidelines. *https://www.diabetes.org.uk/Documents/About2014.*

[22] Oxford English Dictionary. Tortuous. Oxford University Press. http://oxforddictionaries.com/definition/english/tortuous, Accessed April*, 30:2006, 1989.*

[23] Karl T Diedrich, John A Roberts, Richard H Schmidt, Chang-Ki Kang, Zang-Hee Cho, and Dennis L Parker. Validation of an arterial tortuosity measure with application to hypertension collection of clinical hypertensive patients. BMC bioinformatics*, 12(Suppl 10):S15, 2011.*

[24] David P Doane and Lori E Seward. Measuring skewness: a forgotten statistic. Journal of Statistics Education*, 19(2):1–18, 2011.*

[25] Geoffrey Dougherty and Jozsef Varro. A quantitative index for the measurement of the tortuosity of blood vessels. Medical engineering & physics*, 22(8):567–574, 2000.*

[26] James S Duncan and Nicholas Ayache. Medical image analysis: Progress over two decades and the challenges ahead. Pattern Analysis and Machine Intelligence, IEEE Transactions on*, 22(1):85–106, 2000.*

[27] G. Gerig S. Aylward S. Joshi J. K. Smith W. Lin E. Bullitt, D. Zeng and M. G. Ewend. Vessel tortuosity and brain tumor malignancy: a blinded study. Academic Radiology*, 12(10):1232–1240, 2005.*

[28] M. Foracchia E. Grisan and A. Ruggeri. A novel method for the automatic grading of retinal vessel tortuosity. Medical Imaging, IEEE Transactions on*, 2006.*

[29] H. Azegrouz E. Trucco and B. Dhillon. Modeling the tortuosity of retinal vessels: Does caliber play a role? Biomedical Engineering, IEEE Transactions*, 57(9):2239–2247, 2010.*

[30] Nidhal Khdhair El Abbadi and Enas Hamood Al Saadi. Automatic retinal vessel tortuosity measurement. Journal of Computer Science*, 9(11):1456, 2013.*

[31] Inma Estevez, Mary C Christman, and Curtis Miller. Movement in a confined space: Estimating path tortuosity [2011].

[32] Andy Field. Discovering statistics using SPSS*. Sage publications, 2009.*

[33] Marco Foracchia, Enrico Grisan, and Alfredo Ruggeri. Luminosity and contrast normalization in retinal images. Medical Image Analysis*, 9(3):179–190, 2005.*

[34] Jeremy J Foster. Data Analysis Using SPSS for Windows Versions 8-10: A Beginner's Guide*. Sage, 2001.*

[35] Farnoosh Ghadiri, Hamidreza Pourreza, and Touka Banaee. A novel automatic method for vessel tortuosity evaluation. In Systems, Signals and Image Processing (IWSSIP), 2012 19th International Conference on*, pages 56–59. IEEE, 2012.*

[36] Devon H Ghodasra, Atiporn Thuangtong, Karen A Karp, Gui-Shuang Ying, Monte D Mills, Clare A Wilson, Alistair R Fielder, Jeffery Ng, and Graham E Quinn. The rate of change in retinal vessel width and tortuosity in eyes at risk for retinopathy of prematurity. Journal of American Association for Pediatric Ophthalmology and Strabismus*, 16(5):431–436, 2012.*

[37] Kheng Guan Goh, Wynne Hsu, M Li Lee, and Huan Wang. Adris: an automatic diabetic retinal image screening system. Studies in Fuzziness and Soft Computing*, 60:181–210, 2001.*

[38] Rafael C. Gonzalez and Richard E. Woods. Digital Image Processing. *Addison-Wesley Longman Publishing Co., Inc., Boston, MA, USA, 2nd edition, 2001.*

[39] Jenny Gosling. Introductory statistics. *Pascal Press, 1995.*

[40] William Richard Gowers. The state of the arteries in bright's disease. British medical journal, *2(832):743, 1876.*

[41] Henry Gray. Gray's Anatomy: With original illustrations by Henry Carter. *London: Greenwich, 2003.*

[42] Robert M Gray and Joseph W Goodman. Fourier transforms: an introduction for engineers. *Kluwer Academic Publishers Norwell, Massachusetts, 1995.*

[43] Enrico Grisan, Marco Foracchia, and Alfredo Ruggeri. A novel method for the automatic evaluation of retinal vessel tortuosity. 1:866–869, 2003.

[44] Enrico Grisan, Marco Foracchia, and Alfredo Ruggeri. A novel method for the automatic grading of retinal vessel tortuosity. Medical Imaging, IEEE Transactions on, *27(3):310–319, 2008.*

[45] Isabelle Guyon and André Elisseeff. An introduction to variable and feature selection. The Journal of Machine Learning Research, *3:1157–1182, 2003.*

[46] Martin T Hagan, Howard B Demuth, Mark H Beale, et al. Neural network design. *Pws Pub. Boston, 1996.*

[47] H-C Han. Twisted blood vessels: symptoms, etiology and biomechanical mechanisms. Journal of vascular research, *49(3):185–197, 2012.*

[48] William E Hart, Michael Goldbaum, B CÃ, et al. Automated measurement of retinal vascular tortuosity. page 459, 1997.

[49] William E Hart, Michael Goldbaum, Brad Côté, Paul Kube, and Mark R Nelson. Measurement and classification of retinal vascular tortuosity. International Journal of Medical Informatics, *53(2):239–252, 1999.*

[50] Leith Hathout and Huy M Do. Vascular tortuosity: a mathematical modeling perspective. The Journal of Physiological Sciences, *62(2):133–145, 2012.*

[51] *Conor Heneghan, John Flynn, Michael OKeefe, and Mark Cahill. Characterization of changes in blood vessel width and tortuosity in retinopathy of prematurity using image analysis.* Medical Image Analysis*, 6(4):407–429, 2002.*

[52] *Julien Jomier, David K Wallace, and Stephen R Aylward. Quantification of retinopathy of prematurity via vessel segmentation. pages 620–626, 2003.*

[53] *Aubrey Kagan, Elizabeth Aurell, and Gösta Tibblin. Signs in the fundus oculi and arterial hypertension: unconventional assessment and significance.* Bulletin of the World Health Organization*, 36(2):231, 1967.*

[54] *J. J. Kanski.* Clinical Ophthalmology onA Systematic Approach*. Butterworth-Heinemann, 6th edition, 2007.*

[55] *Andrej Krenker, Andrej Kos, and Janez Bešter.* Introduction to the artificial neural networks*. INTECH Open Access Publisher, 2011.*

[56] *Jóhannes Kári Kristinsson, María Soffía Gottfredsdóttir, and Einar Stefánsson. Retinal vessel dilatation and elongation precedes diabetic macular oedema.* British journal of ophthalmology*, 81(4):274–278, 1997.*

[57] *J Richard Landis and Gary G Koch. The measurement of observer agreement for categorical data.* Biometrics*, pages 159–174, 1977.*

[58] *Mark W Leitman.* Manual for Eye Examination and Diagnosis*. UK: Blackwell Science, 5th edition, 2001.*

[59] *Mark W Leitman.* Manual for eye examination and diagnosis*. John Wiley & Sons, 2012.*

[60] *Bernd Liesenfeld, Eva Kohner, W Piehlmeier, Stefan Kluthe, Steve Aldington, Massimo Porta, Toke Bek, Marco Obermaier, Hans Mayer, Gerd Mann, et al. A telemedical approach to the screening of diabetic retinopathy: digital fundus photography.* Diabetes Care*, 23(3):345–348, 2000.*

[61] *Richard J Light. Measures of response agreement for qualitative data: Some generalizations and alternatives.* Psychological bulletin*, 76(5):365, 1971.*

[62] Susannah Q Longmuir, Katherine D Mathews, Reid A Longmuir, Vinayak Joshi, Richard J Olson, and Michael D Abràmoff. Retinal arterial but not venous tortuosity correlates with facioscapulohumeral muscular dystrophy severity. Journal of American Association for Pediatric Ophthalmology and Strabismus*, 14(3):240–243, 2010.*

[63] W Lotmar, A Freiburghaus, and D Bracher. Measurement of vessel tortuosity on fundus photographs. Albrecht von Graefes Archiv für klinische und experimentelle Ophthalmologie*, 211(1):49–57, 1979.*

[64] T. T. Nguyen C. Y. Cheung J. E. Shaw & J. J. Wang. M. B. Sasongko, T. Y. Wong. Retinal vascular tortuosity in persons with diabetes and diabetic retinopathy. Diabetologia*, 54(9):2409–2416, 2011.*

[65] Rodriguez Z Martin, P Kenny, and L Gaynor. Improved characterisation of aortic tortuosity. Medical Engineering & Physics*, 33(6):712–719, 2011.*

[66] Maciej Matyka and Zbigniew Koza. How to calculate tortuosity easily? arXiv preprint arXiv:1203.5646*, 2012.*

[67] R Mielke and W-D Heiss. Positron emission tomography for diagnosis of Alzheimer's disease and vascular dementia*. Springer, 1998.*

[68] Tom M Mitchell. Machine learning. 1997. Burr Ridge, IL: McGraw Hill*, 45, 1997.*

[69] Vahid Mohsenin Mohsenin, Amir and Ron A. Adelman. Retinal vascular tortuosity in obstructive sleep apnea. Clinical ophthalmology (Auckland, NZ)*, 7(Null):787, 2013.*

[70] Dr. Ted Montgomery. Anatomy, Physiology and Pathology of the Human Eye process of vision, 1998.

[71] A. Oppelt. Imaging Systems for Medical Diagnostics: Fundamentals, Technical Solutions and Applications for Systems Applying Ionizing Radiation, Nuclear Magnetic Resonance and Ultrasound*. Wiley, 2005.*

[72] *Christopher G Owen, Richard SB Newsom, Alicja R Rudnicka, Sarah A Barman, E Geoffrey Woodward, and Tim J Ellis. Diabetes and the tortuosity of vessels of the bulbar conjunctiva.* Ophthalmology*, 115(6):e27–e32, 2008.*

[73] *Niall Patton, Tariq Aslam, Thomas MacGillivray, Alison Pattie, Ian J Deary, and Baljean Dhillon. Retinal vascular image analysis as a potential screening tool for cerebrovascular disease: a rationale based on homology between cerebral and retinal microvasculatures.* Journal of anatomy*, 206(4):319–348, 2005.*

[74] *Niall Patton, Tariq M Aslam, Thomas MacGillivray, Ian J Deary, Baljean Dhillon, Robert H Eikelboom, Kanagasingam Yogesan, and Ian J Constable. Retinal image analysis: concepts, applications and potential.* Progress in retinal and eye research*, 25(1):99–127, 2006.*

[75] *Waldir L Roque, Katia Arcaro, and Angel Alberich-Bayarri. Mechanical competence of bone: a new parameter to grade trabecular bone fragility from tortuosity and elasticity.* Biomedical Engineering, IEEE Transactions on*, 60(5):1363–1370, 2013.*

[76] *Joseph R Sadek and Thomas A Hammeke. Functional neuroimaging in neurology and psychiatry.* CNS spectrums*, 7(04):286–299, 2002.*

[77] *Emanuel Schmider, Matthias Ziegler, Erik Danay, Luzi Beyer, and Markus Bühner. Is it really robust? reinvestigating the robustness of anova against violations of the normal distribution assumption.* Methodology: European Journal of Research Methods for the Behavioral and Social Sciences*, 6(4):147, 2010.*

[78] *Martin Sewell. Feature selection.* Online http://machine-learning.martinsewell.com/feature-selection*, 2007.*

[79] *Samuel Sanford Shapiro and Martin B Wilk. An analysis of variance test for normality (complete samples).* Biometrika*, 52(3/4):591–611, 1965.*

[80] *Patrick E Shrout and Joseph L Fleiss. Intraclass correlations: uses in assessing rater reliability.* Psychological bulletin*, 86(2):420, 1979.*

[81] *Phil Simon.* Too Big to Ignore: The Business Case for Big Data*. John Wiley & Sons, 2013.*

[82] Pattheera Panitsuk Sinthanayothin, Chanjira and Bunyarit Uyyanonvara. Automatic retinal vessel tortuosity measurement. Electrical Engineering/Electronics Computer Telecommunications and Information Technology (ECTI-CON),International Conference on IEEE*, 2010.*

[83] Örjan Smedby, N Högman, S Nilsson, U Erikson, AG Olsson, and G Walldius. Two-dimensional tortuosity of the superficial femoral artery in early atherosclerosis. Journal of vascular research*, 30(4):181–191, 1993.*

[84] David L Streiner and Geoffrey R Norman. Health measurement scales: A practical guide to their development and use(oxford medical publications). 2003.

[85] Salford Systems. An Introduction to Random Forests for Beginners*. Salford Systems 2014, 2014.*

[86] P Tanser. Blood vessels. 2006.

[87] Mark OM Tso and Lee M Jampol. Pathophysiology of hypertensive retinopathy. Ophthalmology*, 89(10):1132–1145, 1982.*

[88] Rashmi Turior and Bunyarit Uyyanonvara. Curvature-based tortuosity evaluation for infant retinal images. Journal of Information Engineering & Applications*, 2(8):Null, 2012.*

[89] David Vernon. Machine vision-Automated visual inspection and robot vision*. Englewood Cliffs, NJ (US); Prentice Hall, 1st edition, 1991.*

[90] David K Wallace, Julien Jomier, Steven R Aylward, and Maurice B Landers III. Computer-automated quantification of plus disease in retinopathy of prematurity. Journal of American Association for Pediatric Ophthalmology and Strabismus*, 7(2):126–130, 2003.*

[91] David K Wallace, Julien Jomier, Steven R Aylward, and Maurice B Landers III. Computer-automated quantification of plus disease in retinopathy of prematurity. Journal of American Association for Pediatric Ophthalmology and Strabismus*, 7(2):126–130, 2003.*

[92] Clare M Wilson, Kenneth D Cocker, Merrick J Moseley, Carl Paterson, Simon T Clay, William E Schulenburg, Monte D Mills, Anna L Ells, Kim H Parker, Graham E Quinn, et al. Computerized analysis of retinal vessel width and tortuosity in premature infants. Investigative Ophthalmology and Visual Science*, 8(49):3577–3585, 2008.*

[93] Takuya Yoshikawa, Kenya Murase, Naohiko Oku, Masao Imaizumi, Masashi Takasawa, Piao Rishu, Yasuyuki Kimura, Yoshitaka Ikejiri, Kazuo Kitagawa, Masatsugu Hori, et al. Heterogeneity of cerebral blood flow in alzheimer disease and vascular dementia. American Journal of Neuroradiology*, 24(7):1341–1347, 2003.*

[94] Huiyu Zhou, Jiahua Wu, and Jianguo Zhang. Digital Image Processing: Part II. *Bookboon, 2010.*

Appendices

.1 Appendix A:Review paper

Science and Information Conference 2015
July 28-30, 2015 | London, UK

Quantifying Retinal Blood Vessels' Tortuosity - Review

Mowda Abdalla
University of Lincoln
School of Computer Science
Lincoln, UK
Email: mabdalla@lincoln.ac.uk

Prof Andrew Hunter
University of Lincoln
School of Computer Science
Lincoln, UK
Email: ahunter@lincoln.ac.uk

Dr Bashir Al-Diri
University of Lincoln
School of Computer Science
Lincoln, UK
Email: baldiri@lincoln.ac.uk

***Abstract*—Tortuosity of retinal blood vessels has been identified as one of earliest indicators to a number of vascular and nonvascular diseases; therefore, early detection and grading blood vessel tortuosity could help for early diseases prevention of further complications. There have been many attempts to develop an accurate automated tortuosity grading measure or system. These attempts have varied, from classifying vessels as either tortuous or non-tortuous or classifying/grading a number of retinal vessels in increased tortuosity, to evaluate the collective tortuosity of a whole vascular tree. Yet, seem none of these systems has gained a universal acceptance. This paper provides an overview of systems and measures, either automatic or manual, which are most proposed, to quantify tortuosity, and to critically evaluate the strength and limitations of those systems and measures; also it shed light on problems encountered by researchers in this field, such as the absence of unified, publicly available datasets and the limitations of the existing ones in terms of datasets sizes, variety based on pathologies and the suitability of vessels segments used in these datasets.**

Keywords*—Tortuosity measurement; retinal blood vessels; curvature; vascular diseases.

I. Introduction

The retina has been described as the window of the brain, that because of the close analogy between the retinal vasculature and the cerebral circulation; and it is also the only place where blood vessels can be directly visualized non-invasively in vivo. It provides an easy access for studying the microcirculation and the haemodynamic of blood flow in human body. Normal retinal blood vessels are straight or gently curved, but they tend to dilate and start to become tortuous with age and a number of retinal diseases. Tortuous definition according to Oxford dictionary is full of turns and twists [1], which is not quite a useful definition when it comes to describe retinal blood vessels tortuosity, bearing in mind that the blood vessels are spread in a semi spherical shaped eye, and they are already slightly curved and twisted. Ophthalmologists seem to do not have a precise universal or standard description of abnormal retinal blood vessels' tortuosity, or vessels' tortuosity in general. Usually they describe it based on experience, by identifying relative characteristics such as differences to normal healthy vessels, in term of length, width, location, type and number of twists.

Abnormal retinal tortuosity occurs due to accumulations of curvature along the blood vessels. Ophthalmologists attribute these buildups to the natural capabilities of the blood vessels to avoid or to adapt to certain changes in the body, due to factors such as age and diseases [2]–[5]. Accordingly, tortuosity of retinal blood vessels can be defined as the abnormal curvy, loopy or kinky shapes of vessels extending from the optic disc to the peripheral without bifurcation or between two major consecutive bifurcations. These tortuosity resulted from the ability of the blood vessel to dilate, gain more length and become more curvy and twisty to an abnormal state. Tortuosity can be focal, occurs only in a small region of the retinal vessel tree; or general, involving the whole retinal vascular tree [6]. In recent years, tortuosity of the retinal vessels is considered one of the earliest medical indicators to a number of vascular diseases, including but not limited to Diabetic Retinopathy Hypertensive Retinopathy, Retinopathy Of Prematurity (ROP), facioScapuloHumeral Muscular Dystrophy (FSHD) and Coats diseases [7], [8].

Currently, ophthalmologists rely on an ophthalmoscope, which is an instrument used to manually examine the interior of the eye or retinal fundus images; then abnormalities may be indicated and qualitatively evaluated. With improved image processing software, accurate results can be obtained and further complications and misdiagnosis can be prevented. Moreover, vessels tortuosity in general, not just in the retina, has been associated with diseases presents, for example in abdominal arterial tortuosity and compression of the spine a study conducted by [4] proved that there is significant correlation between the tortuosity of the abdominal aorta and subjects age. Another example, blood vessels tortuosity also has been found as a detector of beginning of malignant tumours in the human brain [9], [10].

The rest of this paper is structured as follows: Section II includes most of the tortuosity measures proposed in the literature, datasets used in these studies are discussed in Section III, and Section IV conclude the paper by outlining the problems encountered researchers in this field.

II. Measures and systems for evaluating tortuosity

Although ophthalmologists fail to agree on a universal definition of vessels tortuosity, they seem to agree on what a tortuosity measure should satisfy to become clinically meaningful. They suggested that tortuosity measures should be invariant to translation rotation and scaling; also the position and the orientation of the vessel should not affect the perception or the degree of tortuosity. Currently, there is a great number of tortuosity measures that have been proposed within the last 42 years. These measures are claimed to accurately able

to quantify tortuosity either as independent vessel segments or as a whole vascular tree [6]. Meanwhile, the literature has revealed and reinforced the strong connection between retinal vessels' tortuosity and vascular diseases [11]–[13]. These findings have urged the need for an accurate automated tortuosity measure. The literature included different types of tortuosity measures, used to quantify vessels tortuosity, either as individual segments or as whole vascular tree, some of these measures have been improved to incorporate features associated with blood vessels' structure such as thickness, width and number of twists and their heights and amplitudes or to satisfy the clinical perception of tortuosity. The literature also included attempts of building automated and semi-automated integrated systems that segment, classify and measure blood vessels features respectively such as Retinopathy Of Prematurity Tool (ROPtool) [14] and Computer Assisted Image Analysis of the Retina(CAIAR) [15]. The following sections document the most frequently used tortuosity measures in the literature.

A. Distance approach

These measures are mainly focused on evaluating tortuosity by computing the length of the blood vessel segment or curve, or the length of the path that the blood vessel takes, known as the Arc and denoted by L_C; and the length of the straight line between the two end points of the blood vessel segment or curve, known as the Chord and denoted by L_X, then tortuosity is mainly estimated by taking the ratio between those two lengths. The next sections provide some of the tortuosity measures that are based on this method.

1) Relative length variation: This was the first distance based measure. It was introduced first by Lotmart Freiburghaus [16], and altered later by Bracher [17]. The measure subdivides a vessel segment into series of single arcs with curves heights h_i, and chord lengths l_i, then tortuosity is estimated as the relative length variation 1, where L is the length of the blood vessel. The approximation is derived using a sinusoidal model of a blood vessel segment. Unfortunately, the technique is not fully automated and it requires manual selection of points on the fundus photograph to divide the vessel into a series of single arcs. Using this measure as a part of a suite of tortuosity measures, 91% was achieved in the classification of segments as tortuous or non-tortuous and 95% in the classification of a whole vascular tree [18] on a private dataset with no particular disease.

$$RLV = \frac{L_C}{l} \approx \frac{8}{3}\sum_{i=1}^{n}(\frac{h_i}{l_i}) \tag{1}$$

2) Arc over chord ratio: This is the most simple, basic and most used distance based tortuosity measure, it is introduced by [6]. Given the blood vessel segment as a curve (S), and the length of the curve as (L_C), 3 or 4, and the straight distance between the two end points of the blood vessel segment, known as the chord length as (L_X) equation 5. This measure simply examines how long the curve is, comparing with the straight distance between its two end points. The measure has zero value for straight vessel segments and increasing positive value for segments as they become tortuous. It is also free of any manual manipulations or interactions, see Equation 2.

$$AOC = \frac{L_C(S)}{L_X(S)} - 1 \tag{2}$$

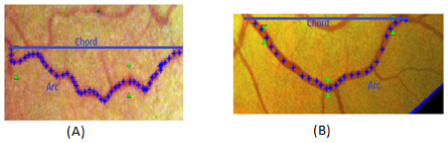

Fig. 1: Two different vessels with the same tortuosity value using Arc over Chord tortuosity measure, (A): Vessel segment tortuosity =1.6, (B):Vessel segment tortuosity =1.6

.

$$L_C = \sum_{i=1}^{n-1}\sqrt{(x_i - x_{i+1})^2 + (y_i - y_{i+1})^2} \tag{3}$$

,

$$L_C 2 = \int_{t_0}^{t_1}\sqrt{x\prime(t)^2 + y\prime(t)^2} \tag{4}$$

,

$$L_X = \sqrt{(x_n - x_1)^2 + (y_n - y_1)^2} \tag{5}$$

This measure found to work very well with short segments; however it assigns the same tortuosity value for a long nicely curved vessel as to a very twisted similar length segment, See figure 1. To sum up, Distance based measures have failed on evaluating retinal vessels tortuosity and that as explained by Emmanuel Trucco [19] that the ratio between the curve and the chord is simply a measure of deviation from a straight line, which is more of a global measure, whereas tortuosity seems more directly related to local measures such as curvature. See Table I for some of the implementations, datasets used and performances achieved using distance approach measures.

B. Curvature approach

Curvature, in mathematics, is the amount by which a surface deviates from a straight line. This deviation or twist can be measured in many ways, it can be measured, geometrically, for each point along a curve by calculating the magnitude of rate of change of angle theta θ, which is the angle made by the tangent line and the positive x-axis, with respect to the curve length or by the measurement of geometrical changes along a blood vessel such as angles between consecutive tangents lines and changes in concavity, such as the Sum Of Angles Measure (SOAM) Equation 15 and the Inflection Count Metric (ICM) Equation 21; or algebraically, by finding the physical rate of change along the blood vessel or the derivative of a function at each point, which it provides a close estimation of curvature at each point along the curve or the blood vessel segment. The curvature measures proposed to estimate tortuosity in the literature were varied between these methods, the following sections are some of the curvature measures discussed and examined in the literature:

1) Curvature at a single point a long a blood vessel: Given a blood vessel segment (S), as a plane curve, where S is represented by centre line points represented by $S = [(x_1, y_1), (x_2, y_2), .., (x_{n-2}, y_{n-2})), (x_{n-1}, y_{n-1}), (x_n, y_n)]$, and given parametrically in the Cartesian coordinates as $(t) = (x(t), y(t))$, The curvature C at point t, $C(t)$, can be estimated as follows:

$$C(t) = \frac{x\prime(t)y\prime\prime(t) - y\prime(t)x\prime\prime(t)}{[x\prime(t)^2 + y\prime(t)^2]^{\frac{3}{2}}} \tag{6}$$

TABLE I: Some of the Implementations, Datasets and Performances achieved using Arc Over Chord Lengths Ratio: (1) as one of suite of measures they achieved 91% for classifying individual segments; (2) 95% for the classification of whole retinal vascular trees as tortuous or non-tortuous; (3) Spearmans Rank Correlation with the clinical order, using numerical differentiation;(4) Spearmans Rank Correlation with the clinical order; (5), using K-nearest neighbour classifier; 6 Comparative study between ROP patients with pre and post treatment.

Implementation	**Dataset**	**Performance**
William E Hart (1997) [6]	Private Dataset	Has a classification rate of 91% $*^1$ and 95%$*^2$ as one of 7 measures.
Conor Heneghan (2002) [13]	Private Dataset	Average increase in tortuosity with the severity of the disease(ROP).
David Wallace (2003) [14]	Private Dataset	80% sensitivity and 91% specificity.
Elizabeth Bullitt (2003) [9]	Private Dataset	It does not differentiate between tight coils and smooth curves.
Julien Jomier (2003) [20]	Private Dataset (ROP)	80% sensitivity and 92% specificity in the prediction of retinopathy compared to experts
Enrico Grisan (2003) [21]	Retinal Vessel Tortuosity DataSet(Public)	Arteries P =0.857, and veins P= 0.036 $*^3$
Enrico Grisan (2006) [22]	Retinal Vessel Tortuosity DataSet(Public)	Arteries P= 0.792, and veins P= -0.656$*^4$.
Enrico Grisan (2008) [23]	Retinal Vessel Tortuosity DataSet(Public)	Arteries P= 0.792, and veins P= -0.656. $*^4$
Crystal S. Y. Cheung etal (2011) [24]	Private Dataset	Significant reductions in all vascular measurements were observed compared to pre-treatment$*^6$
Rashmi Turior (2012) [25]	Private Dataset	Achieved a classification rate of 73% $*^5$
Arunava Chakravarty (2013) [26]	Retinal Vessel Tortuosity DataSet(Public)	It can distinguish between the relative size, shapes and orientations of vessel bends.
Amir Mohsenin (2013) [27]	Private Dataset	80% sensitivity and 92% specificity in predicting retinopathy .

2) Total Curvature of a blood vessel segment: Given the previous curve (S), and the x_n, y_n points representing the centre line points. The total curvature of this segment is the integral curvature along the blood vessel segment with respect to it's length expressed as follows:

$$TC(S) = \int_{t_0}^{t_n} C(t) \tag{7}$$

3) Total Squared Curvature of a blood vessel segment: Given the same blood vessel segment S tortuosity as the total squared curvature is estimated as :

$$TSC(S) = \int_{t_0}^{t_n} C(t)^2 \tag{8}$$

4) Total curvature normalized by the blood vessel arc length: Tortuosity here is estimated by normalizing the total curvature by the blood vessels' arc length as:

$$TC\ normlized\ by\ L_C = \frac{TC_{(S)}}{L_{C_{(S)}}} \tag{9}$$

5) Total squared curvature normalized by the blood vessels' arc length: Tortuosity here is estimated by normalizing the total squared curvature by the blood vessel arc length as:

$$TSC\ normalized\ by\ L_C = \frac{TSC_{(S)}}{L_{C_{(S)}}} \tag{10}$$

6) Total curvature normalized by the blood vessels' chord length: Tortuosity here is estimated by normalizing the total curvature by the blood vessel arc length as:

$$TC\ normalized\ by\ L_x = \frac{TC_{(S)}}{L_{X_{(S)}}} \tag{11}$$

7) Total squared curvature normalized by the blood vessels' chord length: Tortuosity here is estimated by normalizing the total curvature by the chord length between the two end points of the blood vessel segment

$$TSC\ normalized\ by\ L_C = \frac{TSC_{(S)}}{L_{X_{(S)}}} \tag{12}$$

8) Tortuosity Coefficient: This measure proposed by Geoffrey Dougherty [4]. It is based on the second differences of the vessel mid line. Tortuosity is estimates by summing the absolute values of these second differences , represented by δ_i which are the differences between the gradients between two successive segments, then it divided by P which is the sampling interval. The measure is claimed that it could easily be converted and generalized to the use of three dimension measurements. The measure mathematically is expressed as follows:

$$Tortuosity\_Coe = \{\sum_{j=1}^{N} |\delta_i|\}/P \tag{13}$$

9) Tortuosity based on Chain code: The Slope Chain Code tortuosity measure is a measure built on a chain code called Slope Chain Code (SCC). The measure is proposed by Ernesto Bribiesca [28], it is simply based on converting a continuous curve to a discrete one by placing straight-line segments of constant length around the curve (the end points of the straight-line segments always touching the curve), and calculating the slope changes a_i between contiguous straight-line segments scaled to a continuous range from -1 to $+1$. The SCC of a curve is independent of translation, rotation, and optionally of scaling, which considered an important advantage for computing tortuosity, for the mathematical representation of this measure see Equation 14.

$$T\_SCC = \sum_{i=1}^{n} |a_i| \tag{14}$$

10) Sum of angles metric(SOAM): This measure proposed by Semdby, [29] and improved by Elizabeth Bullitt et al. [9], [10]. It measures tortuosity through evaluating the angles between consecutive trios of points along the space curve represented by vessel skeleton, then normalized by path length. Results are in a form of radians/cm. Vessels of high curvature have been noted to have elevated $SOAM$ values. The measure has been found as an effective tool in detecting high-frequency, low-amplitude coils or sine waves. See Equation 15.

$$SOAM = \frac{\sum_{k=1}^{n-3} CP_k}{\sum_{k=1}^{n-1} |P_k - P_{(k-1)}|} \tag{15}$$

11) Mean Curvature(MC): This measure is proposed by Chanjira Sinthanayothin et al. [30], The main principle of MC is fitting circles that fit curves or sub-curves perfectly along a curve. Then radiuses of all circle representing curves will be obtained for the tortuosity of the image to be calculated as the mean curvature (MC). Where 0 is image with low tortuosity and close to 1 is high tortuosity, See Equation 16.

$$MC = AVG[\sum_{i=1}^{n} \frac{1}{r_i}] \tag{16}$$

12) Mean direction Angle change (MDAC): This measure proposed by Chandrinos et al. [31]. It measures tortuosity by averaging the change of angles calculated at reasonable discrete steps along the blood vessel. The measure works by considering two centerline pixels, P-s and P+s for each pixel indicated in the track list, P, pixels that lie ahead and after P, respectively. Consequently two vectors (P-s,P) and (P,P+s) are formed and normalized by dividing each with its norm. Lastly, the dot product is calculated and the inverse cosine of this product. Then MDAC is estimated by averaging those angles over the number of points used along the vessel track. This measure does not work with short segments for instance segments with 10 or less points.

$$MDAC = \frac{1}{(t_{length-2*step})} \sum_{n=step}^{t_length-step} arccos(UV(P_{n-step),P_n}).UV(P_n,Pn+step) \tag{17}$$

13)Absolute direction Angle change (ADAC): This measure proposed by K. G. Goh, et al. (2001) [32]. It is based on tracking vessel centreline and accumulates any direction change along the path of the vessels. At the end of this tracking, the number of changes in direction will indicate how tortuous the segment of the blood vessel is?

$$ADAC = \sum_{i=i+1}^{N-n} (\theta(i) \geq \frac{\pi}{6}) \tag{18}$$

14)Fast Fourier transform based methods: Recently Martin Rodriguez et al. [33] introduced a different approach for evaluating tortuosity; the fast Fourier transform of the vessel's curvature is used as an evaluating method for tortuosity. The method computes the angle variations in three dimensions along the path of the vessel, and then each angle θc is divided by the Euclidean distance Dc between the two points.

$$\theta_C = Cos^{-1}(\frac{\overrightarrow{T_{C-1}}\overrightarrow{T_{C+1}}}{|\overrightarrow{T_{C-1}}||\overrightarrow{T_{C+1}}|}) \tag{19}$$

The overall TC in rad/mm is calculated as the sum of curvatures at each centroid as follows:

$$TSCC = \sum_{C} \frac{\theta_C}{D_C} \tag{20}$$

The amplitude spectra obtained clearly showed differences in tortuosity for the two segments. However, The TSCC obtained for two different tortuous segments were similar although they were completely different in shape. Measures expressed by equations [(6) to (12) were proposed by William E Hart et al. [6]. These measures combined together were able to achieve a classification rate of 91% for the classification of a group of independent retinal blood vessels' segments and achieved 95% for the classification of the whole vascular tree of independent retinal images. The total squared curvature measure was recommended as best measure. See table II for some of the curvature and mixed methods implementations.

C. Mixed methods

These are the methods that combine two or more of the previous methods, some of these methods also might incorporate other blood vessel features such as thickness, width, and inflection points counts.

1) Inflection count metric (ICM): This measure is proposed by Smedby for 2D curves [29] and extended by Elizabeth Bullitt [9], [10] to be implemented on 3D images or space curves. This measure counts "inflection points" along each space or plane curve and multiplies this number (plus one) times the total curve length and then divides by the distance between endpoints, see equation 21.

$$ICM = (n_{i_{c+1}})\frac{L_X}{L_C} \tag{21}$$

2) Tortuosity based on curvature and improved chain code (TCCC): This measure proposed by Danu Onkaew et al. [34], it is an automatic tortuosity measure that classifies retinal images as tortuous and non-tortuous. It is based on the curvature calculated from improved chain code algorithm and the number of inflection points. Where, n_{i_c} and L are the number of inflections and arc length respectively. This measure evaluates vessel tortuosity by summing curvature at every pixels of vessel and also consider number of inflection point at each sub-vessel. This formula has a dimension of 1=L and thus may be interpreted as a tortuosity density. So it can be compared on vessels that have a different length. The advantage of this formula is that it does not depend on segmentation of the vessel tree.

$$TCCC = \frac{(n_{i_{c+1}})}{n_{i_c}} \frac{1}{L} \sum_{n=1}^{n} K(P_i, K) \tag{22}$$

TABLE II: Some of the curvature and the mixed tortousity measures' implementations

Measure	Implementations
Total curvature (TC)	Enrico Grisan [21]–[23], Chanjira Sinthanayothin (2010) , Rashmi Turior (2012), Arunava Chakravarty (2013).
Total squared curvature (TSC)	Enrico Grisan(2003, 2006, 2008), Arunava Chakravarty (2013).
Total curvature normalized by arc length	Enrico Grisan(2003, 2006, 2008), Arunava Chakravarty (2013).
Total squared curvature normalized by the arc length	Enrico Grisan (2003, 2006, 2008).
Total curvature normalized by the chord length	Enrico Grisan (2003, 2006, 2008), Arunava Chakravarty (2013).
Total squared curvature normalized by the chord length	Enrico Grisan (2003, 2006, 2008)
Tortuosity Coefficients	Geoffery Dougherty (2000).
Sum of Angles Metric (SOAM)	Enrico Grisan (2006), Elizabeth Bullitt (2003, 2005), Sodi A,(2013), Arunava Chakravarty (2013).
Inflection count metric (ICM)	Elizabeth Bullitt (2003, 2005), Arunava Chakravarty (2013)
Mean direction angle change (MDAC)	Conor Heneghan (2002),Enrico Grisan (2003, 2006, 2008). , Arunava Chakravarty (2013)
Absolute Direction Angle Change (ADAC)	Enrico Grisan (2006) [22] Arunava et al. (2013) [26] .
Tortousity based on curvature and improved chain code (TCCC)	Onkaew et al. (2011) [34], Abbadi et al. (2013) [35] .
Mean Direction Angle Change (MDAC)	Enrico Grisan (2003, 2008) [21], [23], Conor Heneghan et al. (2002). [13], Arunava et al. (2013) [26]

3) Sub-curves and distance based measurers: Enrico Grison proposed a new tortuosity measure and improved it over the years [21]–[23]. The algorithm based on the partitioning of each vessel into segments of constant-sign curvature and on the combination between the number of such segments and their curvature values. However, this measure requires manual vessel extraction and inflection point placement, the following are the three equations in which the measure has been improved.

$$T1 = \frac{n-1}{L_C} \sum_{n=1}^{n} [\frac{L_{C_S i}}{L_{X_S i}}] \tag{23}$$

,

$$T2 = \frac{n-1}{L_C} \frac{1}{L_C} \sum_{n=1}^{n} [\frac{L_{C_S i}}{L_{X_S i}}] \tag{24}$$

,

$$T3 = \frac{n-1}{n} \frac{1}{L_C} \sum_{n=1}^{n} [\frac{L_{C_S i}}{L_{X_S i}}] \tag{25}$$

where n is the number of curves in a segment.

4) Tortuosity index (TI): This measure proposed by [8]. It evaluates tortuosity by identifying the number of changes in curvature sign. Where n is the number of segments in a single vessel, m represent the angles of curvature θ_i, length of the respective area is denoted by L_C and the length of the chord is represented by L_X.

$$TI = [\frac{(n+1) * [\sum_i^m \theta_i] * [\sum_i^m \frac{L_{C_i}}{L_{X_i}}]]}{L_c * m * m}] \tag{26}$$

5) Tortuosity based on vessel wall thickness: This measure proposed by Hind Azegrouz et al. [36] and extended by Emanuele Trucco and Hind Azegrouz [19], it combines curvature and thickness. It is defined as a weighed Minkowski norm of the curvatures along the vessel boundaries, and is an increasing function of vessel diameter (Thickness).

$$TW = (\sum_{n=3}^{N} \frac{|K_{B_{1(n)}}| + |K_{B_{2(n)}}|}{2})^{\frac{1}{P}} \tag{27}$$

6) Automatic tortuosity image classifier: :
This algorithm can automatically classify images as tortuous or non-tortuous, where n_{i_c} and L are the number of inflection points and arc length respectively. This measure evaluates vessel tortuosity by summing curvature at every pixels of vessel and also consider number of inflection point at each sub-vessel. This formula has a dimension of $1 = L$ and thus may be interpreted as a tortuosity density. So it can be compared on vessels that have a different length. The advantage of this formula is that it does not depend on segmentation of the vessel tree [25], [34].

D. Tortuosity Grading Systems

These are the automatic or semi-automatic systems that, to some extend, segments, extract and classify or measure retinal blood vessels respectively [20]. Examples of these systems are: The ROPTool which is a computer program that traces retinal blood vessels of premature infants and measures their retinal vessels' tortuosity [14], [37], [38]; Another example is the Computer Assisted Image Analysis of the Retina(CAIAR)which measures width and tortuosity of retinal vessels [15].

TABLE III: Some of the tortuosity datasets used in the literature

Author	Pathology /feature measured	Availability	Nature of the dataset
Kagan et al.(1976) [39]	ROP/Tortuosity (segments and whole tree)	Private	Not available
William E. Hart (1997,1999) [6], [18]	Not particular (segments and whole tree)	Private	20 retinal images
Geoffrey Dougherty (2000) [40]	Abdominal Arterial/ Tortuosity	Private	Aortograms of 82 patients
Conor Henghen (2002) [13]	ROP/Width and tortuosity	Private	23 subjects
Elizabeth Bullitt (2003) [9]	Brain tumours/vessels Tortuosity	Private	11 normal and 6 patients
Elizabeth Bullitt (2005) [10]	Brain tumours/vessels Tortuosity	Private	34 Healthy subjects and 30 patients
Enrico Grisan (2003, 2006, 2008) [21]–[23]	Not particular/Tortuosity	Public	60 images of retinal vessels from normal and hypertensive patients.
Christopher G. Owen (2008) [12]	Diabetes/Tortuosity	Private	53 patients and 60 controls
Sodi A(2013) [41]	Fabry disease/Tortuosity + width	Private	35 patients
Susannah Q. Longmuir, et al. (2010) [8]	FSHD /Tortuosity	Private	7 patients
Amir Mohsenin (2013) [27]	ROP/Tortuosity	Private	9 patients and 7 healthy

III. Retinal vessel Tortuosity datasets

One of the tortuosity evaluation main problems is the availability of free public datasets for retinal blood vessels' tortuosity evaluation. Although there are few datasets, the BioImLab Retinal vessel tortuosity dataset appears to be the only publicly available one [23]. Both public and private datasets they differ in sizes, type of segments, segments length, segmentation techniques and the pathologies that affect patients at the moment of screening. Thus comparative tortuosity studies and providing feasible accurate results are proven to be quite surreal given previous circumstances. See table III for some of the tortuosity datasets used in the literature

IV. Conclusion

The literature has proved over and over the strong correlation between some of the vascular and non-vascular diseases and the abnormal tortuosity of retinal blood vessels. Consequently, there is an urgent need for an accurate robust tortuosity measure for early detection and hence diseases prevention. Although there is a healthy number of tortuosity measures proposed in the recent years, non has obtained full-scale acceptance. In our review we came across a few problems that we think might greatly affected the progress of finding such measure, these problems are:

- The ambiguity of tortuosity definition, which has led to the confusion of what to measure and for which disease; for instance: in hypertension tortuosity is associated with Arterial Attenuation, which is decrement in the arterial width or narrowing, while in the other hand the major change associated with diabetes presences is venous dilation or increased tortuosity [7].
- We noticed the absence of unified public datasets for tortuosity, such as the gold standard for retinal vessels segmentation. Even with available datasets, public or private, we observed the differences in the segmentation techniques for extracting blood vessels, lengths and sizes of these segments.
- Sizes of tortuosity datasets, whether they are private or public, most of these datasets fall in the small size side which reflect negatively on the tortuosity measures validations process.
- The majority of tortuosity datasets are private and are not publicly available. Refer to table III.
- Pathologies specialized tortuosity datasets, we believe that different diseases have different tortuosity effects, therefore studying retinal vessel tortuosity from each particular disease point of view is essential.
- Most tortuosity grading algorithms are dependent on one or two factors, factor such as curvature or number of twists. However, retinal blood vessel tortuosity sometimes associated with dilation, elongation and so on, so incorporating measures for these factors in the evaluating process might increase evaluation accuracy.

Given those problems, we suggest and urge the formation of a public and freely available unified datasets. These datasets should cover all main sorts of pathologies associated with retinal vessels tortuosity, with variety of vessels types based on size and the geometric location on the retina, the type of segmentation techniques, information of the imaging tool used to acquire these images and quality. Our future work will be focused on building a robust framework for evaluating tortuosity incorporating the most accurate of the proposed measures in detecting tortuosity.

References

[1] U. Oxford. (2013, April) Tortuous. [Online]. Available: http://oxforddictionaries.com/definition/english/tortuous

[2] Ş. Ţălu, "Characterization of retinal vessel networks in human retinal imagery using quantitative descriptors." *Human & Veterinary Medicine*, vol. 5, no. 2, 2013.

[3] R. Koprowski, S. Teper, B. Weglarz, E. Wylegala, M. Krejca, and Z. Wróbel, "Fully automatic algorithm for the analysis of vessels in the angiographic image of the eye fundus," *Biomed Eng Online*, vol. 11, p. 35, 2012.

[4] G. Dougherty and J. Varro, "A quantitative index for the measurement of the tortuosity of blood vessels," *Medical engineering & physics*, vol. 22, no. 8, pp. 567–574, 2000.

[5] C. G. Owen, A. R. Rudnicka, R. Mullen, S. A. Barman, D. Monekosso, P. H. Whincup, J. Ng, and C. Paterson, "Measuring retinal vessel tortuosity in 10-year-old children: Validation of the computer-assisted image analysis of the retina (caiar) program," *Investigative Ophthalmology & Visual Science*, vol. 50, no. 5, pp. 2004–2010, 2009.

[6] W. E. Hart, M. Goldbaum, B. CÃ *et al.*, "Automated measurement of retinal vascular tortuosity." p. 459, 1997.

[7] J. J. Kanski, *Clinical Ophthalmology onA Systematic Approach*, 6th ed. Butterworth-Heinemann, 2007.

[8] S. Q. Longmuir, K. D. Mathews, R. A. Longmuir, V. Joshi, R. J. Olson, and M. D. Abràmoff, "Retinal arterial but not venous tortuosity correlates with facioscapulohumeral muscular dystrophy severity," *Journal of American Association for Pediatric Ophthalmology and Strabismus*, vol. 14, no. 3, pp. 240–243, 2010.

[9] E. Bullitt, G. Gerig, S. M. Pizer, W. Lin, and S. R. Aylward, "Measuring tortuosity of the intracerebral vasculature from mra images," *Medical Imaging, IEEE Transactions on*, vol. 22, no. 9, pp. 1163–1171, 2003.

[10] E. Bullitt, D. Zeng, G. Gerig, S. Aylward, S. Joshi, J. K. Smith, W. Lin, and M. G. Ewend, "Vessel tortuosity and brain tumor malignancy: a blinded study1," *Academic radiology*, vol. 12, no. 10, pp. 1232–1240, 2005.

[11] C. Incorvaia, F. Parmeggiani, C. Costagliola, P. Perri, S. D'Angelo, and A. Sebastiani, "Quantitative evaluation of the retinal venous tortuosity in chronic anaemic patients affected by β-thalassaemia major," *Eye*, vol. 17, no. 3, pp. 324–329, 2003.

[12] C. G. Owen, R. S. Newsom, A. R. Rudnicka, S. A. Barman, E. G. Woodward, and T. J. Ellis, "Diabetes and the tortuosity of vessels of the bulbar conjunctiva," *Ophthalmology*, vol. 115, no. 6, pp. e27–e32, 2008.

[13] C. Heneghan, J. Flynn, M. OKeefe, and M. Cahill, "Characterization of changes in blood vessel width and tortuosity in retinopathy of prematurity using image analysis," *Medical image analysis*, vol. 6, no. 4, pp. 407–429, 2002.

[14] D. K. Wallace, J. Jomier, S. R. Aylward, and M. B. Landers III, "Computer-automated quantification of plus disease in retinopathy of prematurity," *Journal of American Association for Pediatric Ophthalmology and Strabismus*, vol. 7, no. 2, pp. 126–130, 2003.

[15] C. M. Wilson, K. D. Cocker, M. J. Moseley, C. Paterson, S. T. Clay, W. E. Schulenburg, M. D. Mills, A. L. Ells, K. H. Parker, G. E. Quinn *et al.*, "Computerized analysis of retinal vessel width and tortuosity in premature infants," *Investigative ophthalmology & visual science*, vol. 8, no. 49, pp. 3577–3585, 2008.

[16] W. Lotmar, A. Freiburghaus, and D. Bracher, "Measurement of vessel tortuosity on fundus photographs," *Albrecht von Graefes Archiv für klinische und experimentelle Ophthalmologie*, vol. 211, no. 1, pp. 49–57, 1979.

[17] D. Bracher, "Changes in peripapillary tortuosity of the central retinal arteries in newborns," *Graefe's Archive for Clinical and Experimental Ophthalmology*, vol. 218, no. 4, pp. 211–217, 1982.

[18] W. E. Hart, M. Goldbaum, B. Côté, P. Kube, and M. R. Nelson, "Measurement and classification of retinal vascular tortuosity," *International journal of medical informatics*, vol. 53, no. 2, pp. 239–252, 1999.

[19] H. A. E. Trucco and B. Dhillon., "Modeling the tortuosity of retinal vessels: Does caliber play a role?" *Biomedical Engineering, IEEE Transactions*, vol. 57, no. 9, pp. 2239–2247, 2010.

[20] J. Jomier, D. K. Wallace, and S. R. Aylward, "Quantification of retinopathy of prematurity via vessel segmentation," pp. 620–626, 2003.

[21] E. Grisan, M. Foracchia, and A. Ruggeri, "A novel method for the automatic evaluation of retinal vessel tortuosity," vol. 1, pp. 866–869, 2003.

[22] M. F. E. Grisan and A. Ruggeri., "A novel method for the automatic grading of retinal vessel tortuosity," *IEEE TRANSLATION ON MEDICAL IMAGING*, vol. Null, no. null, p. null, 2006.

[23] M. F. E. Grisan and A. Ruggeri, "A novel method for the automatic grading of retinal vessel tortuosity," *IEEE TRANSACTIONS ON MEDICAL IMAGING*, vol. 27, no. 3, pp. 310–319, 2008.

[24] C. S. Cheung, Z. Butty, N. N. Tehrani, and W. C. Lam, "Computer-assisted image analysis of temporal retinal vessel width and tortuosity in retinopathy of prematurity for the assessment of disease severity and treatment outcome," *Journal of American Association for Pediatric Ophthalmology and Strabismus*, vol. 15, no. 4, pp. 374–380, 2011.

[25] R. Turior and B. Uyyanonvara., "Curvature-based tortuosity evaluation for infant retinal images," *Journal of Information Engineering & Applications*, vol. 2, no. 8, p. Null, 2012.

[26] A. Chakravarty and J. Sivaswamy, "A novel approach for quantification of retinal vessel tortuosity using quadratic polynomial decomposition," *Medical Informatics and Telemedicine (ICMIT)Indian Conference on. IEEE*, vol. Null, no. Null, pp. 7–12, 2013.

[27] V. M. Mohsenin, Amir and R. A. Adelman., "Retinal vascular tortuosity in obstructive sleep apnea," *Clinical ophthalmology (Auckland, NZ)*, vol. 7, no. Null, p. 787, 2013.

[28] E. Bribiesca, "A measure of tortuosity based on chain coding," *Pattern Recognition*, vol. 46, no. 3, pp. 716–724, 2013.

[29] Ö. Smedby, N. Högman, S. Nilsson, U. Erikson, A. Olsson, and G. Walldius, "Two-dimensional tortuosity of the superficial femoral artery in early atherosclerosis," *Journal of vascular research*, vol. 30, no. 4, pp. 181–191, 1993.

[30] P. P. Sinthanayothin, Chanjira and B. Uyyanonvara, "Automatic retinal vessel tortuosity measurement." *Electrical Engineering/Electronics Computer Telecommunications and Information Technology (ECTICON),International Conference on. IEEE*, 2010.

[31] K. Chandrinos, M. Pilu, R. Fisher, and P. Trahanias, "Image processing techniques for the quantification of atherosclerotic changes," *DAI RESEARCH PAPER*, 1998.

[32] K. G. Goh, W. Hsu, M. Li Lee, and H. Wang, "Adris: an automatic diabetic retinal image screening system," *Studies in Fuzziness and Soft Computing*, vol. 60, pp. 181–210, 2001.

[33] P. K. Z. M. Rodriguez and L. Gaynor., "Improved characterisation of aortic tortuosity," *Medical engineering & physics*, vol. 33, 2011.

[34] D. Onkaew, R. Turior, B. Uyyanonvara, N. Akinori, and C. Sinthanayothin, "Automatic retinal vessel tortuosity measurement using curvature of improved chain code," pp. 183–186, 2011.

[35] N. K. E. Abbadi and E. H. A. Saadi, "Automatic retinal vessel tortuosity measurement," *Journal of Computer Science*, vol. 9, no. 11, p. 1456, 2013.

[36] H. Azegrouz, E. Trucco, B. Dhillon, T. MacGillivray, and I. MacCormick, "Thickness dependent tortuosity estimation for retinal blood vessels," pp. 4675–4678, 2006.

[37] D. K. Wallace, "Computer-assisted quantification of vascular tortuosity in retinopathy of prematurity(an american ophthalmological society thesis)," *Transactions of the American Ophthalmological Society*, vol. 105, no. 594, 2007.

[38] D. K. Wallace, S. F. Freedman, Z. Zhao, and S.-H. Jung, "Accuracy of roptool vs individual examiners in assessing retinal vascular tortuosity," *Archives of ophthalmology*, vol. 125, no. 11, pp. 1523–1530, 2007.

[39] A. Kagan, E. Aurell, and G. Tibblin, "Signs in the fundus oculi and arterial hypertension: unconventional assessment and significance," *Bulletin of the World Health Organization*, vol. 36, no. 2, p. 231, 1967.

[40] G. Dougherty and J. Varro, "A quantitative index for the measurement of the tortuosity of blood vessels," *Medical engineering & physics*, vol. 22, no. 8, pp. 567–574, 2000.

[41] A. Sodi, M. Guarducci, L. Vauthier, A. S. Ioannidis, S. Pitz, G. Abbruzzese, F. Sofi, A. Mecocci, A. Miele, and U. Menchini, "Computer assisted evaluation of retinal vessels tortuosity in fabry disease," *Acta ophthalmologica*, vol. 91, no. 2, pp. e113–e119, 2013.

.2 Appendix B: Implementation

Matlab R2014a was used to implement all framework features. The retinal vessels tortuosity dataset RVTDS described in Section 3.3, was used to test the performance of these features. The number of the blood vessel segments in this dataset are 30 arteries and 30 veins represented as (S_N), where $N \subset R$, and each S is represented by given n centreline points expressed as
$S = [(x_1, y_1), (x_2, y_2), \ldots., (x_{n-2}, y_{n-2})), (x_{n-1}, y_{n-1}), (x_n, y_n)]$. The blood vessel segments were sampled, by defining each of which by a series of points with even spacing, by a given parameter. A spline curve was then fitted to the points, and re sampled along the length using a simple piece-wise linear approximation, generating enough spline points to make this reasonably accurate.

.2.1 Distance approach features

Path length:

```
%Path length
    n=length(x);
    x1=(x(2:end));
    x2=x(1:end-1);
    y1=y(2:end);
    y2=y(1:end-1);
    def_x=(x1-x2);
    def_y=(y1-y2);
for i=2:n
    seg_length_item=(power((((x(i)-x(i-1))^2)+(y(i)-y(i-1))^2),1/2));
    seg_length=[seg_length seg_length_item];
end
    segmentlength=sum(seg_length);
```

Curve or arc length measurement:

```
% Curve or Arc length measurement
    Arc_length=sum(sqrt((xprime.*xprime)+(yprime.*yprime)));
```

Chord length measurement:

```
% Chord length measurement
      x_length=length(x);
      x_one=x(1);
      x_n=x(x_length);
      y_one=y(1);
      y_n=y(x_length);
      C_length=abs(sqrt(((x_n-x_one)^2)+((y_n-y_one)^2)));
```

.2.2 Curvature approach features

Curvature along segment length:

```
%Signed curvature for each point a long the segment
       Signed_curvature =((xprime.*ysec) - (xsec.*yprime))./ ...
       power(((xprime.*xprime) + (yprime.*yprime)), 3/2);
%The total signed curvature
       signed_total_curvature=sum(Signed_curvature);
%Unsigned curvature
       unsigned_curvature=abs(Signed_curvature);
%Total unsigned curvature
       unsigned_Total_curvature=sum(unsigned_curvature);
%Total squared unsigned curvature
       tsusc=unsigned_Total_curvature*unsigned_Total_curvature;
%Total squared signed curvature
     tsc=signed_total_curvature*signed_total_curvature;
% Total curvature normalized by arc length1 and total curvature
% normalised by arc length2
      total_unsigned_c_over_seg_Pathlength=unsigned_Total_curvature/...
      seg_Pathlength;
      total_signed_c_over_seg_Pathlength=signed_total_curvature/...
      seg_Pathlength;
      total_unsigned_c_over_arcLength=unsigned_Total_curvature/...
```

```
      Arc_length;
      total_signed_c_over_ArcLength=signed_total_curvature/...
      Arc_length;
%Total squared signed/unsigned curvature normalised by arc length
%total squared signed/unsigned curvature normalised by arc length
      total_squared_signed_curvature_over_PathLength=tssc/...
      seg_Pathlength;
      tsusc_over_pathLength=tsusc/seg_Pathlength;
      total_squared_signed_curvature_over_arcLength=tssc/Arc_length;
      tsusc_over_ArcLength=tsusc/Arc_length;
% Total curvature  normalised by chord length
       total_unsigned_c_over_chordLength=unsigned_Total_curvature/...
       Segment_chord_Length;
       t_signed_c_over_cl=signed_total_curvature/Segment_chord_Length;
%Total squared curvature/chord length
       tssc_over_cl=tssc/Segment_chord_Length;
       tsusc_over_cl=tsusc/Segment_chord_Length;
```

Tortuosity coefficient:

```
for i=2:p-1
    p= length(x);
    Tort_Coefficient_item=sum(abs((y(i)-y(i-1))-(y(i+1)-y(i))));
    Tort=[Tort Tort_Coefficient_item];
 end
    Tort_Coefficient=sum(Tort)/p;
end
```

The Signed and unsigned tortuosity using the gradients along blood vessel segments:

```
            n=length(x);
            M=[];
%x values
            x1=x(1:n-1);
            x2=x(2:n);
```

```
%y values
            y1=y(1:n-1);
            y2=y(2:n);
%Slopes
            M=y2-y1/x2-x1;
            L=length(M);

            m1=M(1:L-1);
            m2=M(2:L);
%The sum of the differences and the absolute
 differences of slopes
            unsign_Tort_Slope= sum(abs((m2-m1)));
            sign_Tort_Slope=sum(m2-m1);
```

Rashmi's measure of tortuosity:

```
%Calculation of the gradients along blood segments
             m=(y2-y1)./(x2-x1);
             ml=length(m);
             m1=m(2:end);
             m2=m(1:ml-1);
%Estimation of the segment tortuosity
             Rashmi_Tortousity=sum(abs(m1-m2));
```

Mean direction angle change:

```
%Identifying two vectors for each point along the segment
%(before and after the point)
      vector_before(1)=x_points(i);
      vector_before(2)=x_points(i-step);
      vector_after(1)=x_points(i);
      vector_after(2)=x_points(i+step);
%Normlization of the two vectors
      vec_b_N =((vector_before-min_b_vec)./(max_b_vec-min_b_vec));
      vec_a_N =((vector_after-min_a_vec)./(max_a_vec-min_a_vec));
```

```
%Estimation of the angle Theta (the dot product of vector_before and
%vector_after, then taking the acos to estimate the angle)
       dot_product_b_a=dot(vec_b_N, vec_a_N);
%Mean Direction Angle Change of a blood vessel segment
       MDAC=(1/Arc_length-2*step)* sum(dot_product_b_a);
```

.2.3 Combined approach features

Grisan's tortuosity measure:

```
  Tort_Grisan = ((all_sub_curves_no -1)/(all_sub_curves_no))*...
  (1/Arc_length)*(sum(all_subcurves_tortousity));
```

Inflection count metrics:

```
all_sub_curves_no=sum(concaved_up_curves_No+...
concaved_down_curves_No+uncurvedCurved_NO);
ICM1=(all_sub_curves_no+1)*(Segment_chord_Length/Arc_length);
ICM2=(all_sub_curves_no+1)*(Segment_chord_Length/seg_Pathlength);
```

.2.4 My combined approach features

Arc over chord and the number of maximum points:

```
  ArcOverchord_times_Maximapoints=(Arc_length *...
   (maximapoints_no+1));
%Path over chord and the number of maximum point
  PathOverChord_maximapoints=(path_over_chord *...
   (maximapoints_no+1));
```

Path length and the sub-curves numbers:

```
   path_length_and_curvesNum=(seg_Pathlength + Subcurves_no) ;
```

Vessel profile features one and two:

```
   vessel_profile2=(path_over_chord + sumSubCurveHeights);
   vessel_profile1=(path_over_chord + sum_all_subcurvesspace);
```

.3 Appendix C: Statistical analysis

.3.1 Regression analysis

.3.2 ANN learning

```
% Initial random weights for a model features
Weights=rand(1,size(model6,2));
% The predicted output
for i=1:size(Features,1)
    FTW = sum(Features(i,:).* Weights(1:end));
    predicted_output(i)=(1/(1+ exp(-FTW)));
end
%Initial performance test of thee neuron
[RHO,~] = corr(desired_output,predicted_output,'Type','Spearman');
```

.3.3 Feature selection

The intersected features of the backward-feed analysis of the arteries include:

1) Segments chord length

2) Tortuosity coefficient

3) Signed tortuosity slope

4) Tortuosity by Grisan

5) Rashmi's tortuosity measure

6) Abs of slopes differences and unsigned curvature

7) Sum of DFT Magnitudes using slopes

8) DFT Magnitudes using xprime

9) Sum of the signal phases norm by path length using xPrime'

10) Sum of Magnitudes normalised by path length using xPrime'

11) Sum of Magnitudes normalised by path length using curvature'

The intersected features of the backward-feed analysis of the veins include:

1) Tortuosity by Grisan
2) Number of minimum points along a segment
3) Sum of sub-curves under spaces
4) Rashmis tortuosity measure
5) Abs of Slops Differences and unsigned curvature
6) The sum of sub-curves heights
7) Sum of DFT Magnitudes using slopes
8) DFT Magnitudes using xprime
9) Sum of the signal phases normalised by path length using xPrime'
10) Sum of Magnitudes normalised by path length using xPrime'

The intersected features of the forward-feed analysis of the arteries include:

1) Path over chord

The intersected features of the forward-feed analysis of the veins include:

1) Mean direction angle change